Development of *in vitro* and *in vivo* models of uveal melanoma

Thesis submitted in accordance with the requirements of the University of Liverpool for the degree of Doctor in Philosophy

Haleh Shahidipour

July 2016

To mum, Farideh Fazel, the angel that walked this earth

Acknowledgements

There will never be enough words, dedications or acknowledgments to thank the most important person in my life, my mum.

I would like to acknowledge my supervisors, Prof. Sarah Coupland, Dr Helen Kalirai, Dr Diana Moss and Prof. Bertil Damato for their help and support in my PhD. I will always treasure Helen's kind heart. I would also like to acknowledge Dr Joseph Slupsky for being a brilliant mentor, Dr Pat Eyers for his input in my project and Dr Kathy Till for her help in the lab.

I thank my truly amazing friends who are so precious to me; Elham for flying across the world at the most difficult time in my life, Afsaneh for sharing so many special moments with, my tall Yosra and the other two crazies Lamia and Rawan, Fatima for being a gem, Fidan - we rock, Vaida for the great workouts and cakes, Cath for always being there with kind words and advice, Isabel my other tall one and my two fabulous, amazing Greeks, Sophia and Lia. I also thank the LOORG team in particular the girls; Martina, Nihal, Dawn, Laura, Sophie and Conni. The Haematology group for being great to be with in the lab and Ahmed, Ola, and the three fabulous girls Athina, Andrea and Ana for the great catching up sessions. I further thank my two lovely Germans, Anne and Amelie. I thank MCS and the brilliant Waterworth family, for one of the best and exciting working opportunities of my life.

I would also like to acknowledge my two amazing brothers Hamed and Hadi and my fiancé Ashkan, thank you all for being tall. I thank all the great family friends and my mum's great friends; Ladan, Laleh, Shiva and Faegheh.

I hope to have contributed to science and research, as small as it maybe, with my hard work in this PhD. I will continue to achieve and strive, and try and be as incredible a person as my mum was.

Abstract

Uveal melanoma (UM) is the most common primary intraocular cancer of the eye in adults. Despite successful treatment of the primary tumour, approximately half of patients diagnosed with UM will develop metastases. To date, treatments for metastatic UM have had only limited effect, hence prognosis remains poor. Metastatic UM occurs predominantly in the liver. The mechanisms responsible for this remain largely unknown. Investigations into the molecular and cellular processes underlying UM development and metastasis are essential to develop therapeutic approaches directed against dissemination of this disease.

In vitro and *in vivo* models play a crucial role in basic and translational oncology research. The scope of the work presented in this thesis was to develop innovative and clinically relevant *in vitro* and *in vivo* preclinical models that reproduce various aspects of metastatic processes in UM. In Chapter 2, primary UM cells were used to establish 3D tumour spheroids which retained many morphological and molecular characteristics of the original tumour. These 3D tumour spheroids more accurately mimic the 3D *in vivo* environment in which cancer cells reside and as a result can be used in co-culture assays, drug assays, and further transferred to an animal model to examine metastatic progression. Chapter 3 outlined one such *in vivo* model; the chick embryo. This model represents an accessible and economical *in vivo* model that has long been used in developmental biology. A panel of UM cell lines that represent the characteristic genetic and morphological profile in UM were used to form tumour nodules on the chorioallantoic membrane (CAM) and metastatic colonisation in internal organs following intravenous injection. Cells predominantly homed to the chick embryo eye spreading widely within the uveal tract, and to the liver, representative of the disease in patients allowing for a better understanding in the spread of this disease. Furthermore, cell lines forming tumour nodules on the CAM can be further used to assess candidate therapeutic drugs in an *in vivo* setting. Chapter 4 aimed to investigate such drug candidates by assessing the effects of targeted clinical inhibitors on UM cell lines. One particular inhibitor, the bromodomain PPI inhibitor JQ1, caused cell cycle arrest in two UM cell lines paving the way for many further insightful investigations.

The models established in this thesis represent valuable, inexpensive and rapid *in vitro* and *in vivo* systems that can improve our understanding of the metastatic process in UM and provide a platform for the preliminary testing of potential new agents to aid molecular-based cancer therapy.

Table of contents

List of abbreviations

BAP1	BRCA1 associated protein-1
BSA	Bovine serum albumin
CAM	Chorioallantoic membrane
MEM	Modified eagle's medium
EDTA	Ethylenediaminetetraacetic acid
EIF1AX	Eukaryotic translation initiation factor 1A, X-linked
FCS	Foetal calf serum
GFP	Green fluorescent protein
GTP	Guanosine-5'-triphosphate
HDACi	Histone de-acetylase inhibitors
H&E	Haematoxylin and eosin
HRP	Horseradish peroxidase
IHC	Immunohistochemistry
LOOB	Liverpool Ocular oncology Biobank
M3	Monosomy 3
MLPA	Multiplex ligation-dependant probe amplification
MAPK	Mitogen-activated protein kinases
PAGE	Polyacrylamide gel electrophoresis
PBR	Proton beam therapy
PCR	Polymerase chain reaction
PBS	Phosphate buffered saline
PKC	Protein kinase C
RPE	Retinal pigment epithemlium
RPMI	Roswell high memorial institute
RT	Room temperature
SDS	Sodium dodecyl sulphate
SRB	Sulforhodamine-B
SF3B1	Splicing factor 3B subunit 1
TCA	Trichloroacetic acid
UM	Uveal melanoma

ULA	Ultra low attachment
αMEM	Minimum essential medium, alpha modification

List of publications, poster and oral presentations

- Kalirai H, **Shahidipour H**, Coupland SE, Moss D, Luyten G. Use of the Chick Embryo Model in Uveal Melanoma. Ocul Oncol Pathol 2015; 1: 133-140

- 05. 2014 Poster presentation at the Association for Research in Vision and Ophthalmology (ARVO) annual meeting. Florida, USA.
  Chick embryo model systems to study uveal melanoma metastasis
  Shortlisted for the MIT Outstanding Poster Award

- 11. 2014 Poster presentation at The National Cancer Research Institute (NCRI). Liverpool, UK.
  Development of in vitro and in vivo models to study uveal melanoma

- 12. 2014 Oral presentation at the 2015 Roy Mapstone Research Prize, Department of Eye and Vision Science, University of Liverpool, UK.
  Chick embryo models systems to study uveal melanoma metastasis
  Winner of the Roy Mapstone Research Prize

Chapter 1

General introduction

1.1 Uveal Melanoma

Uveal melanoma (UM) is a rare and highly aggressive malignancy arising from melanocytes located in the uveal tract of the eye. The uveal tract comprises the iris, choroid and ciliary body (Figure 1).

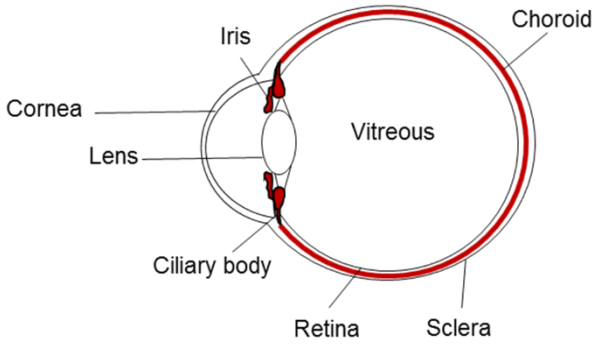

Figure 1.1. The uveal tract consists of the iris, choroid and ciliary body.

1.2 Incidence and risk factors

Although rare, UM is the most common primary intraocular tumour in adults [1]. It accounts for approximately 5% of all melanomas with an incidence of about 6 cases per million individuals per year in Europe [2]. UM is more common in Caucasians, occurring predominately in individuals with blue or grey eyes. Other risk factors include blonde or red hair and cutaneous freckles or nevi [3, 4]. UM incidence increases with age with the majority of cases diagnosed during the fifth decade of life [5]; only 1% of cases occur in younger patients under the age of 18 [6]. Males and females are affected equally [7]. Although there have been reports of familial UM, these are very rare comprising only 0.6% of all UM patients [8].

1.3 Detection, diagnosis and treatment

The majority of UM are detected by optometrists either during routine examinations or when a patient presents with symptoms. The diagnosis of UM is based on clinical appearance of the tumour following ophthalmic examination with the slit lamp and

indirect ophthalmoscope including ultrasonography of the eye [9]. Where possible, treatment of the primary tumour aims to conserve the eye [10]. Eye sparing modalities include brachytherapy, proton beam radiotherapy (PBR), transpupillary thermotherapy, local resection and endoresection. In brachytherapy, a radioactive plaque, usually with Ruthenium 106 or Iodine-125 is used; the former is used more commonly in Europe whilst the latter is applied usually in the US.

Treatment failure, resulting in secondary enucleation, is usually associated with a larger tumour size; however for smaller tumours local recurrences after brachytherapy are reduced to only 3% at 7 years [11]. PBR delivers a focused beam of heavy particle radiation to the region of tumour, enabling the treatment of different sizes and locations of UM tumours [11]. The local recurrence rate in PBR is similar to brachytherapy. Initially there was much interest in transpupillary thermotherapy as it is a minimally invasive procedure where an infrared laser disrupts the metabolic activity of the tumour cells by increasing the temperature for a brief time [12]. However, studies have demonstrated a higher rate of tumour recurrence of small choroidal melanoma after treatment with transpupillary thermotherapy, and thus where possible other methods are used when treating small choroidal melanomas [13]. The tumour can be removed surgically en bloc through a scleral opening i.e. local resection, or in a piecemeal fashion with a vitreous cutter passed through the retina i.e. endoresection. These can be performed in combination with some form of radiotherapy, following surgical resection [7].

If the size or location of the tumour prevents eye sparing therapy, if there are complications with the conservative therapy, or if it is the patient's choice, enucleation, (i.e. removal of the eye globe) is performed with subsequent insertion of a prosthesis [9].

1.4 Prognosis

1.4.1 Clinical and histopathological features

Particular clinical and histopathological features in UM associated with a patients risk to develop metastasis have been identified [14]. Clinical features associated with a poor prognosis include large tumour size, ciliary body involvement and extraocular extension [15]. The histopathological features include the categorisation of UM cell type, the mitotic count, the presence/absence of closed connective tissue loops, as well as inflammatory cell infiltrates (i.e. macrophages and lymphocytes). With respect to cell morphology, UM are either spindle (cells are long and narrow with large nuclei and indistinct cytoplasmic borders), epithelioid (cells are polygonal with large pleomorphic nuclei), or mixed cell type. UM with epithelioid cells are associated with a poorer prognosis [16]. A high mitotic count, the presence of Periodic Acid Schiff positive closed loops and a large number of infiltrating macrophages [17] and lymphocytes [18] are also associated with a poor prognosis and increased risk of death from metastatic disease [15].

1.4.2 Genetic features

1.4.2.1 Chromosomal aberrations

UM is associated with non-random gross chromosomal alterations occurring on chromosomes 1, 3, 6 and 8. Loss of one copy of chromosome 3 (monosomy 3) was first reported in 1996 by Prescher and colleagues to be the strongest predictor of metastatic spread and increased mortality [19]. Monosomy 3 is associated with a reduction in the 5-year survival probability from approximately 100% to less than 50% as a result of metastatic spread predominantly to the liver [15]. Loss of chromosome 1p and chromosome 8 gains (polysomy 8q) are also significantly correlated with reduced survival [20]. Furthermore, analysis of chromosomal data from 602 UMs demonstrated that when occurring in isolation, monosomy 3 and polysomy 8q have

similar impact on survival, however in combination, they reduce the 5-year cumulative survival to 30% [21]. A recent study demonstrated the proto-oncogene *C-MYC*, located on 8q24.21, to be overexpressed in metastasising UM [22]. This is consistent with the overexpression of *C-MYC* in other cancer types thus highlighting its significance as a candidate gene for targeted therapy, discussed in more detail in Chapter 4.

On the other hand, polysomy 6p, which is frequently found in tumours with disomy 3, has been associated with prolonged survival and thus referred to as having a "protective" effect [23]. Although this protective effect may be true in the majority of cases, it has also been observed in a small number of cases with monosomy 3 and additionally found together with polysomy 8q in disomy 3 tumours [24].

1.4.2.2 GNAQ/GNA11

The most common oncogenic driving mutations in UM are activating mutations in the genes *GNAQ* and *GNA11*, the alpha subunits of the heterotrimeric GTP binding proteins. The mutations occur in a mutually exclusive manner and are found in approximately 86% of primary UM [25]. These mutations affect either the glutamine residue at the 209 position (Q209) or the arginine residue at the 183 position (R 183) in exons 4 and 5. Consequently, the genes remain locked in their active GTP bound state which in turn leads to the activation of downstream pathways including protein kinase C (PKC) and mitogen activated protein kinase (MAPK) signalling pathways. As a result, *GNAQ* and *GNA11* have become potential therapeutic targets for the treatment of UM [26], discussed in more detail in Chapter 4. It is important to note that these activating mutations are also seen in uveal melanocytic naevi; believed to be early events in tumour development [27].

1.4.2.3 BAP1

Mutations in the *BRCA1-associated protein 1 (BAP1)* gene, located on 3p21, are associated with a high likelihood of metastasis in UM. Harbour and colleagues identified inactivating somatic mutations in *BAP1* in ~ 85% of metastasising primary UM [28]. *BAP1* is a deubiquitinating enzyme involved in several biological processes, including regulation of cell cycle and cell growth, chromatin dynamics and DNA damage response [29]. Studies have demonstrated an association between the presence of *BAP1* mutations and loss of protein expression. Indeed, a lack of nuclear BAP1 protein expression has been associated with decreased survival time [30, 31]. Knock down of *BAP1* by RNAi has also been found to trigger a loss of cell identity characterised by the emergence of stem-cell like characteristics in UM cells [32]. Germline mutations in *BAP1* have also been reported, although a low frequency, and are associated with a predisposition of individuals with this mutation to a variety of cancers including UM, lung adenocarcinoma and meningioma [33]. *BAP1* plays a key role in UM metastasis, as a result studies have aimed to identify therapeutic agents that reverse the phenotypic effects of *BAP1* loss. This led to the identification of histone de-acetylase inhibitors (HDACi), where UM cells treated with these agents showed reduced growth and a differentiated state *in vitro* and *in vivo* [34].

1.4.2.4 SF3B1

Splicing factor 3B subunit 1 (SF3B1) mutations at arginine-625 were identified in primary UM patient samples by exome sequencing. These mutations are associated with favourable prognostic features such as fewer epithelioid cells, younger age, and inversely associated with poor prognostic features such as monosomy 3 and *BAP1* mutations [35]. However, metastasis may still occur in patients with tumours that harbour *SF3B1* mutations and retain BAP1 expression [36]. *SF3B1* encodes a component of the spliceosome, mutations in this component have been reported to alter gene splicing and in UM are associated with alternative splicing of the 3′ end of

mRNA transcripts [37]. Further investigations are required to understand the functional significance of this alternative splicing and the prognostic significance of *SF3B1* mutations.

1.4.2.5 EIF1AX

The *eukaryotic translation initiation factor 1A, X-linked (EIF1AX)* gene has also been found to be mutated in UM and similar to *SF3B1* mutations is associated with a better prognosis [38]. Martin and colleagues identified the EIF1AX mutation in 3 primary UM that were disomy 3 and lacked *SF3B1* mutation [39].

1.5 UM Metastasis

Despite the advances in the treatment of primary UM, almost 50% of all patients develop metastatic disease [2]. Due to the lack of a lymphatic system in the eye, UM dissemination occurs via the blood stream with the highest tendency of metastasis, up to 90%, in the liver. Less common sites of metastasis include the lungs, bone and skin. The prognosis for liver metastasis is very poor, with a median survival of approximately 8 months [40]. Systemic treatment options, such as intravenous chemotherapy and immunotherapy do not seem to give promising results for survival in patients with UM metastasis [41]. Emerging treatments for metastatic UM has aimed to target molecular drivers in UM including the MEK/MAPK pathway, discussed in more detail in Chapter 4. However, although improvement in progression free survival with MEK inhibitor treatment have been reported, these results need to be taken with caution given the small number of patients in the trial [42]. In selected patients, surgical resection of liver metastases can be beneficial, however this will only prolong survival.

Clinically evident metastasis may occur several years, even decades [43] after treatment of the primary tumour and this has led to speculation about the timing of the haematogenous spread from the eye and also the possibility of tumour dormancy at

distant sites. Since tumour cells can remain dormant, metastasis may occur long before the primary tumour is of a detectable size and as a result patients may already have micrometastatic UM [40]. Clinically evident metastasis at the time of primary tumour diagnosis is infrequent, found in only 1–2% of cases [44].

To better understand metastatic UM, Grossniklaus evaluated the histological sections of livers obtained at autopsy from patients who died of metastatic UM. He categorised these into 3 stages based on size; avascular stage 1 metastases that progress to stage 2, to larger stage 3 tumours that become vascularised as they progress and enlarge [45]. It is still unclear how and when this progression occurs. Furthermore, the majority of UM cells in the liver present with 'miliary' disease (multiple, diffuse, millimetre-sized tumour cells), as a result treatment of UM metastasis has to date proved difficult [9].

1.6 Models of UM

Since little is known about the characteristics of UM cells that metastasise and grow in the liver, it is essential that the metastatic process is better understood. Experimental models of UM that are able to faithfully replicate aspects of tumour development and metastasis are therefore essential to facilitate this. In the past, the majority of *in vitro* models have focused on two-dimensional (2D) cultures using established cell lines, however more recently there has been increasing interest in 3-dimensional (3D) cultures. Traditional 2D environment does not allow for areas of hypoxia, heterogeneous cell populations, varying cell proliferation zones or extracellular matrix influences, and as a result may not accurately mimic the 3D *in vivo* environment in which cancer cells reside. However 3D culture systems exhibit features that are closer to the complex *in vivo* conditions, hence prove a more valuable model with which to study tumour cells and potential chemotherapeutics, discussed in more detail in Chapter 2.

Animal models also play a vital role in providing further insight into the behaviour of the disease in a more representative microenvironment. Many attempts have been made to develop a suitable animal model to study UM, and to induce intraocular melanoma. Generally, these models are divided into spontaneous, transgenic and induced models. Spontaneous tumours and their metastasis occur naturally, and have been reported in certain animals including, mice, rats, cats, dogs, horses, birds and fish [46]. However, their use as a model in UM is limiting since these tumours are very rare, occur randomly and in an unpredictable manner.

Transgenic models in which key genes are knocked out or knocked in to induce tumour growth, offer the opportunity to study the earlier stages of malignancies. The majority of transgenic UM models have been developed in mice where tumours either grow from retinal pigment epithelium (RPE) or are mixed tumours of RPE and UM. An exception to this is the TollTyr-RAS+ Ink4a/Arf-/- transgenic mice, which do not contain RPE cells [47]. Unfortunately metastasis has not been reported in any of these models, and only occur when tumour cells are cultured and then transferred [48]. Recently, Schiffner and colleagues used the Tg (Grm1) transgenic mice, known to spontaneously develop highly pigmented nodular melanomas in hairless skin regions, to demonstrate development of choroidal thickening with a ciliary body tumour [49]. However further studies are required to demonstrate whether these cells have the capacity to metastasise or not.

In induced animal models, tumour development occurs following exposure to chemical agents, radiation, virus or when tumour cells and tissues are xenografted into the animal [50]. These models are easier to use as the experiments can be repeated yielding similar results.

One cell line commonly used for this purpose is the Greene melanoma cell line, a spontaneous cutaneous melanotic melanoma discovered in Syrian golden hamsters, which developed into an amelanotic melanoma after continuous passage [51]. In one

study, the Greene melanoma cell line was implanted subcutaneously to investigate the effect of hyperthermia on developing tumours. The results of this study led to the use of transpupillary thermotherapy in the treatment of UM patients [52-54]. A further cell line, the Bomirski cutaneous melanoma, identified in a male Syrian golden hamster that had developed a black skin tumour [55], has also been used in ocular melanoma research. Small fragments of melanoma tissues were implanted into the anterior chamber of hamsters to investigate radio sensitivity, and tumour vascularisation [56, 57]. Although these cell lines have been reported to metastasise in the hamster model, as summarised in Table 1.1, they are not of ocular origin and therefore not representative of ocular tumours. Furthermore, the small size of the hamster eye limits its practicality as a model.

Table 1.1 Hamster model

Cell line	Inoculation site	Metastasis	Reference
Greene	Subcutis Vein and artery	Liver Lung, liver, kidney, thymus, heart	[51, 58]
Greene	Subcutis	None reported	[52, 53]
Greene	Subcutis	None reported	[54, 59]
Bomirski	Subcutis	Lung, kidney, lymph node	[55]
Bomirski	Anterior Chamber	Lymph node	[56]
Bomirski	Anterior Chamber	Lung, kidney	[57]

Attempts to establish UM cell lines from rats have not been successful and as a result, cell lines from other species have been used in the rat model. Braun and colleagues used the athymic albino WAG/RijHs-rnu rat to implant human UM cells (Table 1.2) either by placing tissue or minced tissue into the choroidal space or by injecting tumour spheroids in the suprachoroidal space [60, 61]. The majority of the animals injected with the spheroids developed intraocular tumours. However no metastasis was reported in any of the investigations hence limiting this model to studying primary intraocular tumours only.

Table 1.2 Rat model

Cell line	Inoculation site	Metastasis	Reference
OCM-1, C918, M619	Suprachoroidal	None reported	[60-63]

Unlike the hamster and the rat, rabbits have larger eyes allowing for much easier access and examination. The different cell lines used in this model include the B16F10 cell line of murine cutaneous origin, the Greene melanoma cell line and the human UM cell lines (Table 1.3). The well-characterised B16F10 cell line has been placed in the subchoroidal space of the rabbit eye in many studies, however not only does this cell line require the injection of cyclosporin A (CsA) which reduces the immunity and life span of the rabbits, it is also of cutaneous origin. The Greene melanoma cell line on the other hand does not require immunosuppression in the rabbit [46] and has been placed into the anterior chamber (AC) or subchoroidal space of the rabbit eye to develop ocular tumours and to investigate treatments [64]. Both the B16F10 and Greene melanoma cell lines have failed to show metastasis to the liver in this model (Table 1.3). Human UM cell lines have been successfully implanted in the rabbit eye and have shown metastatic spread to distant organs (Table 1.3) [44]. Blanco and colleagues injected the human UM 92.1 cell line into the suprachoroidal space of rabbit eyes; all the animals developed metastasis to the lungs and 18% developed micrometastasis to the liver [65].

Table 1.3 Rabbit model

Cell line	Inoculation site	Metastasis	Reference
B16F10	Subchoroidal	None reported	[66-68]
B16F10, OCM1	Subchoroidal	None reported	[69]
OCM1	Suprachoroidal	None reported	[70]
MKT-BR	Suprachoroidal	Lung	[71]
IPC227	Anterior chamber	None reported	[72]
MKT-BR, OCM1, 92.1, SP6.5	Suprachoroidal	Lung	[73]
92.1	Suprachoroidal	Lung, liver	[65]
92.1	Suprachoroidal	Lung, liver	[74, 75]
92.1	Suprachoroidal	None reported	[76]
92,1	Suprachoroidal	None reported	[77]
Greene	Subchoroidal	Kidney	[78]
Greene	Suprachoroidal	None reported	[64]
Greene	Anterior chamber	None reported	[79]
Greene	Anterior chamber	None reported	[80]

Due to the similarity of the mouse genome to human genome, mice are widely used in cancer research [50]. The B16F10 and the Queens melanoma cell line, a subculture of the B16F10 cell line, have both been successfully transplanted in the AC of the mouse eye as summarised in Table 1.4, resulting in tumour development. Metastatic spread in the liver, however, was not observed in any of the studies. A derivative cell line of B16 cell line, B16LS9 cell line, has been shown to metastasise to the liver when injected in the posterior chamber (PC) [81]. Dithmar and colleagues demonstrated that transcorneal inoculation of these cells into the murine PC leads to haematogenous metastases to the lung and liver [46]. This model has further been used in several studies to investigate tumour angiogenesis and tumour biology, summarised in Table 1.4.

Table 1.4 Mouse model

Cell line	Inoculation site	Metastasis	Reference
B16F10	Anterior chamber	Lung	[82]
B16F10	Anterior chamber	None reported	[83]
B16F10, Queens	Anterior chamber	None reported	[84]
B16F10, Queens	Posterior chamber	Lung	
B16F10	Anterior chamber	None reported	[85]
B16F10	Anterior chamber	None reported	[86]
B16LS9	Posterior chamber	Lung, liver	[87]
B16LS9	Posterior chamber	Lung, liver, lymph node	[46]
B16LS9	Posterior chamber	Liver	[88]
B16LS9	Posterior chamber	None reported	[89]
B16LS9	Posterior chamber, spleen	Liver	[90]
B16LS9	Posterior chamber, spleen	Liver	[91]
OCM1, OCM3, OCM8, EOM3, 92.1, OM431, MEL202	Anterior chamber	Liver	[92-94]
C918, MUM2B	Subcutis	None reported	[95]
OCM1, MUM2B	Subcutis	None reported	[96]
OMM1.3	Retro-orbital	Lung, liver	[97]

Human xenografts with human cell lines and human tumour fragments are now more widely used in research to investigate metastasis and treatment strategies. Orthotopic and ectopic xenografts have been established where human UM cell lines are placed subcutaneously in the flanks of athymic mice [95, 96]. Similarly, Heegaard and colleagues implanted UM specimens subcutaneously into the flanks of nude mice, in order to establish a serially transplantable tumour model, however the take rate of the transplantable tumour was very low (13%) [98]. Furthermore, metastasis was not reported in any of these studies (Table 1.4). However, Surriga and colleagues transplanted EGFP labelled UM cells by retro-orbital injections and reported metastasis to lung and liver of the mice 6-7 week after injection [97]. Other studies have placed xenografts derived from primary human UM or from UM metastasis in the interscapular fat pad of immunodeficient mice; these tumours show the original human gene expression profiles and mutations, and have allowed for the evaluation of drug candidates and for predicting therapeutic efficacy by screening molecular markers [99, 100]. Nemati and colleagues established a panel of

primary human UM xenografts obtained from patient tumour samples transplanted into severe combined immunodefficient (SCID) mice [101]. These patient derived xenografts (PDX) showed complete concordance with the patient material with regard to the *GNA11*, *GNAQ*, *BAP1* and *SF3B1* mutations. Recently, Amirouchene-Angelozzi and colleagues established a panel of 7 UM cell lines from either patient's tumours or PDXs. All the cell lines displayed *GNAQ* or *GNA11* mutations, with four of these displaying BAP1 deficiency [102]. However, the relative tumour take in these models is rather low and liver metastasis have not been reported. In many studies, although tumour growth is reported, tumour metastasis has proved more difficult to achieve. As a result some of these models can only be used to study the primary tumour. However, each model has its own relevance; PDX models are used to generate tumours that are representative of the tumour of origin and not always employed as a spontaneous metastasis model. On the other hand, orthotopic models have been used to study both the tumour in its natural environment and to examine the possibility of spontaneous metastasis. Therefore, collectively each model can address the different questions surrounding tumour biology and tumour metastasis.

Until recently the current available cell lines did not completely reflect the genetic alterations found in UM, for example, many of the models use cell lines derived from cutaneous melanoma that are biologically and genetically different to UM (i.e. they harbour *BRAF* mutations) [103]. Furthermore, models have failed to recapitulate the metastatic processes that occur in UM, as many do not show any metastasis to key organs such as the liver. It is unclear why so few tumours give rise to xenografts and why many fail to induce liver metastasis. In an effort to use well established representative UM cell lines in a cost effective model and to investigate the effect of inhibitors, van der Ent and colleagues used the zebra fish and injected fluorescently labelled UM cell lines into the yolk sac of the embryos

[104]. However, as a model, zebrafish lack some of the mammalian organs, such as lung and mammary gland. In order to be able to study the mechanism of UM metastasis and assess drug therapeutics, we still require suitable animal models which are cost effective, do not require immunosuppression, easily accessible / visualised, and efficient in terms of achieving results in a short period of time. One such model, the chick embryo model has previously been used in a small number of studies in UM, however as discussed in more detail in Chapter 3 these have failed to either use representative cell lines or to demonstrate liver metastasis.

UM is a complex and diverse disease, this thesis has set out to investigate and provide baseline platforms, from 3D *in vitro* environments to *in vivo* setting of an animal model with which to better understand UM and the mechanisms involved in the metastasis, and finally to establish therapeutic targets for the treatment of this disease.

Chapter 2

Formation and characterisation of UM spheroids in a 3D *in vitro* model

2.1 Introduction

The introduction of mammalian cells in *in vitro* culturing systems has led to many advances in cell biology and the understanding of formation and function of tissues, as well as disease states such as cancer. The majority of these discoveries have been through the traditional two-dimensional (2D) culture techniques. However, 2D culture systems can inadequately reflect the biological features of original tumours and their environments; for example, in 2D culture cell-to-plastic interactions prevail rather than the crucial cell-to-cell and cell-to-extracellular matrix (ECM) interactions, which are the basis of normal cell function. Thus, alternative culture systems of cancer cells that realistically reflect the characteristics of parental tumours have been established to study cancer biology. Three-dimensional (3D) culture systems have become a popular method to recapitulate the *in vivo*-like growth and differentiation of tissues as compared to 2D-models. The most widely used 3D model system at present is the 3D tumour spheroid assay, which preserves the characteristics of the original tumour and has further shown correlation with the *in vivo* situation when testing the effects of anticancer agents [105]. Spheroids have been produced from either a single cell type or as complex multicellular spheroids, reflecting the *in vivo* cells found in the tumour of interest. Multicellular tumour spheroids resemble avascular tumour nodules or micrometastases with respect to growth kinetics and some histomorphological features [106]. With increasing size of either the mono- or multi-cellular spheroids, proliferation and oxygen/nutrient gradients are observed, features that affect not only cellular RNA and protein expression but also the penetration and bioactivity of drugs [106].

As highlighted in Chapter 1, there are currently no effective treatment options once UM has disseminated. Our knowledge about the processes involved in UM metastasis is limited, and there are currently no well-characterised *in vitro* models with which to investigate these processes or perform preclinical drug testing. As a result,

developing a 3D model system that can be used to explore the biology of UM and assess therapeutic drugs preclinically, can pave the way in discovering better treatment options for metastatic UM.

Sutherland and colleagues were the first to describe the use of 3D spheroids in cancer research [107]. By utilising the spinner culture method, they cultured Chinese hamster lung cells as spheroids and described an outer zone containing many proliferating cells, an intermediate zone that is poorly nourished and oxygenated and contains few cells in mitosis, and a central zone of necrosis. They further dissociated the spheroids and used the single cells for colony formation and highlighted the use of this model for assessment of the effects of nutrition and oxygenation on growth and for determination of the cell growth fraction after treatment with drugs or radiation [107]. The spinner culture method creates mass spheroid culture by preventing cells in suspension from settling and by stimulating cell-to-cell collision via constant stirring. Using this method, culture conditions, such as changes in medium and addition of growth factors or drugs, can be easily carried out [108]. Firth and colleagues showed fundamental differences between the cells cultured in monolayer and in spinner flasks; they reported altered immunophenotypes, including loss of human leukocyte antigen (HLA) class I molecules, and enhanced osteogenic and adipogenic differentiation in mesenchymal stem cells (MSCs) cultured using the 3D techniques when compared with 2D monolayers [109]. Following Sutherlands work, several other methods have been developed to generate tumour spheroids including; micro-moulded non adhesive hydrogels, scaffolds, liquid overlay, and hanging drops.

Micro-moulded non-adhesive hydrogels have been used to form spheroids with different shapes. Micro-moulds are created using computer-aided design software from which non-adhesive hydrogels are cast. Cells settle and form spheroids at the bottom of each recess created. In a single mould, a large number of spheroids with homogenous size, shape and cellular compositions can be created. Desroches and

colleagues used this technique with 822 moulds creating cardiac myocyte (CM) and cardiac fibroblast (CF) spheroids. Neonatal rat ventricular CMs and CFs, alone or in combination, self-assembled into viable spherical-shaped microtissues. Furthermore, when seeded simultaneously or sequentially, CMs and CFs self-sorted were interspersed, creating cellular structures reminiscent of their *in vivo* myocardial distribution [110].

The liquid overlay method prevents cells from adhering to the culture plates and therefore encourages cell-cell aggregation. Tissue culture flasks or dishes are coated with agarose or poly-2-hydroxyethyl methacrylate (polyHema) and allowed to dry [111]. In an early study, liver cells isolated from new-born rats cultured in polyHema coated Petri dishes were found to spontaneously form aggregates and within a few days form spheroids. Furthermore, after further analysis by immunohistochemistry (IHC), cell types such as hepatocytes that regrouped in small islands often defining a central lumen, and cells that reorganised into bile duct-like structures were reported [112]. This method is simple, widely-utilised to date, and is also cost effective.

In the hanging drop method, small volumes of cell suspensions are placed on the inside of a Petri dish lid and inverted. This method relies on gravitational force as the droplets stay attached to the lid via surface tension and cells settle at the bottom of the drop, resulting in the formation of a single spheroid. Kelm and colleagues used this method to generate tumour spheroids from hepatoma and adenocarcinoma cell lines, which revealed highly organised, three-dimensional, tissue-like structures with an extensive extracellular matrix [113]. Spheroid size in this technique can be controlled by altering the cell density in the drop, and high throughput methods have been developed producing up to 384 spheroids in a single assay [114].

More recently, however, studies have used the ultra-low attachment (ULA) 96-well round bottom plates that, in comparison to the other standard methods, do not require pre-coating to prevent cell adhesion. In addition, the well shape promotes the

formation of single, centrally located spheroids of reproducible size [106]. Vinci and colleagues used this method to test 40 cell lines and classified each according to their morphology; tight spheroid, compact aggregate and loose aggregate. They further evaluated the sensitivity of the tumour spheroids in 2D and 3D cultures to three specific molecularly-targeted agents. Tumour cells were found to be generally less sensitive to compounds in 3D culture than in 2D culture, highlighting the importance of accurately evaluating drug responses under appropriate conditions *in vitro* in order to avoid overestimating or underestimating the effect of compounds prior to *in vivo* studies [106]. This high throughput and reproducible method of tumour spheroid formation allows for simple and time efficient analysis from imaging, comparing, treating, characterising and collecting the 3D tumour spheroids to further enhance our understanding of *in vivo* processes.

The focus of this chapter was to assess the ability of UM cell lines and primary UM cells to form tumour spheroids and to reproduce aspects of the *in vivo* tumour and its microenvironment.

2.2 Materials and Methods

2.2.1 Cell culture

For routine cell line culture, UM cell lines (Table 2.1) were maintained in UM medium A; RPMI (PAA Laboratories, Somerset, UK) supplemented with 10% fetal calf serum (FCS; PAA Laboratories), 2 mM l-glutamine (Sigma, Dorset, UK), and antibiotics (penicillin 50 IU/ml, streptomycin 500 µg/ml) [115]. They were incubated under standard conditions (37°C, 5% CO_2, 95% humidity). For all studies, UM cell lines (~70% confluent) were harvested with 0.05% trypsin/EDTA (Life Technologies, Paisley, UK) and re-suspended in appropriate medium at varying cell density as indicated below. The primary human UM cell line MEL270 and the cell lines OMM2.5 and OMM2.3 derived from a liver metastasis of the same patient [116], the primary UM cell line 92.1 [80] and the subcutaneous metastasis cell line OMM1 were all kindly provided by Martine Jager (Leiden University, Leiden, The Netherlands). The patient-derived tumour xenograft (PDX) cell line, MM66, established from a liver metastasis [102], was kindly provided by Sergio Roman-Roman (Institut Curie, Paris) (Table 2.1).

Following approvals from the local and national ethics committees (NRES reference: 15/SS/0097), fresh UM specimens were acquired via the Liverpool Ocular Oncology Biobank (LOOB) from patients undergoing enucleation or local resection. For primary cell culture, a small sample of fresh UM tissue from an enucleation or local resection was finely minced with a sterile scalpel blade. It was then digested with 5 ml of type I collagenase (Sigma) at 37°C for approximately 40 minutes. To assess the presence of single cells, 10 µl of the suspension was placed onto the haemocytometer and observed under a microscope. The debris was then allowed to settle and the supernatant containing the single cells transferred to a new tube and centrifuged at 1800 rpm for 2 minutes. The cell pellet was resuspended in primary cell culture medium, UM medium B; α-MEM (Sigma), AmnioSelect (Metachem Diagnostics LTD), FCS (Labtech), 2 mM l-glutamine (Sigma, Dorset, UK) and antibiotics

(penicillin 50 IU/ml, streptomycin 500 µg/ml). A minimum of 1 million cells were plated in T75 flasks and placed in an incubator until cells reached ~80% confluence. Primary cells were pre-cultured to ensure sufficient number of cell for the assays to be carried out, as not all primary samples successfully survive in culture.

Table 2.1 UM cell lines characteristics

	Cell line				
	92.1	**MEL270**	**OMM2.3**	**OMM2.5**	**OMM1**
Origin	Primary	Primary	Liver metastasis	Liver metastasis	Subcutaneous metastasis
BAP1	wt	wt	wt	wt	wt
GNAQ/GNA11	GNAQ Q209	GNAQ Q209	GNAQ Q209	GNAQ Q209	GNA11 Q209
Chromosome 3	Partial deletions	wt	wt	wt	wt
Chromosome 8	G	N	N	N	G

Wt = wild type, G = gain, N = normal

2.2.2 Cell suspension assay

PolyHema solution was prepared at 12 mg/ml in 95% ethanol, the solution was stirred overnight at 37 °C. 6 cm Petri dishes were coated with 300 µl of polyHema solution and allowed to dry overnight. The UM cell lines 92.1, MEL270, OMM2.3 and OMM1 were plated at 30,000 cells in the polyHema coated Petri dishes in 6 ml of UM medium A. Following 10 days of incubation, images were taken on an inverted light microscope.

2.2.3 Hanging drop assay

The UM cell lines 92.1, OMM2.3, OMM2.5 and OMM1 were harvested as described in 2.2.1 and plated as individual droplets of 7,500 cells on an inverted 6 cm Petri dish lid with a pipette. The Petri dish lid was then carefully inverted on to the dish containing PBS to prevent the cell suspension droplets drying. Images of the individual droplets were taken on an inverted microscope at 4x magnification, after 2 and 4 days of incubation respectively.

2.2.4 ULA 96-well plate spheroid assay

UM cell lines 92.1, OMM2.3 and OMM2.5 and primary cells, were harvested as described in 2.2.1, 100 µl/well of cell suspensions were dispensed into the ULA 96-well-round-bottom plates (Appleton Woods LTD, Birmingham, UK) using a multichannel pipette. The cells were plated at varying cell densities indicated below to assess their ability to form tumour spheroids. They were imaged after 7 days of incubation using an inverted microscope, at 4x magnification. Further spheroid assays with primary cell lines were carried out similarly with cells plated at densities indicated and imaged on the Axio ObserverZ1 Zeiss Microscope. Spheroid measurements were taken by measuring the diameter of each tumour spheroid horizontally and vertically since not all spheroids were completely spherical in shape (Figure 2.1).

At days 3, 6 and 9 of incubation, measurements and images of each spheroid was taken, and two spheroids from each cell density were removed and fixed in 10% neutral buffered formalin overnight, and were then placed in molten agar to set. The formalin-fixed spheroids were then placed in tissue cassettes before being loaded onto the BAYER VIP E300 tissue processor. The spheroids underwent dehydration in a series of alcohol and xylene incubations before being finally maintained in hot wax ready for embedding. Spheroids were then embedded in paraffin by carefully orienting them in the wax to set in the centre of the block.

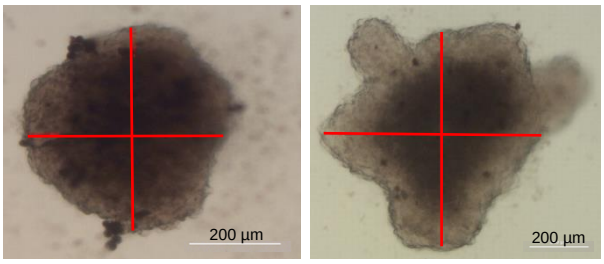

Figure 2.1. Representative images of UM tumour spheroids showing measurements of the diameter in the different shapes.

2.2.5 Histological assessment and immunohistochemistry (IHC)

Sections (4µm) were cut from paraffin-wax-embedded spheroid samples, and floated onto X-tra® adhesive slides (Leica, Milton Keynes, UK), which have a positive charged surface to help bond tissue sections onto the glass. For histological analysis, sections were stained with Haematoxylin and Eosin (H&E): slides were first deparaffinised in xylene, and rehydrated to water through a series of decreasing ethanol concentrations. Following immersion in haematoxylin, the slides were incubated in tap water to allow the stain to develop; and then acid alcohol to destain. They were then stained with eosin and dehydrated through ethanol before coverslipping with using DPX mountant (Sigma, Dorset, UK).

IHC assays were undertaken using the FLEX Envision kit (DAKO) as follows. Applying a PT Link (DAKO, Ely, UK) pre-treatment module, high-pH (Tris/EDTA buffer, pH 9.0) antigen retrieval was performed at 96°C for 20 minutes. The slides were then washed in FLEX wash buffer (Tris-buffered saline solution containing Tween 20, pH 7.6) prior to loading onto the automated DAKO autostainer system. Using the FLEX Envision system (DAKO) according to the manufacturer's instructions, IHC was performed as follows; (1) blocking of endogenous peroxidase (phosphate buffer containing hydrogen peroxide, 15 mmol/L NaN3 and detergent) for 5 minutes at room temperature (RT); (2) incubation with primary antibodies or isotype controls as appropriate (Table 2.2) for 30 minutes at RT; (3) incubation with mouse linker for 15 minutes at RT; and, (4) incubation with horseradish peroxidase for 20 minutes at RT. Positive staining was visualised with 3-amino-9-ethylcarbazole (AEC, Vector Laboratories Ltd., Peterborough, UK, 30min) or 3,3'-Diaminobenzidine (DAB, DAKO, Ely, UK, 10min). Slides were washed between each incubation with 1× FLEX wash buffer.

Counterstaining was performed with Mayer's haematoxylin (VWR, Leicestershire, UK) and slides were mounted with either Aquatex aqueous mounting medium (Merck Millipore, Nottingham, UK) for slides using the AEC detection system or dehydrated through a series of alcohol and xylene before mounting with DPX mountant (Sigma, Dorset, UK) for slides using the DAB detection system. Tissues known to express the proteins were included in each run as positive controls; negative controls included omission of the primary antibody or use of isotype specific controls where appropriate (Table 2.2).

Table 2.2. Details of antibodies used

Antibody	Species	Isotype	Dilution / Concentration	Supplier	Positive human control tissue
MelanA	Mouse	IgG_1k Mouse monoclonal	1:100 0.96 µg/ml	Dako	Eye containing UM
Ki67	Mouse	IgG_1k Mouse monoclonal	1:200 0.4 µg/ml	Leica	Tonsil
αSMA	Mouse	IgG_1k Mouse monoclonal	1:600 0.1 µg/ml	Dako	Colon
BAP1	Mouse	IgG_1k Mouse monoclonal	1:200 1 µg/ml	Santa Cruz	Pancreas
CD68	Mouse	IgG_1k Mouse monoclonal	1:200 0.15 µg/ml	DAKO	Tonsil

2.2.6 Clinical, histopathological and genetic information

Clinical and histopathological information from the primary UM used in 3D spheroid assays were provided in an anonymous format by the LOOB (Table 2.3).

DNA extracted from the 3D spheroids was analysed for copy number variation of chromosomes 1p, 3, 6, and 8 by applying MLPA as described [117]. This was performed as part of the Ocular Oncology Molecular Pathology Service by Miss Sophie Thornton (University of Liverpool, UK).

Table 2.3 Clinical, histopathological and genetic information from primary UM tumours

		Patient tumour										
		S084-15	**S093-15**	**S104-15**	**S119-15**	**S121-15**	**S125-15**	**S143-15**	**S114-15**	**S145-15**	**S006-15**	**S082-15**
Clinical information	**Tumour location**	Ciliochoroidal	Ciliochoroidal	Choroidal	Choroidal	Choroidal	Ciliochoroidal	Choroidal	Choroidal	Choroidal	Choroidal	Choroidal
	Previous treatment	No	No	No	No	No	No	No	No	No	No	No
Histopathological information	**Specimen type**	E	E	ED	E	E	E	LR	E	E	E	E
	Cell type	Epithelioid	Spindle	Mixed	Mixed	Mixed	Mixed	Epithelioid	Mixed	Epithelioid	Spindle	Mixed
	Presence/absence of vascular loops	Yes	No	NA	Yes	Yes	Yes	ND	Yes	Yes	Yes	Yes
	Mitotic count/40HPF	4	4	NA	3	2	6	2	8	14	3	38
	Presence/absence of necrosis	No	No	NA	No	No	No	No	Yes	No	No	Yes
	Macrophages	Scattered	Scattered	ND	ND	Mild infiltration	Heavy infiltration	Numerous	Scattered	ND	Scattered	ND
	nBAP1 protein expression	-ve	+ve	ND	+ve	+ve	-ve	+ve	ND	-ve	+ve	-ve
Genetic information	**Chr3**	L	N	N	N	L	L	N	N	L	N	L
	Chr6p	G	G	N	G	G	G	G	G	N	G	N
	Chr8q	N	G	N	N	N	G	N	G	G	G	G

E = Enucleation, ED = Endoresection, LR = Local resection, ND = Not detailed, NA = Not applicable L = Loss, N = Normal, G = Gain

2.3 Results

2.3.1 Cell suspension assay

To assess the ability of the UM cell lines to spontaneously from tumour spheroids in culture, they were plated in polyHema coated Petri dishes which renders the plates non-adhesive. By preventing cell adhesion, the cells are encouraged to migrate towards each other. Using this method, the UM cell lines formed loose aggregates of varying sizes (Figure 2.2). Collecting the aggregates in this assay proved difficult as they would simply disintegrate once any attempt at manipulation e.g. pipetting was made.

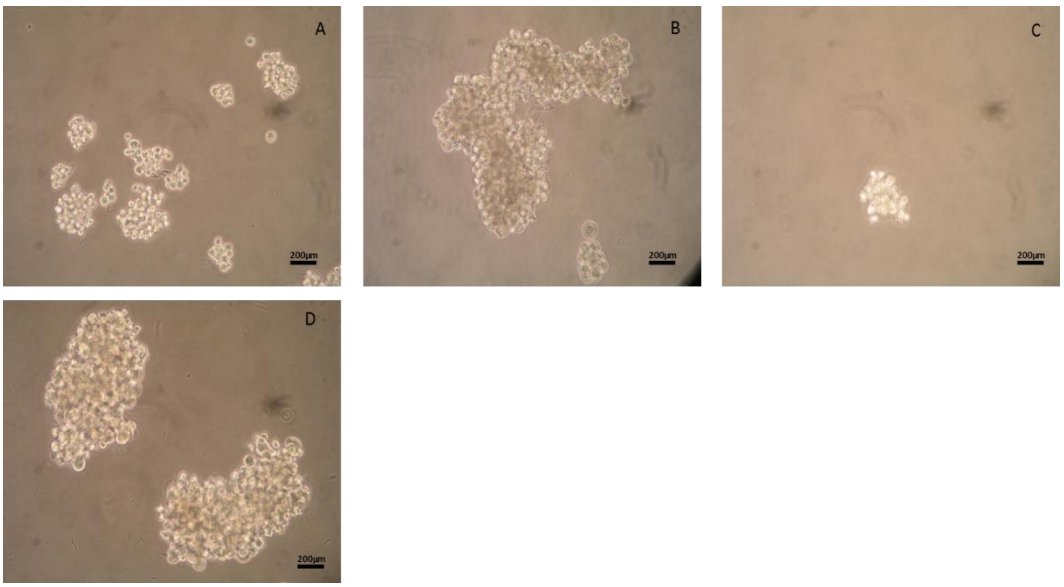

Figure 2.2. Representative images (200 µm) of UM cell lines grown in suspension. Cell lines were plated at 30,000 cells in polyHema coated Petri dishes, in 6 mls UM medium A (as described in materials and methods). Images were taken after 10 days incubation. **A.** MEL270 cell line formed small dispersed aggregates. **B.** 92.1 cell line formed loose aggregates containing some pigmented cells. **C.** OMM2.3 cell line formed small and few, dispersed loose aggregates. **D.** OMM1 cell line formed large loose aggregates.

2.3.2 Hanging drop assay

In the hanging drop method, UM cell suspensions were plated on a Petri dish lid as single droplets. Due to gravitational force, the droplets “hang” from the Petri lid once inverted and cells assemble together at the base of the droplet (Figure 2.3 A). In this assay, after 4 days of incubation, the 92.1, OMM2.3 and OMM1 UM cells formed tumour spheroids of varying size and compactness, 92.1 and OMM2.5 UM cells formed more compact spheroids, OMM1 UM cells formed loose spheroids and OMM2.3 UM cells formed loose aggregates (Figure 2.3 B). This assay required great care and diligence, during the whole process of depositing the droplets to inverting the Petri dish lid, and any subsequent manipulation e.g. imaging, feeding and collecting the droplets. The majority of the spheroids would disintegrate following any manipulation to collect them; in particular, those that had formed less compact spheroids, e.g. OMM2.3 cells.

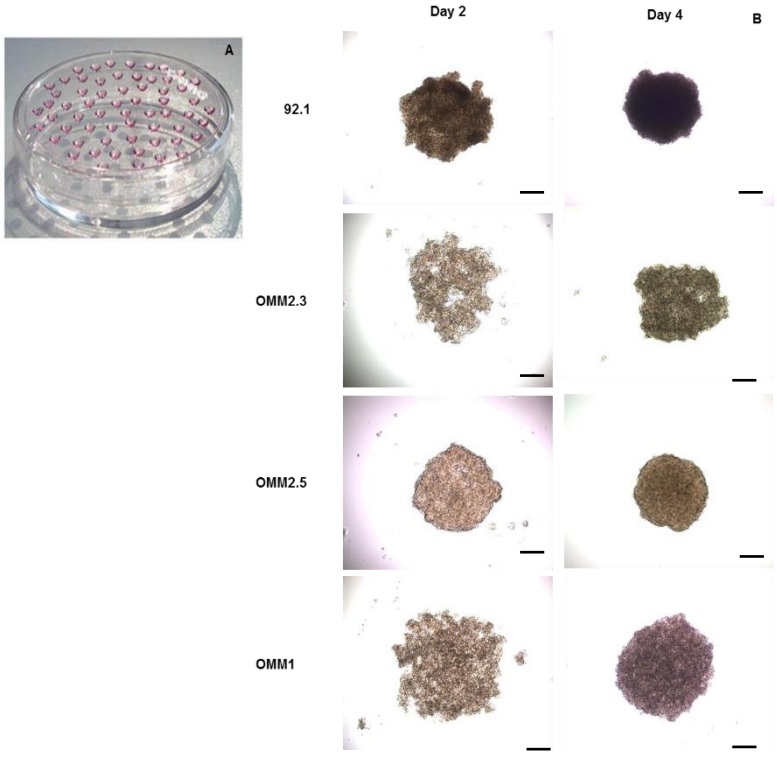

Figure 2.3. Representative images (scale bar 200 µm) of UM cells in hanging drop assay. **A.** Cells were plated as individual droplets of 7500 cells in 20µl’s UM medium A onto Petri dish lid, then inverted. PBS was added to Petri dish to prevent droplets of cells from drying. **B.** Cell lines forming tumour spheroids of varying size and compactness. Images were taken after 2 and 4 days of incubation, on an inverted microscope at 4x magnification.

2.3.3 ULA 96-well plate spheroid assay

ULA 96-well round bottom plates were used to assess the ability of the UM cell lines and primary UM cells to form tumour spheroids. UM cells OMM2.3 formed loose aggregates (Figure 2.4 B and 2.5 A), which were again difficult to manipulate further, since once they were removed from the wells they did not maintain their structure (Figure 2.4 C). The UM cell lines OMM2.5 and 92.1 formed more compact spheroids (Figure 2.4. B and 2.5 B) however they also failed to maintain their compact structure when removed from the wells. In contrast, the primary UM cells S104-15, formed compact spheroids in culture and further maintained their 3D spheroid structure when removed from the wells for fixation and assessed by IHC (Figure 2.4 C).

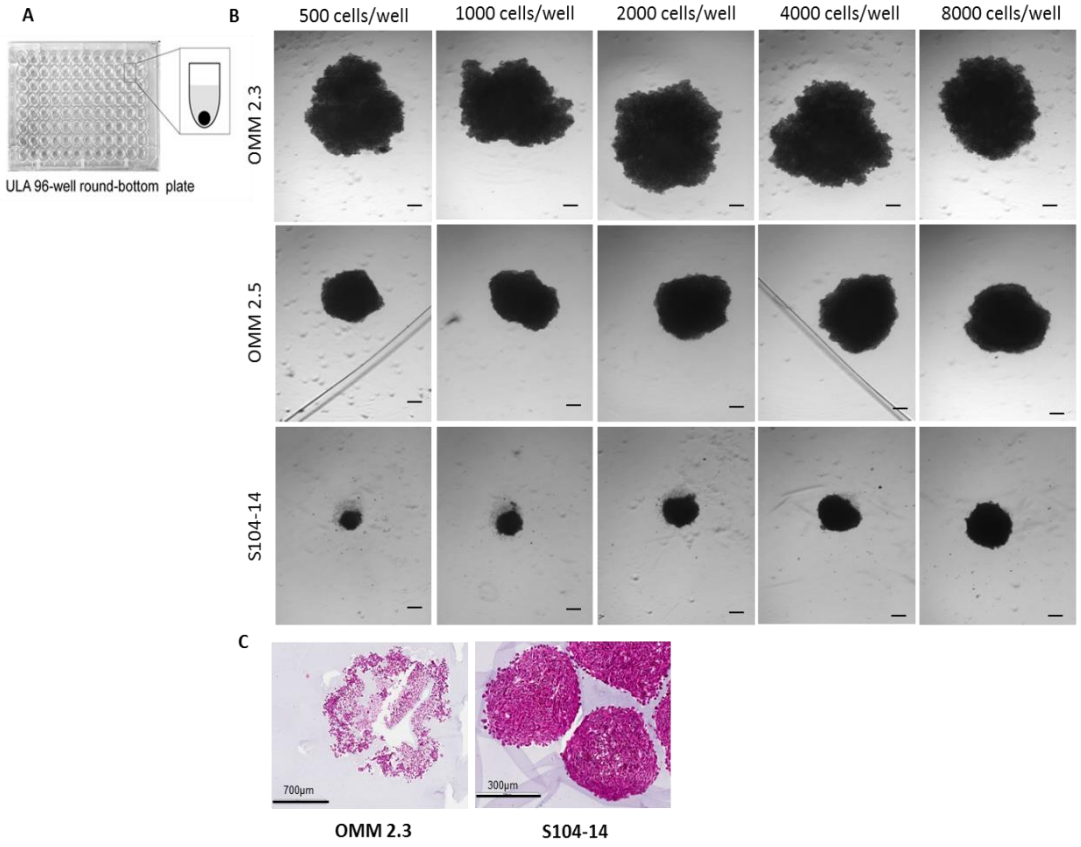

Figure 2.4. Representative images of UM and primary cells in ULA 96 well plate. Cells were plated at increasing densities indicated in ULA 96 well round bottom plates to generate spheroids. **A.** ULA 96 well plate showing schematic representation of spheroid formation at the base of individual wells. **B.** OMM2.3 and OMM2.5 cell lines in UM medium A, and S104 primary cell line in primary cell culture medium plated as spheroids. Images taken at day 7 using an inverted microscope, at 4x magnification (200µm). **C.** H&E image of OMM2.3 cells showing viable UM cells towards the edge of the spheroid and S104-14 spheroids of plump spindle cells at day 7.

Based on UM cell line evidence and the initial success with the primary tumour in the ULA plate, further assays were performed with this method. Eleven primary UM tumour specimens were cultured. The clinical, histopathological and genetic information of each patient specimen was recorded (Table 2.4). Of the eleven primary UM specimens, six were disomy 3 and five demonstrated chromosome 3 loss. Normal chromosome 3 status or a loss of chromosome 3 was irrespective of the cell type (Table 2.4). Only one case (S114-15), which was a enucleation with mixed cell type and normal chromosome 3 status, failed to grow in culture. The remaining ten successfully grew in 2D culture and were further utilised for 3D spheroid culture. These cases were enucleations with one endoresection (S104-15) and one local resection (S143-15). Six of these UM were of mixed cell type, three were epithelioid, and the remaining two were spindle. Six of the ten cases formed tumour spheroids in the 3D culture assay (Figure 2.5 A - F). Although the other four cases were successfully cultured in 2D, they formed aggregates or a flat sheet of cells when plated for 3D culture and failed to form spheroids, it was unclear why these six UM failed to grow as tumour spheroids.

At the earlier time point of 3 days and at the lower plating cell density, in the majority of cases UM primary cells formed loose aggregates or loose spheroids. In particular, the UM case S119-15 demonstrated rather dispersed cells until day 9 (Figure 2.5 F). However, at 6 and 9 days of culture and at the higher plating densities, the primary UM cells begin to form more compact structures (Figure 2.5 A - F).

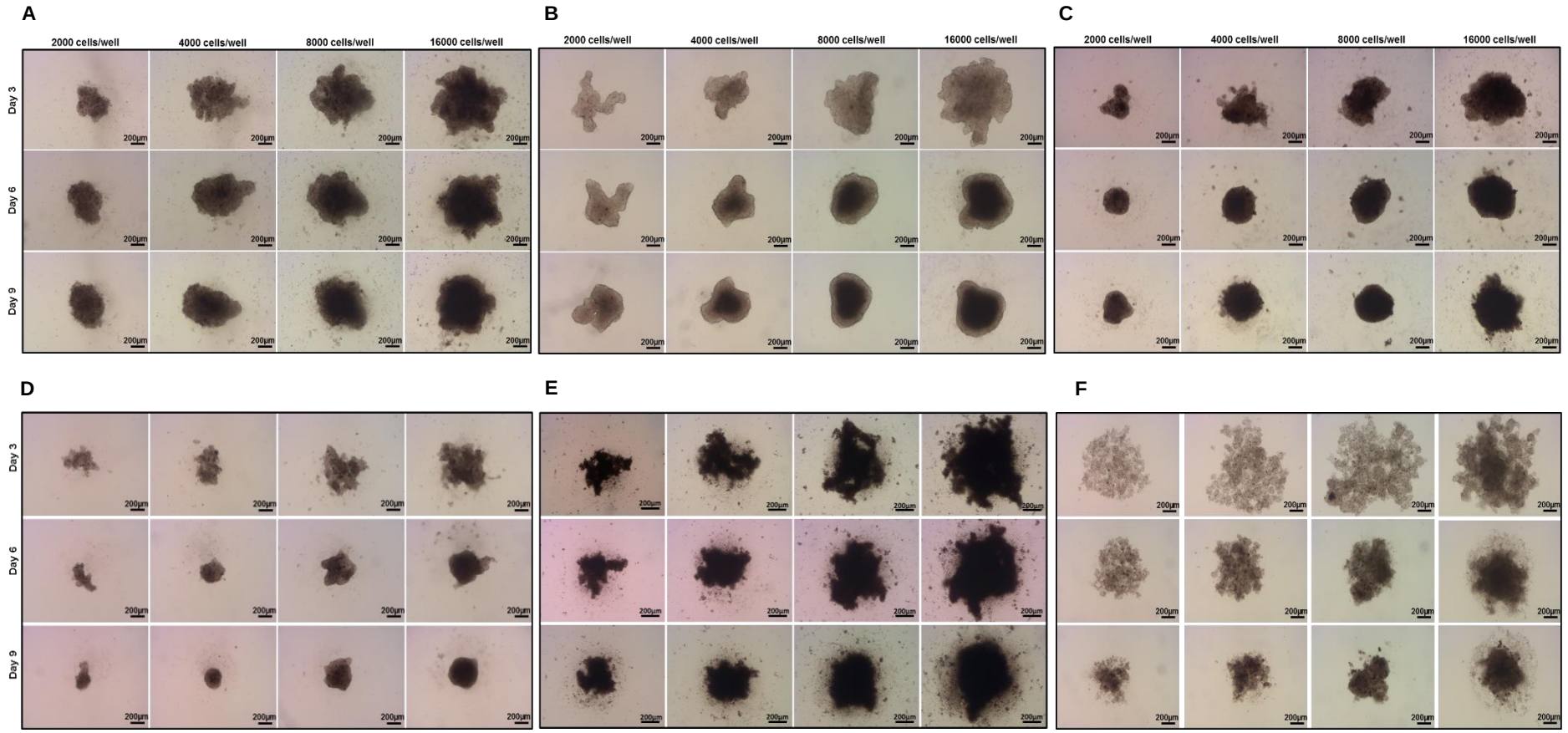

Figure 2.5. Primary UM cells in ULA 96 well plates. **A.** S084-15, **B.** S093-15, **C.** S104-15, **D.** S121-15, **E.** S125-15, **F.** S119-15 were digested and cultured in a tissue culture flask in culture medium B. Following growth of primary human cells to 80% confluence cells were harvested and plated in ULA 96 well plates at the indicated cell densities in 100 µl of primary cell culture medium. Spheroids were imaged and measured at days 3, 6 and 9 using the Axio ObserverZ1 Zeiss Microscope.

The IHC analysis of each primary UM specimen allowed for the establishment of an immunophenotype for each case. For example, the specimen S093-15 can readily be analysed and studied by comparing the tumour cells in the cross-section of the enucleated eye with those in the 2D and 3D cultures. Furthermore, comparisons can be made of nuclear BAP1 and MelanA expression (a classic marker of the melanocytic lineage, Ki67 growth fraction, and macrophages. The S093-15 melanocytes seen in the sections of the enucleated eye were predominantly spindle in shape; however, a mixed cell type was observed when isolated cells were cultured in 2D. Interestingly, when grown in 3D culture, these UM cells were more spindle in shape (Figure 2.6 and table 2.4 A). This was also observed with the case S125-15, where the tumour cells were of mixed cell types within the original tumour sections, had a spindle cell morphology in 2D culture, and were of mixed cell type when grown in 3D culture (Table 2.4 D).

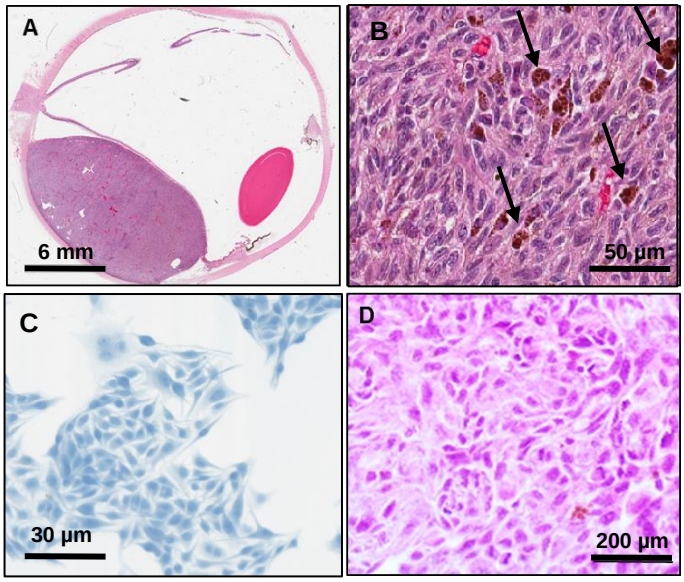

Figure 2.6. S093-15 tumour cell types. **A.** H&E Cross section of enucleated patient eye. **B.** Higher power of spindle tumour cells within patient eye (macrophages highlighted with arrows). **C.** Mixed cell type of tumour cells cultured in 2D. **D.** Spindle cell type of tumour cells in cultured in 3D.

In addition to similarities in UM cell type observed between the primary tumour and the 3D spheroid, the presence of macrophages was also retained. For example in case S093-15, macrophages are seen throughout the original tumour (Figure 2.6 B arrows) and are also present in the 3D spheroids (Figure 2.7 A). These macrophages were also present in both primary tumour and tumour spheroids in S084-15, S121-15 and S125-15 cases as indicated by CD68PG staining (Figure 2.7 A – D). In the case of S104-15, analysis of the original tumour for the presence of macrophages was not possible as the tissue was very fragmented since it had been obtained via an endoresection procedure. Despite this, these UM cells successfully grew as 3D spheroids and IHC analysis clearly showed the presence of macrophages (Figure 2.7 E). Although macrophages were not reported for S119-15 case (Table 2.3), they were observed in the 3D tumour spheroids (Figure 2.7 F).

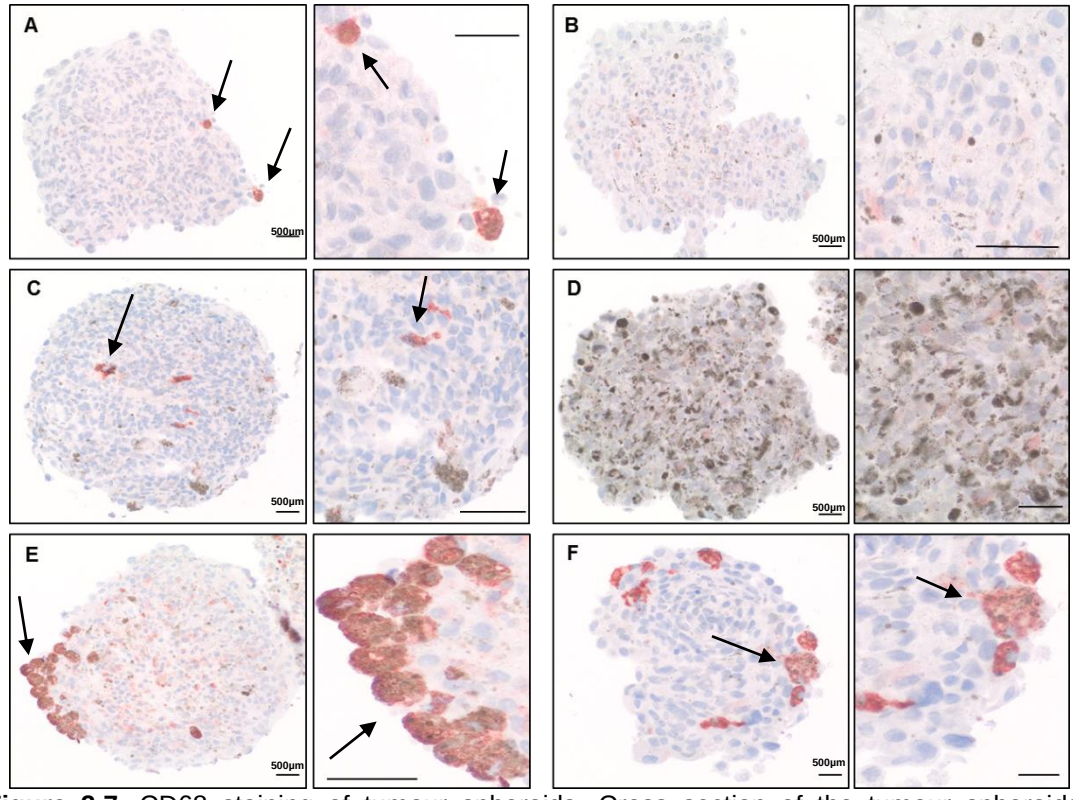

Figure 2.7. CD68 staining of tumour spheroids. Cross section of the tumour spheroids showing distinct macrophages (arrows) in **A.** S093-15, **B.** S084-15, **C.** S121-15, **D.** S125-15, **E.** S104.15, **F.** S119.15.

Interestingly after 6 days in culture, and more evidently at the higher cell densities of 8,000 and 16,000 cells per well, necrotic centres were observed in some of the more compact spheroids (Figure 2.5 B). This is evident in other tumour spheroids, where a gradient of proliferation develops as spheroids become more compact, correlated with tumour hypoxia [106]. Not all of the UM tumour spheroids developed a necrotic centre; in some cases the spheroids would form compact shapes after 9 days in culture (Figure 2.5 E and F). When the UM spheroids were analysed further, proliferating cells could be observed towards the edges of the spheroids and less so in the centre (Figure 2.8).

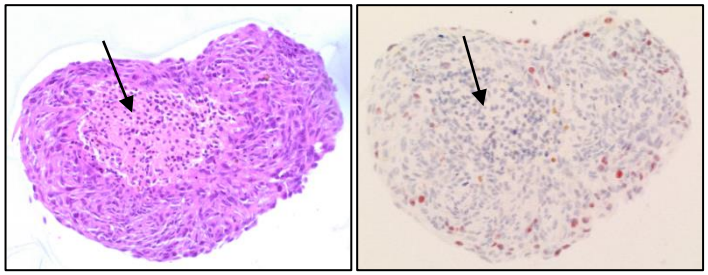

Figure 2.8. Cross section of primary UM spheroids (S093-15) at day 9. H&E image showing a less proliferative core (arrows) as also indicated by lower Ki67 staining in adjacent image, in this region compared to the outer regions.

The presence or absence of nuclear BAP1 was consistent between the original patient tumour and the 3D spheroid in all cases (Table 2.4 and Appendix 1 – 6). Surprisingly, however, three cases that displayed nuclear BAP1 staining in the original tumour and/or 3D spheroid, demonstrated a loss of nuclear BAP1 expression in 2D culture (Table 2.4 A – F). The genetic status of the primary UM for chromosomes 3, 6 and 8 was consistent with the data obtained from the 3D spheroids (Table 2.4 A – F).

Table 2.4. Histopathological and genetic information from the original primary UM tumour and in 2D and 3D culture

A	S093-15	2D culture	3D culture
Cell type	Spindle	Mixed	Spindle
Macrophages	Scattered	NA	Present
melanA	+ve	++++	++++
nBAP1 protein expression	+ve	-ve	+ve
Chr3	N	ND	N
Chr6p	G	ND	G
Chr8q	G	ND	G

B	S104-15	2D culture	3D culture
Cell type	Mixed	Spindle	Spindle
Macrophages	ND	NA	Present
melanA	+ve	+++	++++
nBAP1 protein expression	ND	-ve	+ve
Chr3	N	ND	N
Chr6p	N	ND	N
Chr8q	N	ND	N

C	S119-15	2D culture	3D culture
Cell type	Mixed	Spindle	Spindle
Macrophages	ND	NA	Present
melanA	+ve	++	++++
nBAP1 protein expression	+ve	-ve	+ve
Chr3	N	ND	N
Chr6p	G	ND	G
Chr8q	N	ND	N

D	S125-15	2D culture	3D culture
Cell type	Mixed	Spindle	Mixed
Macrophages	Heavy infiltration	NA	No
melanA	+ve	++++	+++
nBAP1 protein expression	-ve	+ve	-ve
Chr3	L	ND	L
Chr6p	G	ND	G
Chr8q	G	ND	G

E	S121.15	2D culture	3D culture
Cell type	Mixed	Nd	Spindle
Macrophages	Mild infiltration	ND	Present
melanA	+ve	ND	++++
nBAP1 protein expression	+ve	ND	+ve
Chr3	L	ND	U
Chr6p	G	ND	N
Chr8q	N	ND	G

F	S084-15	2D culture	3D culture
Cell type	Epithelioid	ND	Epithelioid
Macrophages	Scattered	ND	Present
melanA	+ve	ND	++++
nBAP1 protein expression	-ve	ND	-ve
Chr3	L	ND	ND
Chr6p	G	ND	ND
Chr8q	N	ND	ND

NA= not applicable, N= normal, G = gain, L = loss, ++++ = 80 – 100% positive staining, +++ = 60 – 80% positive staining, ++ = 40 – 60% positive staining.

2.4 Discussion

Development of *in vitro* models for studying cell biology and cell physiology has been of great importance in cancer research and drug discovery, as well as the emerging fields of tissue engineering and regenerative medicine. The traditional 2D methods of mammalian cell culture have several limitations, and it has become increasingly recognised that cells grown in a 3D environment more closely represent normal cellular function because of the increased cell-to-cell interactions present [108].

The use and advantages of the different 3D culture methods that have been described in the literature were outlined in the introduction of this chapter; however these methods do present with some limitations. Due to constant mixing in the spinner flask method, cells cannot be visualised as they aggregate, and furthermore, it may not be a useful method for cells that are sensitive to shear forces. Spheroids formed in the liquid overlay method are often heterogeneous in size and shape, and as a result a uniform homogenous set of spheroids cannot always be obtained for comparison and further studies [108]. This was consistent with the results obtained with the UM cell lines. The hanging drop assay requires diligence and care as the droplets are in close vicinity to each other and any sudden movements to the Petri dish can cause the droplets to fall or to join together. In addition, tracking these spheroids during culture can be difficult and further manipulations such as media change or the addition of drugs can be challenging.

The most efficient method used in this chapter was the ULA 96-well plates for the culture of the 3D spheroids. UM primary cells in particular formed individual spheroids in each well of the plate and were easily imaged and further manipulated. Furthermore, these tumour spheroids retained many of the features of the original patient tumour, including cell morphology, nuclear BAP1 expression and the presence or absence of macrophages. Macrophages are a key feature of UM, associated with a poorer prognosis in UM patients [118]. Surprisingly, these macrophages were found

in the tumour spheroids, even after their culture in 2D. The majority of the macrophages were found closer to the edges of the tumour spheroids, further investigation could establish whether these macrophages would infiltrate further into the spheroid chore with a longer period of time in culture, or remain on the edges of the tumour spheroids. It was not possible to obtain further histopathological information for case S104-15, since an endoresection was performed for this patient and since only a small sample, only a cytospin was made, which is limiting with respect to the amount of IHC that can be performed. When cultured in 3D and analysed further by IHC however, macrophages were identified, as a result providing a more complete profile for this tumour based on culture as spheroids.

Since *BAP1* plays a key role in UM metastasis and is used as a prognostic marker [28], as described in Chapter 1, it was important to assess its expression in the different culture environments. In both the original tumour and in the spheroids, nuclear BAP1 expression remained the same. However, this was not the case in 2D culture as tumours originally expressing BAP1 lost this expression in 2D culture (Table 2.4 A and C). The difference in expression highlights the importance of the correct environment for tumour growth, and the more representative 3D environment. This representative environment is further noted in the UM tumour spheroids at the later days in culture; when observed under a microscope, the spheroids present with a lighter outer layer and a darker inner centre (Figure 2.5 B). As spheroids grow in size, the inner cells become necrotic; this is paralleled by a decrease in Ki67 cell proliferation staining in the primary UM spheroids. After further IHC analysis, the UM spheroids showed a less proliferative core compared to the more proliferative outer layer, similar to micrometastases and avascular tumours [119]. When spheroids reach a critical size of ≥ 500 µm in diameter, they begin to form gradients that more faithfully mimic *in vivo* solid tumours, including an outer proliferating zone an inner quiescent zone, and a central necrotic core [119]. In order to grow further, tumours require a

blood supply, as a result a cascade of signalling factors are activated to supply the proliferating cancer cells with oxygen [120].

The 3D spheroid culture system, further offers the unique opportunity to culture cancer cells with various cell types. This co-culture system, allows interactions that cause the cells to acquire morphological and cellular characteristics relevant to *in vivo* tumours. Holliday and colleagues utilised this system by co-culturing breast cancer cells with luminal cells, myoepithelial cells and stromal fibroblasts and reported features in 3D similar to ductal carcinoma *in situ* [121]. Furthermore, breast cancer cells co-cultured with fibroblasts showed an invasive phenotype, and formed a tissue more similar to primary breast cancer tissue [122]. A co-culture system may provide a great advantage in better understanding UM metastasis to the liver. Liver resections are uncommon, and culturing liver cells have proven a challenge in research. When hepatocytes are cultured in 2D, they lose their differentiation function; however, when cultured as spheroids, they retain their polarity, form tight junctions and have hepatocyte-like functions [123]. Co-culturing hepatocytes with hepatic stellate cells encourages the rapid formation of hepatic spheroids on a modified surface. Multicellular spheroids formed via this method retained hepatospecific functions for more than two months in culture [124]. A co-culture spheroid system with UM cells and hepatocytes as a future direction in these spheroid assays could shed some light into the current questions regarding the preference of UM cells settling primarily in the liver. Furthermore, they will provide a platform for drug discovery and the treatment of metastatic UM.

3D *in vitro* culture systems have been shown to recapitulate the drug sensitivity patterns of tumour cells *in vivo*. Spheroids cultured from a breast cancer cell line had a lower IC_{50} to cisplatinum than the same cells cultured in 2D. Moreover, when treated with DNA damaging therapeutic agents, TGF-βs are upregulated *in vivo*, consistent with the treatment of the spheroids; however, similar results were not observed in 2D

[125]. In designing effective treatment strategies, tumour heterogeneity introduces significant challenges. The difference between the size and necrotic core of the tumour spheroids investigated in this chapter is a small reflection of the different tumour types in patients. This results in different sensitivities to drugs among different patients. Model systems can typically lack the heterogeneity seen in human cancers. In order to accurately study tumour heterogeneity, more accurate preclinical models are required. The heterogeneity observed among the patient tumour spheroids in this investigation, is a step towards recapitulating and understating the individual patient tumour and allowing for the assessment of different potential therapeutic targets.

It is unclear why some UM cases in this investigation failed to form tumour spheroids, perhaps a larger panel of cases would not only offer an explanation for this, but also provide a more representative quantitative data set than that presented here. In addition, measuring tumour volume would better demonstrate the reproducibility in spheroid size, in particular if the spheroids were to be treated with potential therapeutic drugs. This can easily be achieved since there are currently imaging systems designed for 96 well plates and measuring spheroids such as the Celigo™ cytometer [106]. As well as recapitulating the tumour environment, these 3D tumour spheroids can further be utilised for potential therapeutic targets. Since there has been no influence on the survival of UM patients with the current treatment options for metastasis, discussed in more detail in Chapter 4, these tumour spheroids can provide an efficient, simple and reproducible setting with which to assess different drugs. Furthermore, to recapitulate the behaviour of the UM tumour spheroids in an *in vivo* environment, they can be utilised as xenografts in animal models described in the following chapter.

Chapter 3

Chick embryo as a model to study uveal melanoma metastasis

3.1 Introduction

3.1.1 Historical background

The chick embryo has been widely used in cancer research and has proved itself as an essential *in vivo* model for understanding tumour biology, angiogenesis, metastatic spread and drug testing. The history of the chick as a model organism dates back to 330 B.C.; by opening chick eggs at different stages, Aristotle studied the chick development and made detailed observations, recorded in his *Historia Animalium.* Later, in the 17th century, Marcelo Malpighi used the chick embryo to define and describe blood vessels, followed in the late 19th century by the first complete atlas of chick morphology, *Atlas d'embryologie* [126]. These advances further led to the universally used Hamburger-Hamilton staging system, which illustrates 46 morphologically distinct stages of chick development beginning with a freshly laid egg to a fully developed and hatched chick [127].

The absence of a full immune system early in chick embryo development has also widely contributed to its tractability as a cancer model. In 1911, Francis Peyton Rous discovered the Rous Sarcoma Virus; he prepared an extract from a sarcoma found on a hen by mincing a sample of the tumour in saline and passing it through a filter to eliminate bacteria and tumour cells. He then injected the extract into healthy chickens and found that new tumours arose [128]. This ultimately led to the discovery of viral oncogenes and fundamentally, changed our understanding of cancer growth and the applications of the chick model in human cancer research.

Following on from Rous and Murphy's work demonstrating growth of chicken sarcoma tumours transplanted on the chorioallantoic membrane (CAM) [129], Murphy continued to show successful heterologous transplantations of tumours through continuous passage from one egg to another, in a similar manner to the more recently described propagation of patient derived xenografts in mice [101]. Furthermore, he

demonstrated that although rat tissues could not grow on adult chickens, transplants successfully grew on the CAM up to embryonic day 18 of chick development [130, 131]. These studies revealed the utility of the natural immunodeficiency in this model and the CAM has since become a predominant feature of the chick embryo for the study of spontaneous metastasis [132].

3.1.2 Development of the chick embryo

Of particular help to cancer researchers using the chick embryo model is the detailed description of the stages of chick embryo development, from the first cleavage division through to hatching as defined by Hamburger and Hamilton. Development of internal organs commence early in chick development: by embryonic day 2 (E2) the heart is beating, and by the end of E3 the limb buds for the wings and legs are visible. Between E5 and E6 formation of the reproductive organs takes place. The embryo begins to move into position for hatching at E14 and enters a further growth phase before hatching on E20 - E21 [133].

Of particular relevance to this chapter are the timing of eye and the liver development in the chick embryo. The liver is formed from both the mesoderm and endoderm and the liver primordium is visible at the end of E2. Haemopoiesis in the liver of the chick embryo begins at E7 and peaks at E14. The liver is a closely packed mass of dendriform cords and discontinuous sinusoids. In both birds and mammals, the discontinuous linings of the sinusoids consist of endothelial cells and Kupffer cells [134].

The first sign of eye development, the rudiments of the primary optic vesicles, is around E1 – E2 [135]. By E4, the lens has begun to acquire its shape, and around E7, the ciliary body which develops close to the lens, secretes the fluid of vitreous chamber. The iris and the retina also form around E7 and at this stage the choroid begins to develop pigment and the eyelids start to form [135].

3.1.3 Development of the Chorioallantoic membrane

The CAM, a highly vascular extraembryonic membrane, begins to form between E3 and E4 from the fusion of the chorion and the allantois [132]. The chorion is the outermost membrane that surrounds an embryo and the allantois is a sac-like structure that forms part of a developing amniote's conceptus, consisting of all embryonic and extra-embryonic tissues (Figure 3.1). The CAM consists of three layers: the ectoderm from the chorion that attaches to the shell membrane, and the mesoderm and endoderm from the allantois enriched in blood vessels, all of which then form a thin transparent collagenous matrix. A fully developed capillary plexus has developed by E10, and by E16 the CAM has surrounded the yolk sack pressing against the egg shell membrane. This allows it to serve as a set of lungs for the developing embryo enabling the exchange of gasses through the pores in the shell [136]. The chick immune system does not begin to function until around two weeks into its development. By E10 and E12 respectively, monocytes and macrophages can be found and from E10 to E15 the two major inflammatory cell types, heterophils and monocytes are present. By E18, the chick embryo is fully immunocompetent [137].

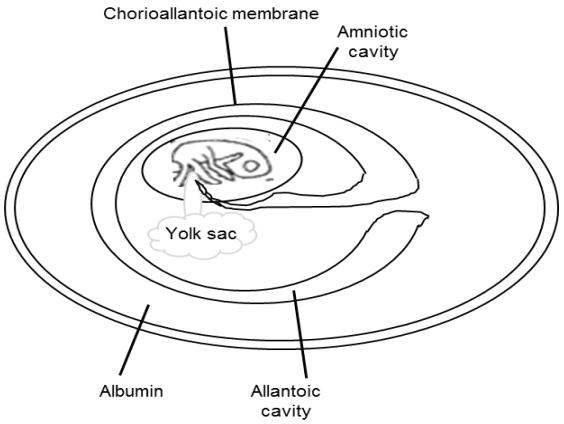

Figure 3.1. Developing chick embryo surrounded by the chorioallantoic membrane

3.1.4 Chick embryo as a model in cancer biology

The chick embryo as a model to study tumour development and metastasis has been reported in many different cancers including ovarian, renal, colorectal and prostate [138-141]. Studies have used this model in two main experimental approaches 1) inoculation of tumour cells directly on to the CAM to study tumour development and spontaneous metastasis; and 2) inoculation of tumour cells intravenously as a direct metastasis model.

The CAM has become invaluable in developmental studies and has provided a platform for cell intravasation and spontaneous metastasis models. Studies using human fibrosarcoma cells showed their capacity to form tumour nodules on the CAM as well as in distant portions of the CAM, and also in internal organs by PCR [142]. Several important steps of metastasis, including tumour invasion, angiogenesis and metastasis have been explored in this assay. Nasopharyngeal carcinoma (NPC), a highly invasive and metastatic head and neck cancer has been difficult to study due to lack of tissue and *in vivo* models for this disease. Recently, Xiao and colleagues reported 100% tumour formation of four NPC cell lines, and 35 primary tumour biopsies after 3 days of inoculation on the CAM, including extracellular matrix interaction and induced angiogenesis [143].

Chambers and colleagues injected B16F1 cutaneous melanoma cells into the blood vessels of the chick embryo CAM at E11 and the tail vein of mice. After 7 and 20 days respectively, the chick embryos and mice were examined for tumour formation. The total number of tumours per animal was much greater in the chick than in the mouse (~25 fold) [144]. In another study B16F1 cells were injected into the optic cup of the chick embryo at E3.5. Histological examination demonstrated that some cells remained at the site of transplantation while other cells formed tumours and invaded the choroid. Furthermore, the malignant growth of the melanoma cells in the optic cup was enhanced by bone morphogenetic protein-2 (BMP-2), highlighting the utility of

orthotopic studies and the ease of access and manipulation in this model [145]. B16F10 tumour cells inoculated into the chorioallantoic vein at E10 disseminated throughout the vascular system of the chick and more than 80% of injected cells survived the microcirculation and successfully extravasated by 1 - 3 days later [146]. Therefore within a few days after inoculation, tumour cells can be identified in the CAM distant from the inoculation site and in organs. For example, following injection of leukaemia cells, they were found engrafted in the chick brain, similar to central nervous system involvement in the human disease and in hematopoietic organs, as early as 7 days post injection, in contrast to the 4 weeks and more required for engrafting severe combined immunodeficient mice [147]. As early as 10 minutes after intravenous injection of fluorescently labelled B16-F10 cells, they were found arrested in the capillary bed. Six hours later, they had changed their shape and spread in close contact with the capillary wall [148].

Advances in imaging technologies have made it possible to visualise vascular perfusion, vascularisation of the CAM and the distinct steps of angiogenesis. Following small nanoparticles through the vascular beds that feed solid tumours can predict how intravenously administered drugs will localize within tumours and their surrounding tissues. Imaging tumour vascular dynamics in the CAM is faster, easier and less expensive than in mammals, promoting its utility for screening drugs or new designs for drug carriers and potential targeting agents [149]. Furthermore, GFP-labelling of cells enables them to be easily visualised in this model, compared to the original PCR methods. Lewis lung carcinoma cells stably expressing GFP were injected at E12. The GFP-labelled cells were visualised by fluorescence after 7 days in the brain, heart, and the sternum, with the most frequent site being the brain. The E12 chick embryos were injected intravenously with GFP-Lewis lung cancer cells along with two agents (streptokinase and gemcitabine) either alone or in combination. The combination of these agents inhibited metastasis at all sites, showing that the

GFP-tumour chick-embryo model should be very useful for rapid screening of anti-metastatic agents [149].

To date, there are only three studies that have used UM cells and the chick embryo as a model to study this disease. Luyten and colleagues microinjected 10^2 - 10^3 UM cells into the developing eye of twenty embryos. These cells were cultivated from the subcutaneous metastatic lesion of a 46 - year old patient who had undergone enucleation 28 years earlier. At E19, the eyes were removed for histological examination: 18 of the 20 injected embryos had survived; four showed intraocular tumour growth. UM cells were observed adherent to the ciliary body, along the hyaloid artery and tunica vasculosa lentis. Immunohistochemical analysis showed positive expression of S100P and HMB45 highlighting UM cells in these regions. UM cells were not reported by these authors in the choroid. Interestingly, when they repeated the same experiments injecting human skin melanoma cells into the optic cup, these cells had also infiltrated the choroid [150].

Berube and colleagues used the CAM assay to study the tumourigenic potential of four cell lines; SP6.5, SP8.0 and TP31 derived from the primary UM of three different patients, and H79 cells derived from a metastatic UM in the liver. All four cell lines formed vascularised tumour masses on the CAM following inoculation of 5 x10^6 cells at E10 for seven days; however, histological analysis of these tumours was not reported [151].

Laurent and colleagues, examined the effects of protein tyrosine phosphatase type IV A member 3 (PTP4A3), when introduced into the OCM1 UM cell line, on tumour cell dissemination using the CAM assay. They reported increased migration and invasiveness in the chick femur, although no information was provided with regard to tumour formation and mass of the OCM1 cells, or metastasis to any organs [152].

The aim of this chapter was to investigate the chick embryo as an *in vivo* model to study UM tumour development, intravasation, extravasation and metastatic colonisation. To achieve this two approaches were used: 1) various UM cell lines were grafted onto the CAM as a spontaneous metastasis model, and 2) UM cell line injections were performed into the chick embryo circulation mimicking a direct metastasis (or dissemination) model.

3.2 Materials and Methods

3.2.1 Chick egg preparation

Fertilised white leghorn chicken eggs (obtained from Lees Lane poultry, Neston, UK) were incubated at 37°C. At embryonic day 2 (E2) or E3 a small incision was made at one end of the egg using a 19 gauge needle (Terumo) and syringe and approximately 4 ml of albumin was removed to detach the embryo and surrounding vessels from the shell. A small rectangular window was then cut into the “top surface” of the egg shell using a Power Craft PKW-160N Combitool and the window then sealed using Scotch Magic adhesive tape (Figure 3.2). Eggs were then further incubated at 38°C and 40% humidity.

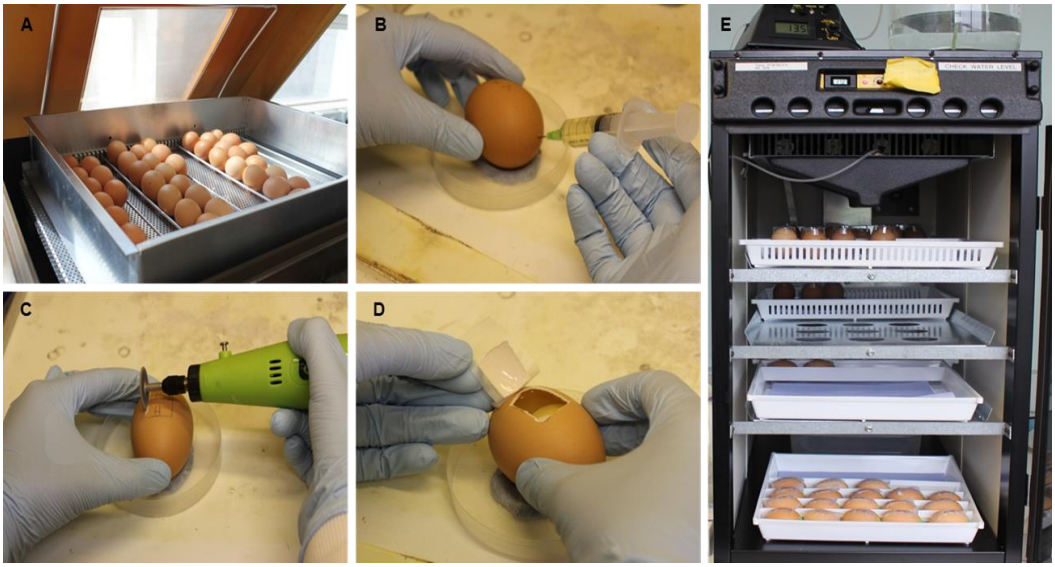

Figure 3.2. Outline of chick embryo egg preparation for CAM and injection assays. **A.** Fertilised eggs are incubated at 37°C. **B.** At E3, approximately 3ml of albumin is removed with a 5ml syringe and 18-gauge needle to lower the CAM. **C.** A small window is cut into the egg shell using a rotating disc drill. **D.** The window is sealed to allow normal development until experimental day where it will provide access for CAM laceration and tumour cell injection. **E.** Eggs are incubated at 38°C and 40% humidity.

3.2.2 Cell preparation

UM cells 92.1, MEL270, OMM1 and OMM2.3 were cultured and harvested as described in Chapter 2. The breast cancer cell line MCF-7, was cultured in DMEM (Sigma, Dorset, UK) supplemented with 10% fetal calf serum (FCS; PAA Laboratories), 2 mM l-glutamine (Sigma), and antibiotics (penicillin 50 IU/ml, streptomycin 500 µg/ml). MCF-7 cells were used to compare the behaviour of a non-mesenchymal cell line to the mesenchymal UM cell lines.

The UM and MCF-7 breast carcinoma cells were transduced with an enhanced green fluorescent protein (EGFP)-expressing HIV-based lentivirus. In brief UM cell lines plated at 500 cells/ well (24 well plate) were transduced and following an incubation of 24 hours, the lentivirus was removed and transduction efficiency was examined microscopically. Wells containing >90% EGFP expressing cells were propagated and banked down for all future experiments. Transducing the cells was kindly carried out by Dr Anne Herrmann.

3.2.3 CAM inoculation

GFP-labelled 92.1, OMM1, MEL270, OMM2.3 UM cells and MCF-7 breast carcinoma cells were counted using a haemocytometer and 2 x 10^6 cells were removed and pelleted at 1500rpm for 1 minute. A small volume of RPMI (approximately 3 µl) was mixed with each pellet to create a wet pellet and facilitate pipetting.

Cell pellets were kept on ice and occasionally re-triturated by flicking the tube. At E7, the junction of two or more small blood vessels was selected as the graft site. The vessels were then gently traumatised using a pipette tip to induce a small bleed and the wet cell pellet was introduced on-to the site. A minimum of 5 embryos underwent inoculation in each experimental replicate. Embryos were incubated until E14 at which point the CAM was observed under a Leica M165 FC fluorescence microscope for the presence of tumour nodules. Tumour nodules formed on the CAM were imaged

and dissected from the surrounding membrane and fixed in 10% neutral buffered formalin overnight. All CAM inoculations experiments were replicated (Appendix 7).

3.2.4 Chick embryo injections

GFP-labelled 92.1, OMM1, MEL270, OMM2.3 UM cells and MCF-7 breast carcinoma cells were harvested from culture flasks using 0.05% trypsin/ETDA (Life Technologies, Paisley, UK) and centrifuged at 1500 for 2 minutes. The resulting cell pellet was then resuspended as single cells at a density of $1x10^5$ cells/µl in RPMI 1640 (Life Technologies) containing 0.05% fastgreen (Sigma).

Cells were kept on ice and occasionally re-triturated by flicking the tube. Borosilicate glass capillary tubing (thin wall with filament, Harvard Apparatus Ltd., Kent, UK) was pulled under heat (settings: heat 580, velocity 15, pull 130, time 15, pressure 20; Sutter Instrument Co.) to produce needles for microinjection. The needles were then snapped using dissecting forceps to create a fine needle end allowing for cell suspension uptake. At E7, approximately 2µl of the cell suspension was injected by mouth pipetting (Sigma) directly into the chick embryo circulation under a stereo microscope. A minimum of 5 embryos underwent injection in each experiment replicate. Embryos were then incubated until E14 at which point they were dissected under a Leica M165 FC fluorescence microscope. Organs containing GFP-labelled cells were imaged, and subsequently removed and fixed in 10% neutral buffered formalin overnight.

The formalin fixed tissues were then placed in tissue cassettes before being loaded onto the BAYER VIP E300 tissue processor. The tissues underwent dehydration in a series of alcohol and xylene incubations before being finally maintained in hot wax ready for embedding. Tissues were then embedded in paraffin by careful orientation in the wax to fix them in the centre of the block.

3.2.5 Histological assessment and immunohistochemistry

Sectioning and immunohistochemical assays were performed as described in Chapter 2.

Tissues known to express the proteins of interest were included in each run as positive controls; negative controls included omission of the primary antibody or use of isotype specific controls where appropriate (Table 3.1).

Table 3.1. Details of antibodies used.

Antibody	Species	Isotype	Dilution / Concentration	Supplier	Positive human control tissue
MelanA	Mouse	IgG_1k Mouse monoclonal	1:100 0.96 µg/ml	Dako	Eye containing UM
Ki67	Mouse	IgG_1k Mouse monoclonal	1:200 0.4 µg/ml	Leica	Tonsil
αSMA	Mouse	IgG_1k Mouse monoclonal	1:600 0.1 µg/ml	Dako	Colon

3.3 Results

3.3.1 Chick embryo CAM inoculation

Following inoculation of GFP-labelled 92.1, OMM1, MEL270, OMM2.3 and MCF-7 cells onto the CAM at E7, tumour nodule formation was assessed at E14. The success rate/tumour nodules forming efficiency, as determined by size and histological assessment of nodule viability, was recorded (Appendix 7). MEL270, OMM2.3 and MCF-7 cell lines failed to form tumour nodules on the CAM. The tumour nodule forming efficiency of 92.1 and OMM1 cells varied between experiments ranging from a 30 – 100% success rate (Appendix 7). After the seven days of incubation at E14, UM cells were not observed in any internal organs, either using the fluorescence microscope or on histological examinations.

3.3.1.1 CAM inoculation of 92.1 cells

92.1 UM cells formed nodules that were pigmented and surrounded by a network of blood vessels (Figure 3.3).

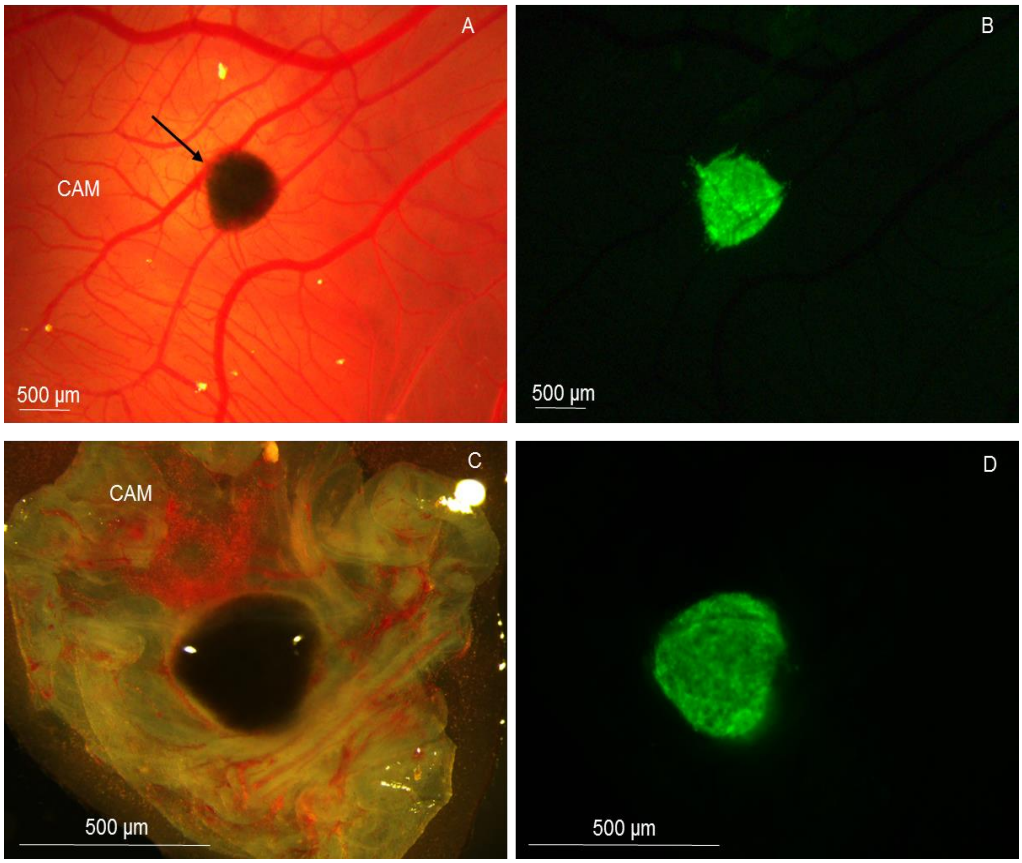

Figure 3.3. Macroscopic detection of 92.1 cell line tumour nodule formed in the CAM assay. A. 92.1 uveal melanoma cells formed a visible nodule on the CAM at E14, 7 days following cell grafting, arrow shows pigmented tumour nodule. **B.** Fluorescent image showing GFP-labelled 92.1 cells within nodule *in ovo*. **C.** Tumour nodule dissected from embryo with surrounding CAM tissue for further analysis. **D.** Fluorescent image of dissected tumour nodule.

Histological analysis of the tumour nodule sections clearly showed the tumour nodule surrounded by the CAM tissue (Figure 3.4 A). Melan A was expressed by some of the cells within the CAM nodule (Figure 3.4 B) and a small number of MelanA positive tumour cells were also seen in the surrounding CAM tissue (Figure 3.4 C). αSMA staining highlighted the presence of blood vessels within the tumour nodule (Figures 3.4 D and 4E) and nuclear Ki67 staining within the tumour nodule indicated the presence of large numbers of viable proliferating cells (Figures 3.4 F and 3.4 G).

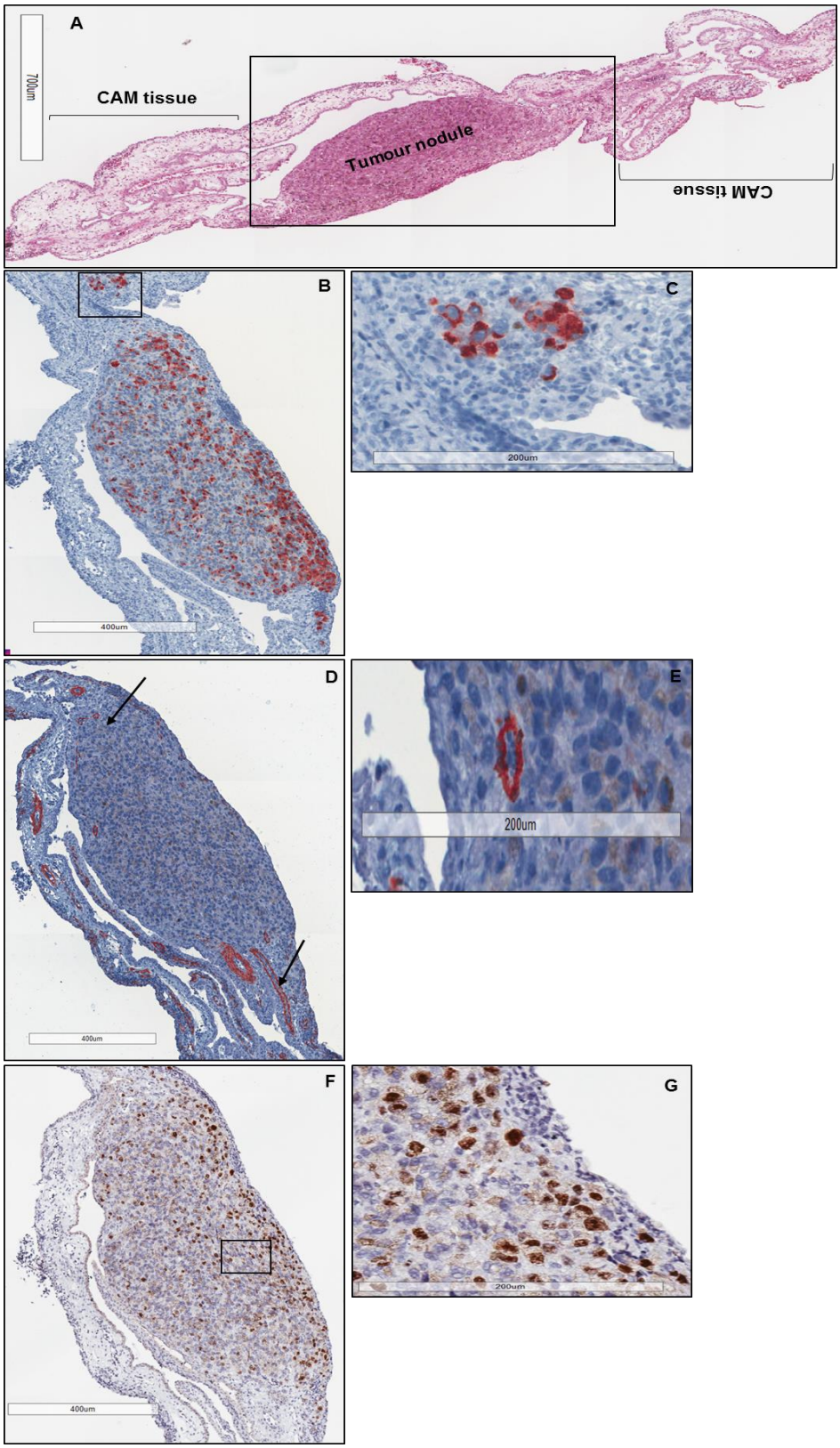

Figure 3.4. Immunohistochemical analysis of a representative 92.1 tumour nodule formed in the CAM assay. **A.** H&E-stained cross-section of the 92.1 tumour nodule on the CAM at E14. **B.** MelanA positive cells within the tumour nodule. **C.** High power image of MelanA positive tumour cells located in the surrounding CAM tissue. **D.** Cross section of tumour nodule stained with αSMA showing blood vessels within the tumour nodule. **E.** High power image of individual blood vessel within the tumour nodule. **F.** Nuclear Ki67 expression highlighting proliferating tumour cells. **G.** High power image of Ki67 nuclear staining.

3.3.1.2 CAM inoculation of OMM1 cells

Unlike the nodules formed with the 92.1 cell line, OMM1 tumour nodules were not pigmented. A network of blood vessels was also observed surrounding the nodules (Figure 3.5).

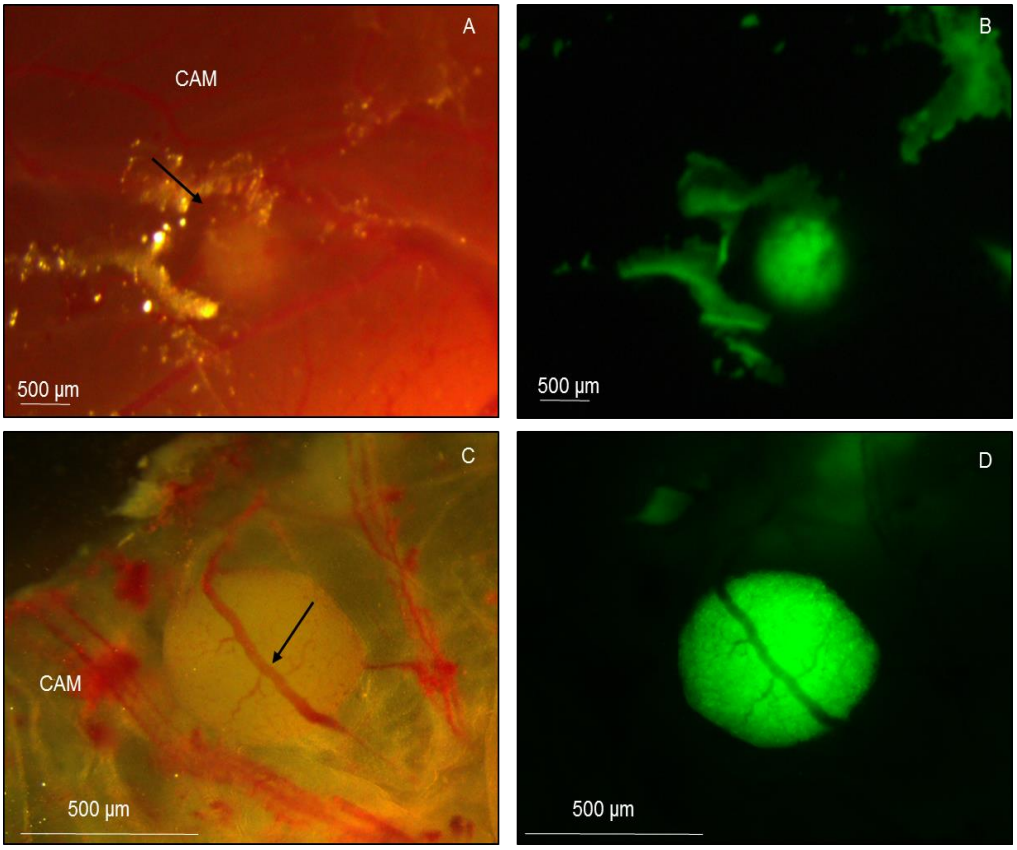

Figure 3.5. Macroscopic detection of OMM1 cell line tumour nodule formed in the CAM assay. A. OMM1 uveal melanoma cells formed a visible non pigmented nodule (arrow) on the CAM at E14, 7 days following cell grafting. **B.** Fluorescent image showing GFP-labelled OMM1 cells within nodule *in ovo*. **C.** tumour nodule dissected from embryo with surrounding CAM tissue for further analysis, arrow shows large blood vessel *ex ovo*. **D.** Fluorescent image of dissected tumour nodule.

Histological analysis of the tumour nodule sections clearly showed the tumour nodule surrounded by the CAM tissue (Figure 3.6 A). Melan A was expressed by some of the cells within the CAM nodule (Figure 3.6 B) and a small number of MelanA positive tumour cells were also seen in the surrounding CAM tissue (Figure 3.6 C). αSMA staining highlighted the presence of blood vessels within the tumour nodule (Figures 3.6 D and 3.6 E) and nuclear Ki67 staining within the tumour nodule indicated the presence of large numbers of viable proliferating cells (Figures 3.6 F and 3.6 G).

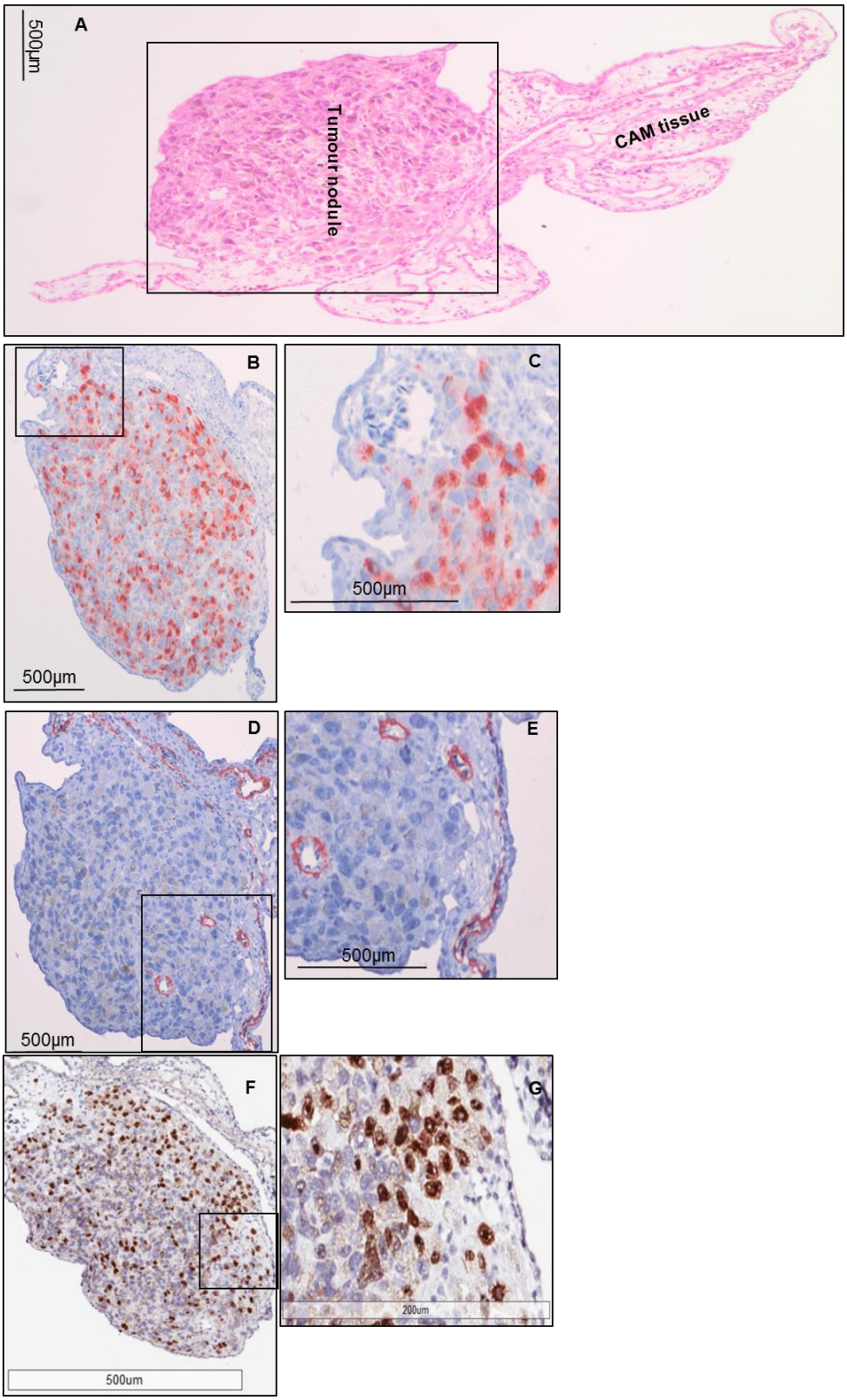

Figure 3.6. Immunohistochemical analysis of a representative OMM1 tumour nodule formed in the CAM assay. **A.** H&E-stained cross-section of the OMM1 tumour nodule on the CAM at E14. **B.** MelanA positive cells within the tumour nodule. **C.** High power image of MelanA positive tumour cells located in the surrounding CAM tissue. **D.** Cross section of tumour nodule stained with αSMA showing blood vessels within the tumour nodule. **E.** High power image of individual blood vessel within the tumour nodule. **F.** Nuclear Ki67 expression highlighting proliferating tumour cells. **G.** High power image of Ki67 nuclear staining.

3.3.2 Chick embryo injections

Following direct injection of GFP-labelled 92.1, OMM1, MEL270, OMM2.3 and MCF-7 cells into the chick circulation at E7, their movement and colonisation of internal organs was assessed at E14 (Table 3.2). MEL270, OMM2.3 and MCF-7 cell lines failed to form metastatic deposits in any of the organs examined at E14. 92.1 and OMM1 cells, however, were found in most neural crest-derived tissues and the most frequent colonisations occurred in the liver and eye.

Table 3.2. Distribution of 92.1, OMM1, MEL270, OMM2.3 UM, and MCF7 breast cancer cell lines within chick embryo organs at E14.

Chick tissue	92.1	OMM1	MEL270	OMM2.3	MCF-7
Liver	+++	+++	-	-	-
Eye	+++	+++	-	-	-
Lungs	-	-	-	-	-
Spleen	-	-	-	-	-
Heart	+	-	-	-	-
Gut	+	+	-	-	-
Kidney	+	+	-	-	-
Brain	++	++	-	-	-
Number of embryos examined	19	15	10	10	10

+++ = 70 - 100% of embryos examined had GFP-labelled cells in organ, ++ = 40 - 70%, + = 1 – 40%, - = no tumour cells observed.

3.3.2.1 Chick embryo injections of 92.1 cells

92.1 UM cells were found in the liver and could be seen macroscopically under a fluorescence microscope upon dissecting the chick embryo at E14 (Figure 3.7 A and 3.7 B). Histological analysis of the liver sections showed numerous infiltrating tumour cell aggregates of varying sizes next to blood vessels that stained positively for MelanA (Figures 3.7 D and 3.7 E). A small number of cells within each foci stained positively for Ki67, indicating ongoing proliferation. Ki67 does not stain chick cells [153] hence proliferating cells are confirmed tumour cells (Figure 3.7 F and 3.7 G).

Cells were also abundant in the eye of the developing chick embryo and these could be clearly visualised under the fluorescence microscope (Figure 3.8 B). When further dissecting the anterior part of the eye, UM cells were found in the ciliary body and iris, as confirmed by MelanA staining (Figures 3.8 D and 3.8 E). Furthermore, cross section of the whole eye and close examination of the choroid revealed infrequent UM cells within this compartment (Figure 3.8 F).

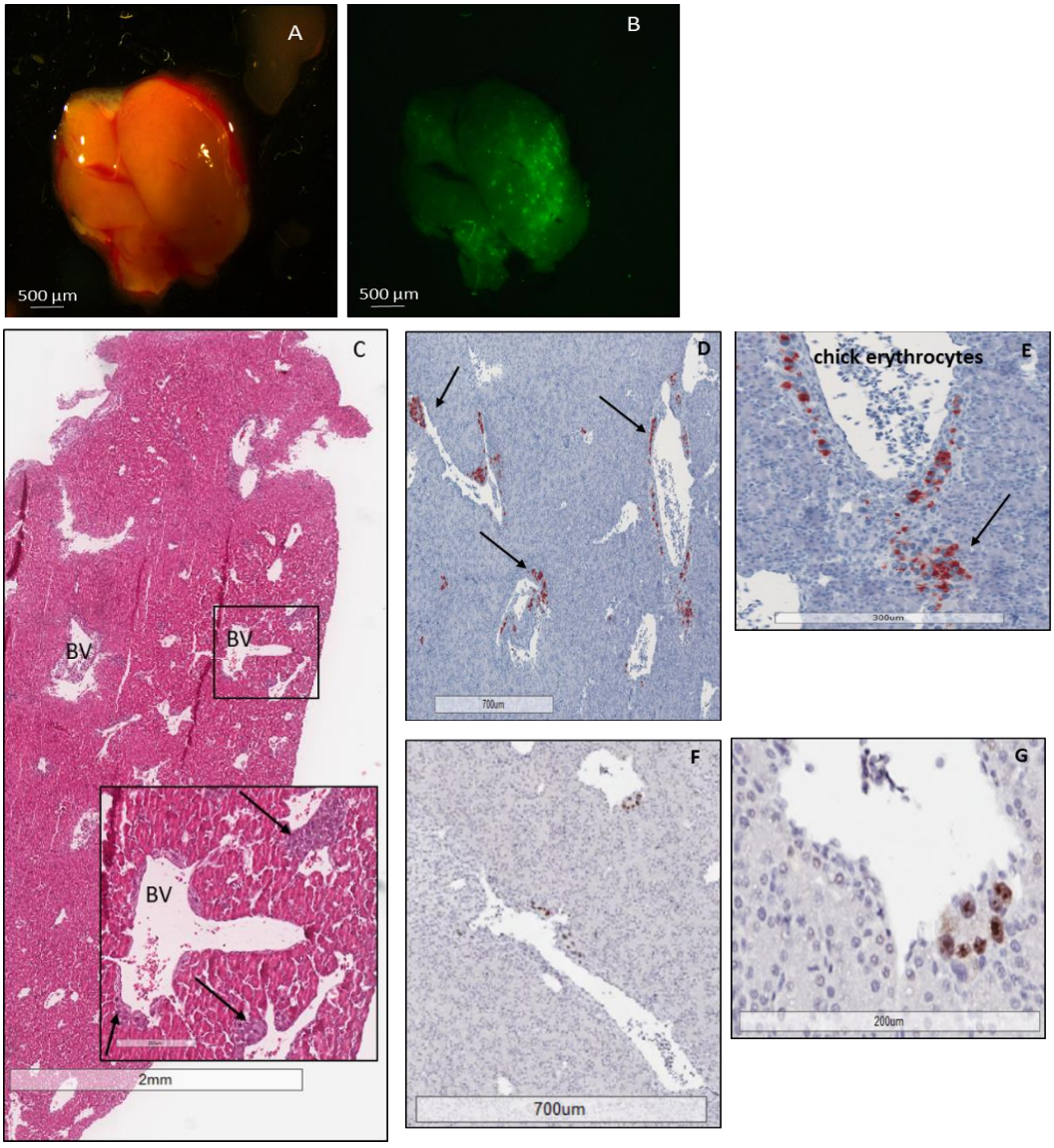

Figure 3.7. Detection and immunohistochemical analysis of 92.1 GFP-labelled UM cells in the chick embryo liver at E14. A. Macroscopic image of a dissected chick embryo liver at E14. **B.** Detection of 92.1 GFP-labelled cells in the chick embryo liver under fluorescence. **C.** H&E-stained cross section image of liver. Inset shows higher power of infiltrating melanoma cells (arrows). D. MelanA staining of the tumour cells within the liver showing adjacent blood vessels (arrows). E. High power image showing escaping tumour cells from blood vessel (arrow). **F.** A low Ki67 proliferation index is also visible (arrow). **G**. High power image showing proliferating tumour cells.

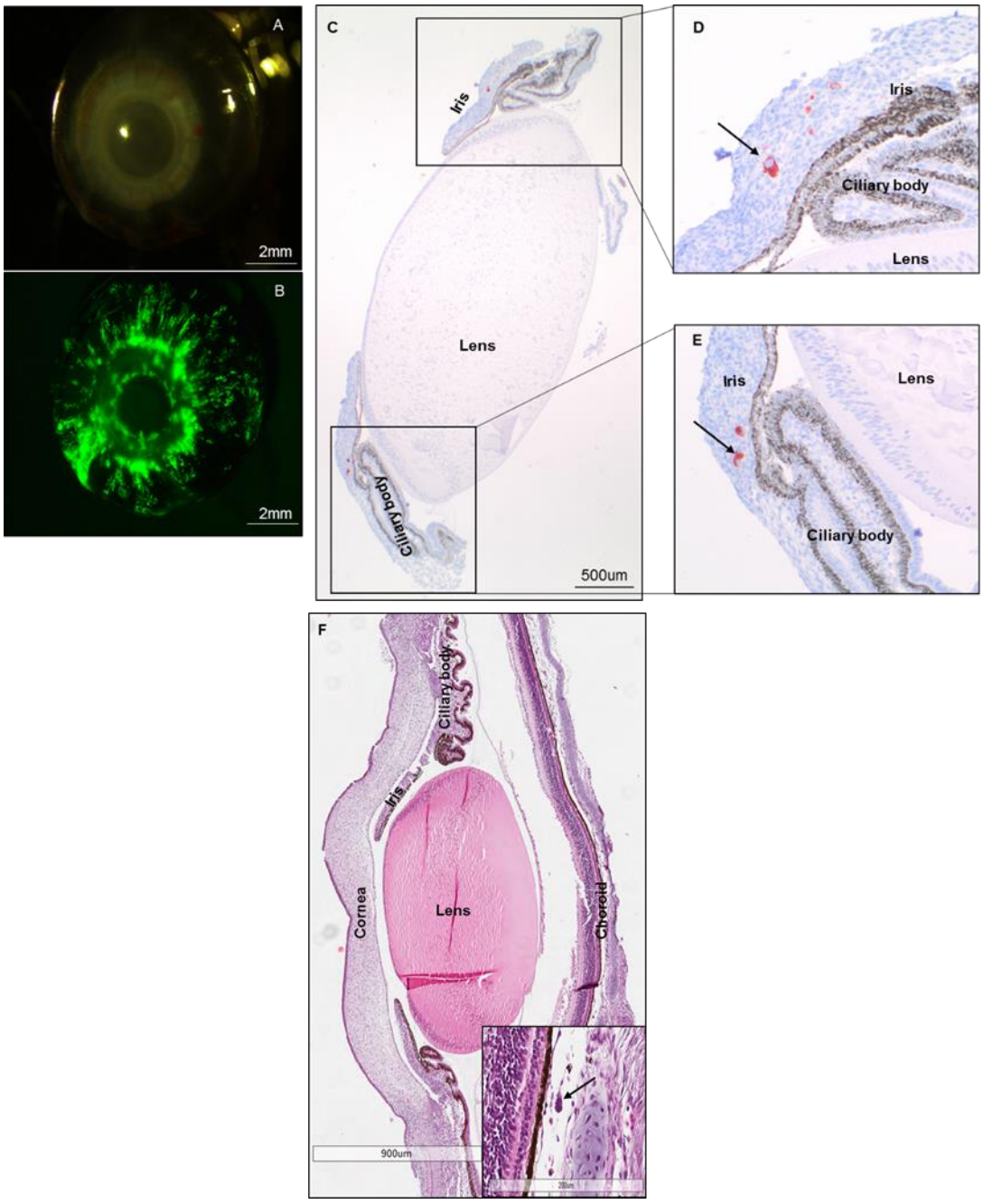

Figure 3.8. Homing of 92.1 GFP-labelled UM cells to the chick embryo eye. A. Macroscopic analysis of a dissected chick embryo eye. **B.** GFP-labelled 92.1 cells injected at E7 are visible in the anterior. **C.** Cross section of anterior segment of eye showing MelanA positive cells within the iris. **D** and **E.** High power image of MelanA positive tumour cells within the iris (arrows). **F.** H&E cross section of whole eye, inset shows melanoma cell within the choroid (arrow).

3.3.2.2 Chick embryo injections OMM1 cells

Similar to 92.1 cell injections at E7, OMM1 cells were found predominantly in the chick embryo liver at E14. These were clearly visualised using a fluorescence microscope and further with MelanA staining. Larger groups of infiltrating OMM1 cells compared with 92.1 cells were identified adjacent to blood vessels in the liver. A small number of proliferating cells can also be seen as indicated by Ki67 staining (Figure 3.9).

OMM1 cells were also abundant in the eye of the embryo and these could clearly be visualised under the fluorescence microscope. When further dissecting the anterior part of the eye, aggregates of cells were found in the iris and ciliary body, and were confirmed by MelanA staining (Figure 3.10).

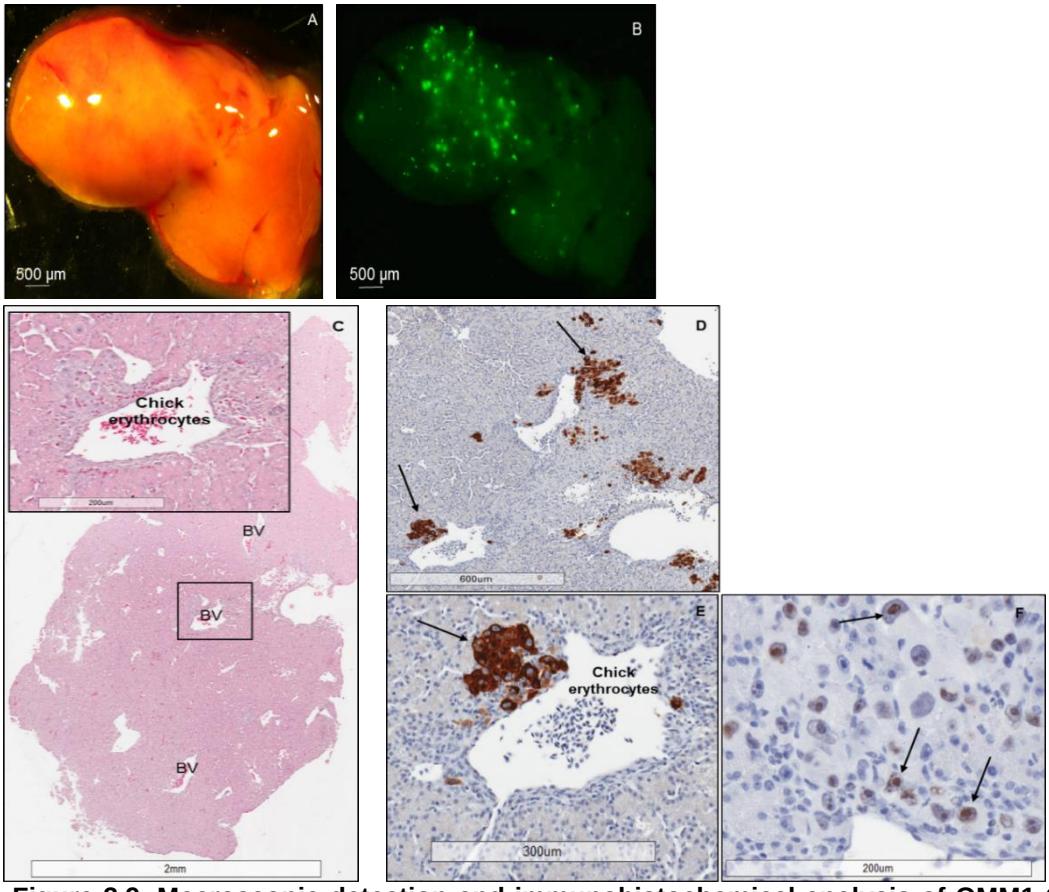

Figure 3.9. Macroscopic detection and immunohistochemical analysis of OMM1 GFP-labelled UM cells in the chick embryo liver at E14. A. Macroscopic images of a dissected chick embryo liver at E14. **B.** Detection of OMM1 GFP-labelled cells in the chick embryo liver under fluorescence. **C.** H&E-stained cross section image of liver. Inset shows higher power of infiltrating melanoma cells surrounding the blood vessel. **D.** MelanA staining of liver showing tumour cells across the liver, particularly adjacent to blood vessels (arrows). **E.** High power image showing extravasation of tumour cells from blood vessel (arrow). **F**. A low Ki67 proliferation index is also visible (arrows).

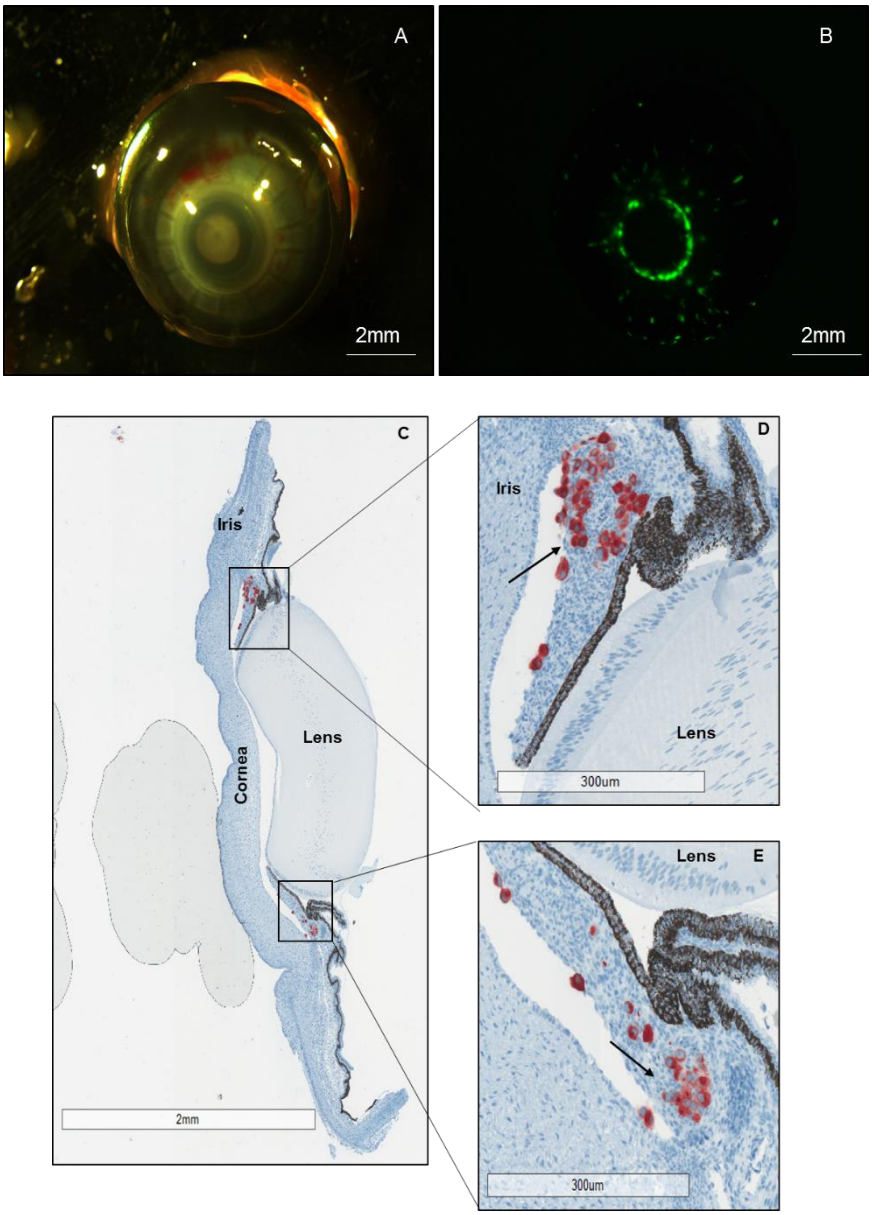

Figure 3.10. Homing of OMM1 GFP-labelled UM cells to the chick embryo eye. A. Macroscopic analysis of a dissected chick embryo eye. **B.** GFP-labelled 92.1 cells injected at E7 homed to the uveal tract by E14. **C.** Cross section of anterior part of eye showing MelanA positive cells within the ciliary body and iris of the uveal tract. **D** and **E.** High power image of MelanA positive tumour cells within the iris (arrows).

3.4 Discussion

The chick embryo model has been used successfully to date in a limited number of studies assessing the ability of UM cells to; undergo orthotopic growth in the chick eye, form tumour masses on the CAM and undergo dissemination via the chick circulation to internal organs. This chapter has highlighted that the chick embryo model can be used successfully for xenografting UM cells onto the CAM as well as direct injection and survival of UM cells in the circulation, facilitating the biological analysis of many aspects of tumour development and metastasis.

UM can be characterised by chromosomal aberrations and genetic mutations that are either early events in tumour development i.e. *GNAQ* and *GNA11* mutations or that influence the metastatic capacity of the UM cells, in particular loss of one copy of chromosome 3, *BAP1* and *SF3B1* mutations, as discussed in Chapter 1. To date, the published studies examining UM cells in the chick embryo model have either failed to recapitulate this genetic landscape, having instead *BRAF* mutations that call into question the origin of the tumours [152], or detailed histological examination of the tumours formed has not been performed [151]. Berube and colleagues used three cell lines derived from enucleated UM and one from a UM metastasis to the liver [151]. However, one of the cell lines, SP6.5, harbours a *BRAF* mutation, which is found in cutaneous melanomas and not in UM [103]. In this study, two of the four UM cell lines examined, 92.1 (*GNAQ* mutants) and OMM1 (*GNA11* mutant), formed vascularised tumour masses on the CAM. Of interest, the two cell lines failing to form tumour masses on the CAM, MEL270 (*GNAQ* mutant) and OMM2.3 (*GNAQ* mutant) were derived from the primary UM and metastasis of the same patient. As a result, a correlation between the G protein mutation status and the ability of the cell lines to form tumour masses could not be made. However it is not of great surprise that not all the UM cell lines failed to form tumour masses on the CAM tissue. Balke and colleagues screened eight osteosarcoma cell lines for their ability to form vascularized

tumours on the CAM. They reported that three out of these eight cell lines were successful in forming nodules on the CAM [154]. As in Balke's investigation and in this study, the inability of all the cell lines to form tumour masses on the CAM highlights the importance of continued baseline analyses using a larger panel of well-characterised UM cell lines, as well as primary cell cultures, covering the spectrum of genomic and phenotypic alterations observed in UM patients.

While spontaneous metastases have been observed following the topical inoculation of mouse tumours on the CAM, most tumours do not give rise to spontaneous metastases [50]. Similarly the UM cells in this chapter, when inoculated onto the CAM, did not spontaneously metastasise to any organs within the chick embryo, despite forming tumour nodules surrounded by blood vessels after only 7 days of incubation. Degradation and penetration of basement membranes and their underlying stroma are hallmarks of tumour invasion and metastasis [155]. It is possible that invading the superficial epithelial layer of the CAM could be achieved by incubating the chick embryo eggs until a later embryonic stage; in this way allowing the cells more time to intravasate the CAM tissue and escape into the blood stream. Indeed, MelanA positive UM cells were observed outside the large tumour nodule that formed on the CAM (Figure 3B). Earlier steps in inducing this invasion from the CAM and certain characteristics of cell lines such as their ability to release proteases can also provide a "push" to promote metastasis. For example, Deryugina and colleagues demonstrated the existence of two variants of fibrosarcoma cells with different intravasation capacity on the CAM. They showed that specific inhibition in the variant with the higher invasion capacity of matrix metalloproteinase-9 (MMP-9) expression and activity with MMP-9 small interfering RNA and anti-MMP-9 monoclonal antibody resulted in an increase of intravasation indicating that targeting certain MMPs may lead to enhanced malignancy [142]. Other experimental approaches, such as addition

of trypsin to the CAM tissue prior to placing tumour cells can assist the cells in digesting through the CAM tissue (unpublished work by Dr Diana Moss).

Increased tumour progression and metastasis have previously been associated with hypoxic regions in primary tumours [156], and thus an approach may be to incubate the UM cells in hypoxic conditions prior to grafting onto the CAM. One such study showed that pre-conditioning neuroblastoma (NB) cells to hypoxia leads to metastasis to organs in the chick embryo. NB cells successfully form tumours on the CAM without spontaneous dissemination, however after pre-conditioning to hypoxia (1% O_2) for 3 days, they not only formed tumours larger in volume but also metastasised in the chick embryo organs, mainly to the gut and the liver [157]. This method may further provide insight to better understanding the behaviour and characteristics of metastasising UM cells in the liver.

The tissue composition and accessibility of the CAM for experimental manipulation, makes it an attractive preclinical *in vivo* model for drug screening. Hagedorn and colleagues showed that tumour growth with key features of human glioblastoma at the cellular and molecular levels occurred in a highly reproducible manner after human Glioblastoma multiforme (GBM) cell grafting on the CAM. Subsequent treatment of the glioma cells with receptor tyrosine kinase inhibitors abrogated tumour growth [139]. The simplicity, rapidity, and low cost of the different assays that can be performed with chick embryos strengthen the interest of routinely using this model in pharmaceutical technology.

As with the CAM assays, studies using direct injection methods have failed to use a representative panel of UM cell lines and to mimic UM metastasis. Laurent and colleagues used the OCM1 cell line to investigate the effect of PTP4A3 overexpression on tumour cell dissemination [152]. The OCM1 cell line harbours a *BRAF* mutation, this is inconsistent with the spread to the liver that is generally seen

in UM patients, as this cell line spread to the chick femur. In another study, Luyten and colleagues injected UM cells from a subcutaneous metastasis directly into the eye of E3.5 chick embryos, and although cells were found in the ciliary body at E19, they weren't reported in the iris or the choroid. Furthermore, metastasis was not reported in any other organs [150].

Two out of the four UM cell lines used in the chick embryo model, MEL270 and OMM2.5, failed to form both tumour nodules on the CAM or produce tumour deposits in the chick embryo organs when injected directly into the circulation. Of interest, these two cell lines are derived from the same patient; one from the primary UM (MEL270) and from a metastatic liver lesion (OMM2.3), suggesting an inherent property of the two cell lines and a lack of ability to invade through the epithelial sheet of the endothelial cell layer. As shown in this chapter, 92.1 and OMM1 UM cells "homed" to organs within the chick embryo, that are representative of tumour development and metastatic spread in patients i.e. the eye and the liver (Table 2.1). Within the eye, cells were found in the ciliary body, iris and the choroid, all of which are the sites human UM cells are found in the patient eye. Within the liver, the cells were found adjacent to the blood vessels with metastatic foci throughout the liver in a similar manner to multiple UM deposits that are seen in the liver of patients with metastatic UM [9]. The tumour cell foci, identified by MelanA immunohistochemistry, were located close to blood vessels and Kupffer cells; specialised macrophages found in the lumen of liver sinusoids [158]. This is consistent with the presence of metastatic UM cells in the perisinusoidal space of the liver, also known as the space of Disse, in patient specimens [45]. This similarity is of great importance as latency of UM metastatic cells in the liver has long puzzled researchers thus a representative model could shed significant insight. Borthwick and colleagues suggested that UM latency is due primarily to the inability of cells at metastatic sites to grow [159], consistent with low Ki67 staining in the chick embryo liver in this investigation. In this study, cells were

also found in other organs outlined in table 2.1, but not observed in the lungs or spleen, which are the other sites of UM metastasis. As Borthwick and colleagues pointed out, metastasising UM cells must pass through the lungs first [159], however details of the steps of metastasis still remain poorly understood, in part because of the difficulty of direct observation of ongoing *in vivo* processes. Chambers and colleagues have used intravital video microscopy to visualize cells labelled with fluorescent beads as they arrest in the microcirculation, extravasate, and form micrometastases in the chick embryo. Tumour cell division was seen only after extravasation [160]. In a further study, the invasiveness between two murine mammary tumour cell lines were investigated and in light of their differences in invasiveness, no differences were found between the high- and low-metastatic cell lines in either the timing or mechanism of extravasation. However, after extravasation, the more metastatic and invasive cells showed a greater ability to migrate to sites which favour tumour growth and to replicate to form micrometastases [161]. Therefore highlighting the post-extravasation events, migration and growth, as being critical in metastasis formation. As discussed previously, certain genetic alterations, e.g. *BAP1* mutations that are found in the majority of metastasising UM's, could cause the cells to perhaps only migrate to the common sites of metastasis found in UM patients. Thus isogenic cell lines or the more recently established *BAP1* mutant cell lines would be ideal future experimental procedures in this model.

This chapter has highlighted the many studies and different techniques and methods used to investigate a variety of cancers and potential therapeutic treatment using the chick embryo model. Not to mention the chick embryo as a brilliant cost efficient model; the accessibility of the CAM, the well-vascularized extra-embryonic tissue located underneath the eggshell, and its acceptance of xenografted tumour cells all make it easy to use. The underlying steps of metastasis in UM are still of question, however in an effort to mimic metastasis of UM in the chick embryo model this

investigation has successfully shown the metastasis and the similar behaviour of UM cells in the liver and the uveal tract of the chick embryo. These experiments have provided a baseline for further studies and further for preliminary testing of potential new agents to aid molecular-based cancer therapy.

Chapter 4

Targeted therapy in MYC amplified uveal melanoma

4.1 Introduction

Despite increased knowledge of UM biology and despite the advances in primary UM treatment, as discussed in Chapter 1, patient mortality remains high in those who develop metastatic disease. Metastatic disease occurs in approximately 50% of UM patients. The liver is the main site of metastasis and, due to the disseminated spread of the UM cells within the liver, with typically numerous metastatic deposits, liver resections are possible in only a small number of UM patients with isolated/solitary masses [162]. Unfortunately, only limited improved survival of UM patients with metastatic disease has been reported with chemotherapy, such as dacarbazine (DTIC) [163], hepatic intra-arterial chemotherapy with fotemustine [164] or interferon-α-2a [165]. Thus, there is a lack of effective treatment for metastatic UM.

Recently, targeted therapy has become a growing part of many cancer treatment regimens. For example, the identification of *BRAF* V600 somatic mutations in 66% of cutaneous melanomas [166], led to the development of molecularly targeted therapies, which initially improved survival of these patients compared with previous treatments [167]. However, *BRAF* V600 mutations are not present in UM [168]. Nevertheless, activation of the MAP-kinase pathway occurs in both cutaneous melanoma and UM. In cutaneous melanoma *BRAF* and *NRAS* mutations activate the MAP-kinase pathway; in UM, this occurs through oncogenic mutations in the G-protein α-subunits q or 11 [25, 169], which are found in greater than 80% of UM (discussed in Chapter 1). These mutations result in activation of Protein Kinase C (PKC), and are thought to drive downstream signalling leading to activation of the mitogen-activated protein kinase kinase (MEK) and extracellular signal regulated kinase (ERK) pathways [170] (Figure 4.1).

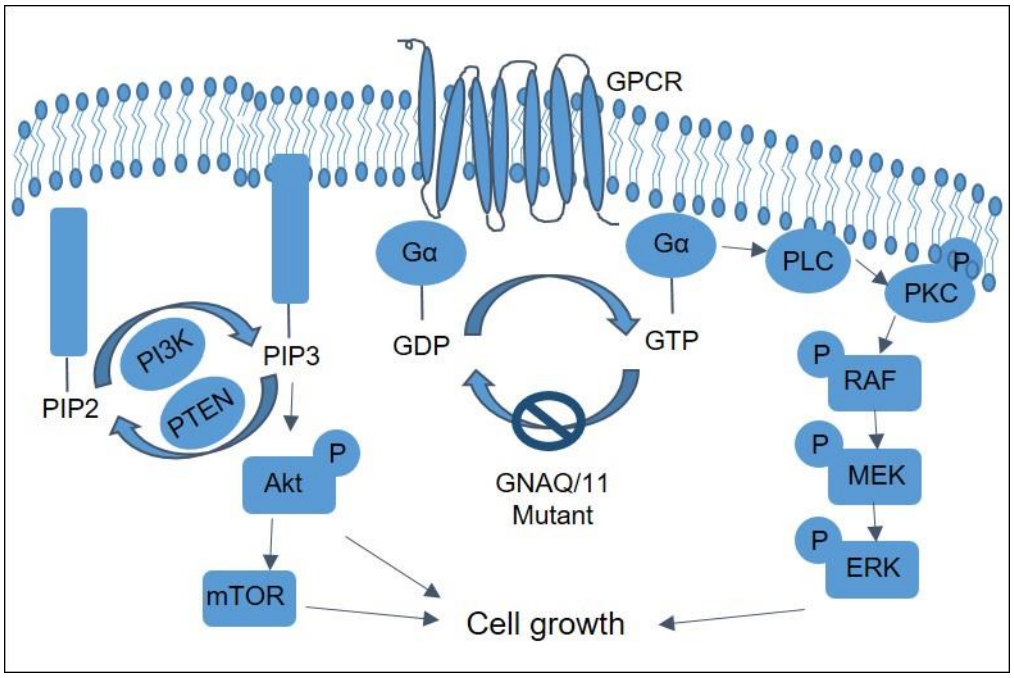

Figure 4.1. Simplified signalling cascade in *GNAQ* and *GNA11* mutant UM. Hydrolysis of GTP results in increased Gα protein. Gα signals to phospholipase C (PLC), activating protein kinase C (PKC). The MAP kinase pathway is in turn activated by PKC signal. Phosphatidylinositol-3 kinase (PI3K, class I) which is upregulated in UM cells, signals through Akt and mammalian target of rapamycin (mTOR) to affect cell growth (adapted from Shoushtari *et al* [171]).

As a result, recent efforts in the understanding of the biology of UM have outlined therapies that target mutant G-protein signalling [42]. In this regard, targeted therapies in the form of kinase inhibitors that diminish the activity of MEK or PKC in UM patients with metastatic disease might be relevant. In a randomised open-label phase 2 study, 101 metastatic UM patients received the MEK inhibitor selumetinib alone or chemotherapy (temozolomide or DTIC); 14% of patients treated with MEK inhibitor had an objective radiographic response (either partial or complete response), whereas there was no response with chemotherapy alone [172]. Unfortunately, almost all patients treated with selumetinib had treatment-related adverse events, with 37% requiring dose reduction [172]. In this study, selumetinib compared with chemotherapy therefore resulted in a modestly improved progression-free survival and response rate; however, no improvement in overall survival was observed.

Other targeted kinase inhibitors - such as imatinib, sunitinib and sorafenib - are also undergoing clinical testing. Both imatinib and sunitinib were used in NCRI-sponsored national UK Trials – ITEM and SUAVE, respectively - led by medical oncologists based at the Clatterbridge Cancer Centre in Liverpool [173, 174]. Unfortunately, neither trial demonstrated any clear benefit. Hence, there is a compelling need for effective therapeutic strategies to manage metastatic UM.

Chen and colleagues demonstrated that chemical inhibition of PKC led to selective growth arrest in UM cell lines with *GNAQ* and *GNA11* mutations, and that PKC inhibitors can partially or temporarily suppress activation of the MAP-kinase pathway. Furthermore, the combination of PKC and MEK inhibitors, synergistically resulted in sustained growth inhibition and apoptosis *in vitro*, and led to tumour regression in a mouse model *in vivo* [175]. In a further study, treatment of *GNAQ* and *GNA11* mutant UM cell lines with a combination of the PI3Kα inhibitor BYL719 and PKC inhibitor AEB071, showed synergistic inhibition of cell proliferation and apoptotic cell death as compared with the effects of either agent alone. In addition, reduced xenograft tumour growth with the combination therapy was demonstrated in a *GNAQ* mutant mouse model [176]. These preclinical findings highlight that a combination of targeted agents may improve the outcome of metastatic UM, and also highlight the importance of identifying novel targets in this disease.

Dysregulated pathways in solid cancers commonly involve *c-MYC* located on chromosome 8q, which is thought to influence expression of ~15% of the genome responsible for cell growth, proliferation and apoptosis [177]. As a result, this transcription factor is thought to be an attractive drug target in the majority of cancers. However, although the importance of *c-MYC* in cancer progression is well documented, until recently it has been difficult to target this oncogene since the gene product is a transcription factor rather than an enzyme or extracellular receptor. However, Delmore and colleagues showed that the Bromodomain (BRD) and

ExtraTerminal (BET) family of proteins regulate c-Myc expression and function [178]. BET proteins such as bromodomain-containing 4 (BRD4) recruit proteins comprising macromolecular transcription complexes to specific chromatin sites. They contain an extraterminal domain and tandem bromodomains that recognise acetylated lysine residues on histones. BET inhibitors have been shown to block c-MYC expression in a variety of cancers, including multiple myeloma [178], medulloblastoma [179], neuroblastoma [180] and glioblastoma [181]. In one study, treatment with BET inhibitors impaired cutaneous melanoma cell proliferation *in vitro* and tumour growth and metastatic behaviour *in vivo* [182]. Furthermore, displacement of BET led to the downregulation of key cell cycle genes such as *c-MYC*, accumulation of cyclin-dependent kinase (CDK) inhibitors (p21 and p27), and subsequent cell cycle arrest.

JQ1, a chemical protein-protein interaction (PPI) bromodomain inhibitor, binds to the BET domain of BET proteins that interacts with acetylated histones and functions to silence transcription downstream of *c-MYC*. This includes *c-MYC* itself, and BET domain inhibitors are therefore able to decrease *c-MYC* levels in cells [183]. Shao and colleagues showed that JQ1 induced cell cycle arrest and decreased cell proliferation of Merkel cell carcinoma, an aggressive skin tumour of neuroendocrine origin exhibiting c-MYC protein overexpression. Moreover, JQ1 significantly attenuated xenograft tumour growth in vivo [184]. As discussed in Chapter 1, high-risk UM are usually characterised by monosomy 3 and polysomy 8q [185]. Parrella and colleagues showed that in a cohort of 43 UMs, 70% had increased MYC expression and of these, 43% had amplification of the *c-myc* gene, 47% had an intermediate relative increase in the *c-myc* copy number and 10% had a simple gain of chromosome 8 [186]. In a recent investigation, Ambrosini and colleagues explored the potential therapeutic effect of JQ1 in UM cells. Treating UM cell lines with JQ1 induced suppression of c-MYC and triggered apoptosis in only a subset of cell lines, including those with *GNA11/GNAQ* mutations [187].

Other targeted kinase inhibitors that affect the cell cycle, include Aurora and Polo-like kinases inhibitors; these can also target *c-MYC*, although the mechanism is unclear. One study showed that Small Cell Lung Cancer (SCLC) cells with c-*MYC* amplification are highly susceptible to specific kinase inhibitors targeting the mitotic Aurora and Polo-like kinases. Patient-derived SCLC cell lines were highly sensitive to both the Aurora B inhibitor AZD1152 (Barasertib) and the Polo-like kinase inhibitor BI2536, and these compounds inhibited proliferation at 3 orders of magnitude lower concentrations than in non-*MYC* amplified lines [188]. The Aurora kinases, A, B and C play an essential role in mitotic events regulating cell cycle transit from G2 to cytokinesis. MLN8237 (Alisertib) is an Aurora kinase A selective inhibitor that has shown encouraging anticancer effects in preclinical studies [189], whilst the Aurora kinase B inhibitor Barasertib, has been found to be an essential regulator of chromosome segregation in mitosis [190]. Polo-like kinase inhibitors, such as the advanced phase III inhibitor BI6727 (Volasertib) and the related probe compound BI2536 are also potent and selective cell-cycle kinase inhibitors that induce mitotic arrest and apoptosis by targeting Polo-like kinases [191]. Importantly, these drugs have recently been shown to target bromodomains [192]. Therefore, these inhibitors have gained great attention in targeted therapy and as possible anti-cancer drugs.

The aim of this chapter was to investigate the cellular effects of a panel of 5 UM cell lines to four targeted clinical inhibitors (Table 4.1); the specific Aurora A inhibitor MLN8237 (Alisertib), the specific Aurora B inhibitor AZD1152 (Barasertib), the dual Polo-like kinase inhibitor and bromodomain inhibitor BI6727 (Volasertib) and the bromodomain PPI inhibitor JQ1 (and its inactive stereoisomer JQ1-).

Table 4.1 Targeted clinical inhibitors and their current status in clinical trials

Compound	Mechanism of action	Clinical trials
Alisertib	Aurora kinase A inhibitor	Phase I: Breast cancer, Non-Hodgkin's lymphoma Phase I/II: Gynaecological cancer, Non-small cell lung cancer, Solid tumours Phase II: B cell lymphoma; Brain cancer; Mesothelioma; Prostate cancer; Small cell lung cancer Phase III: Discontinued but many others recruiting
Barasertib	Aurora kinase B inhibitor	Phase I: Acute Myeloid Leukaemia, Myeloid Leukaemia, Lymphoma, Solid tumours Phase II: Acute Myeloid Leukaemia Phase III: Acute Myeloid Leukaemia
Volasertib	Polo-like kinase 1 inhibitors	Phase I: Chronic myelomonocytic leukaemia; Leukaemia; Solid tumours Phase II: Myelodysplastic syndromes; Non-small cell lung cancer; Ovarian cancer Phase III: Acute Myeloid Leukaemia
JQ1	Bromodomain and extraterminal domain protein inhibitors	Not currently in clinical trial due to short half-life however structurally similar BET inhibitors to JQ1; Phase I: NUT Midline carcinoma, Acute Myeloid Leukaemia, Lymphoma, Multiple myeloma, Leukaemia, Multiple Indications Cancer, Advanced Cancer, Solid tumours Phase II: Multiple Indications Cancer, Advanced Cancer, Brain and Central Nervous System Tumours, Head and Neck Cancer, Lymphoma Phase III: Diabetes Mellitus

4.2 Materials and Methods

4.2.1 Small molecule inhibitors

Four small molecules were tested: Bromodomain PPI inhibitor JQ1 and its inactive isomer JQ1-, Aurora kinase A inhibitor Alisertib (MLN8237), Aurora kinase B inhibitor Barasertib (AZD1152) and Polo-like kinase inhibitor Volasertib (BI6727). The inhibitors were kindly provided by Dr Patrick Eyers (University of Liverpool, UK) and diluted from a stock concentration of 10 mM in DMSO. Each experiment / assay was repeated three times.

4.2.2 Cell culture

The UM cell lines 92.1, OMM1, OMM2.5, MEL270 and MM66 were cultured as described in Chapter 2. Each cell line was harvested by standard trypsin procedures, using 0.05% trypsin after cells reached 70% confluence, prior to use in the assay described below.

4.2.3 Sulforhodamine B (SRB) assay

Cells were plated in 96 well plates at 6,250 cells/cm^2 (92.1) and 12,500 cells/cm^2 (OMM1, OMM2.5, MEL270 and MM66), using a multi-pipette, in 100 µl of UM medium A. One plate was fixed at 24 hours, and after 72 hours the appropriate kinase or BRD4 inhibitors were added at varying concentrations to the appropriate wells. Following addition of medium alone or the compounds, plates were fixed every 24 hours by removing the cell culture medium and adding 100 µl 10% trichloroacetic acid (TCA) (10 g TCA flakes/crystals (FisherScientific, UK) in 100 ml H_2O) to each well for 1 hour at 4 ºC. The TCA solution was removed and the plate washed gently with tap water and left to air dry. To visualise cells, 50 µl of Sulforhodamine B (SRB, Sigma) solution (0.4% in 1% acetic acid) was added to each well and the plate incubated for 30 minutes at room temperature. Excess SRB was removed and wells washed with 1% acetic acid until all unincorporated dye had been removed. Plates were air dried

and the incorporated SRB was solubilised in 100 µl 10 mM Tris Base (pH 8.8). The absorbance was measured at a wavelength of 565 nm and background absorbance at 690 nm, measured using a POLARstar Omega plate reader (BMG Labtech, Aylesbury, UK).

4.2.4 Western blotting

4.2.4.1 Preparation of whole cell lysates

92.1 and OMM1 cells were plated at 6,250 cells/cm^2 and 12,500 cells/cm^2 respectively in 10 cm Petri dishes and cultured for 3 days in medium A. On day 3, 92.1 cells were treated with either 220 nM JQ1 (the EC_{50} concentration established in 92.1 cells) or 1 µM JQ1 and OMM1 cells with 1 µM JQ1. Both JQ1$^-$ and DMSO were included as experimental controls. At 24, 48, 72, 96 and 120 hours post addition of compounds, cells were washed once with cold PBS and lysed with 300 µl of lysis buffer (1% SDS, 125 mM Tris pH6.8, 5 mM EDTA, and 10% glycerol). Lysates were kept on ice for 30 minutes then scraped from the Petri dish using a cell scraper into a microfuge tube. The lysates were then sonicated for 30 seconds at 40% power setting and then heated at 95 ºC for 10 minutes. Lysates were centrifuged at 12,000 rpm for 10 minutes, and the supernatant was transferred to a clean microfuge tube for storage at -20 ºC until further use.

4.2.4.2 Protein determination

The protein concentration in lysates was determined using a Bio-Rad DC protein assay kit (Bio-Rad laboratories Ltd, Hertfordshire UK). In brief, a serial dilution of BSA standard (0-2 mg/ml) prepared in SDS lysis buffer was added to wells in a 96 well plate. In separate wells, 5 µl of cell lysate was pipetted. 1 ml of reagent A was mixed with 20 µl of reagent S and 25 µl of this mixture was added to all wells. Finally, 200 µl of reagent B was added to all wells and the plate was incubated in the dark for 15 minutes at room temperature. Absorbance readings were taken at 650 nm, and

protein concentration within the samples was determined by comparison with a standard curve prepared with BSA protein standards. Measurements were considered valid if there was a linear doubling of absorbance with each doubling of protein standard concentration, and the correlation coefficient value for the standard curve was 0.99.

For SDS-PAGE, 10 µg of cell lysates were loaded per well. The volume of each sample applied was equalised with SDS lysis buffer, and then 5X loading sample buffer (5% SDS, 625 mM Tris pH6.8, and 50% glycerol, β- mercaptoethanol and bromophenol blue) was added prior to boiling and gel loading.

4.2.4.3 SDS PolyAcrylamide Gel Electrophoresis (SDS–PAGE) and western blotting

Acrylamide gels (10% Running/Resolving and 5% Stacking gels) (Appendix 8) were used to separate proteins in lysates. In general, 10 µg of total protein was loaded per lane of gel. The Full-Range Rainbow Molecular Weight Marker (GE Healthcare Life Sciences, UK) was also loaded for assessing the molecular weight. Membranes were blocked with the blocking buffer (5% milk in TBS-T (150 mM NaCl, 25 mM Tris pH 7.5, 0.1% Tween 20)) for an hour to reduce non-specific binding between the membranes and antibodies.

Membranes were blocked then probed with the primary antibodies, as detailed in Table 4.2, then washed and incubated with the appropriate secondary antibody (Table 4.3). After a final wash, membranes were developed with Immobilon™ Western Chemiluminescent HRP substrate (MerckMillipore, Watford, UK), and imaged using an LAS-1000 imager (Fujifilm, Japan). Equal protein loading was confirmed by probing the blots with anti β-Actin or Histone H3 antibodies (Table 4.3). Different loading controls were used to avoid overlap of bands with protein of interest, due to the similarities of protein size.

Table 4.2. Primary antibodies

Primary antibody	Species	Dilution	Supplier
Monoclonal c-MYC	Rabbit	1:1000	New England Biolabs 5605
Monoclonal Histone H3	Rabbit	1:10000	Merck Millipore 17-10051
Monoclonal Anti-B-Actin	Mouse	1:10000	Sigma A5316

Table 4.3. Secondary antibodies

Secondary antibody	Dilution	Supplier
Goat anti rabbit HRP	1:5000	Santa Cruz Biotechnology sc-2004
Goat anti mouse HRP	1:10000	Santa Cruz Biotechnology sc-2031

4.2.5 Cell cycle and apoptosis assay by flow cytometry

Evaluation of cell cycle and apoptotic profiles were performed using a TACS Annexin V-FITC Apoptosis Detection Kit (R&D Systems, Abingdon, UK) and analysed on an Attune NxT Flow Cytometer (ThermoFisher Scientific, Loughborough, UK).

4.2.5.1 Preparation of cells

The UM cell lines 92.1 and OMM1 were plated at 6250 cells/cm^2 and 12500 cells/cm^2 respectively in 10 cm Petri dishes. At 3, 6, 24, 48, 72, 96 and 120 hours post addition of compounds, medium was removed and transferred to a fresh tube. Cells from the Petri dishes were harvested with 4 ml of non-enzymatic cell dissociation solution (Sigma-Aldrich, UK) and pooled with the medium prior to centrifugation at 300 x*g* for 5 minutes at room temperature. The supernatant was discarded and the cell pellet was washed in ice cold PBS.

4.2.5.2 Cell fixation prior to cycle analysis

Cells were counted, and a minimum of 5 x 10^5 cells were fixed in 70% ethanol at 4 ºC overnight. They were then washed in in PBS and centrifuged at 2000 rpm for 5 minutes. Cell pellets were re-suspended in 224 µl PBS and 100 ng of RNase A and incubated at room temperature for 30 minutes. 25 µl of propidium iodide (PI) solution (50 µg/ml) was added prior to analysis on the flow cytometer. At least 20,000 events were collected per sample. Data was analysed using Attune NxT Flow Cytometer Software. Forward and side-scatter profiles were obtained from the same samples.

4.2.5.3 Apoptosis

Buffers were prepared according to the instructions provided by the manufacturer. Cells were counted and a minimum of 5 x 10^5 cells were re-suspended in 100 µl Annexin V Incubation Reagent followed by the addition of 400 µl 1X Binding Buffer and incubated in the dark for 15 minutes. Samples were then analysed on the flow cytometer as above.

4.3 Results

4.3.1 SRB assay and determination of IC_{50}

An initial experiment was perfomed to examine the effects of a relatively specific Aurora A or Aurora B kinase inhibitors, a polo-like kinase inhibitor and a BRD4 inhibitor on the growth of UM cells. The UM cell lines in exponential growth were treated for 72 hours and the cell number examined using the SRB assay. At a concentration of 10 µM the Aurora kinase inhibitor, Alisertib (MLN8237) maximally reduced cell number of 92.1 cell line by 45%, MEL270 cell line by 42% and OMM1 cell line by 9%, as compared with untreated control cells (Figure 4.2 A).

At the same concentration, the Aurora kinase inhibitor, Barasertib (AZD1152) maximally reduced cell number of 92.1 cell line by 38%, MEL270 cell line by12%; however, had no effect on cell number on the OMM1 cells (Figure 4.2 B). In contrast, the effects of the polo-like kinase inhibitor Volasertib (BI6727) and the BRD4 inhibitor JQ1 were very much more striking, in terms of effects on cell survival compared with untreated controls. Indeed, Volasertib reduced cell number in the 92.1 and MEL270 cell lines by up to 84% at a concentration of 1 µM, but was less effective in the OMM1 cell line, requiring a 10-fold higher concentration to reduce cell numbers to similar levels (Figure 4.2 C). JQ1 at 1 µM was also more effective in the 92.1 and MEL270 cell lines when compared with the OMM1 cells reducing the cell numbers by 78%, 48% and 38%, respectively (Figure 4.3 A). JQ1 was then subsequently tested on an additional two UM cell lines: OMM2.5 and MM66 (Figure 4.3 B).

The concentration of JQ1 that reduced cell number by 50% (IC_{50}) was then determined by plotting the values on a log scale (Figure 4.4). The EC_{50} of 92.1 cells treated with JQ1 was 220 nM, which is almost five times lower than that of the MEL270 cell line, which exhibited an IC_{50} of 1 µM. OMM1 and MM66 both harbour *GNA11* mutations, compared to the *GNAQ* mutant cell lines 92.1, MEL270 and OMM2.5, and

were the least sensitive to JQ1. Indeed, it was not possible to calculate the IC_{50} over the range of JQ1 concentrations tested for these cells.

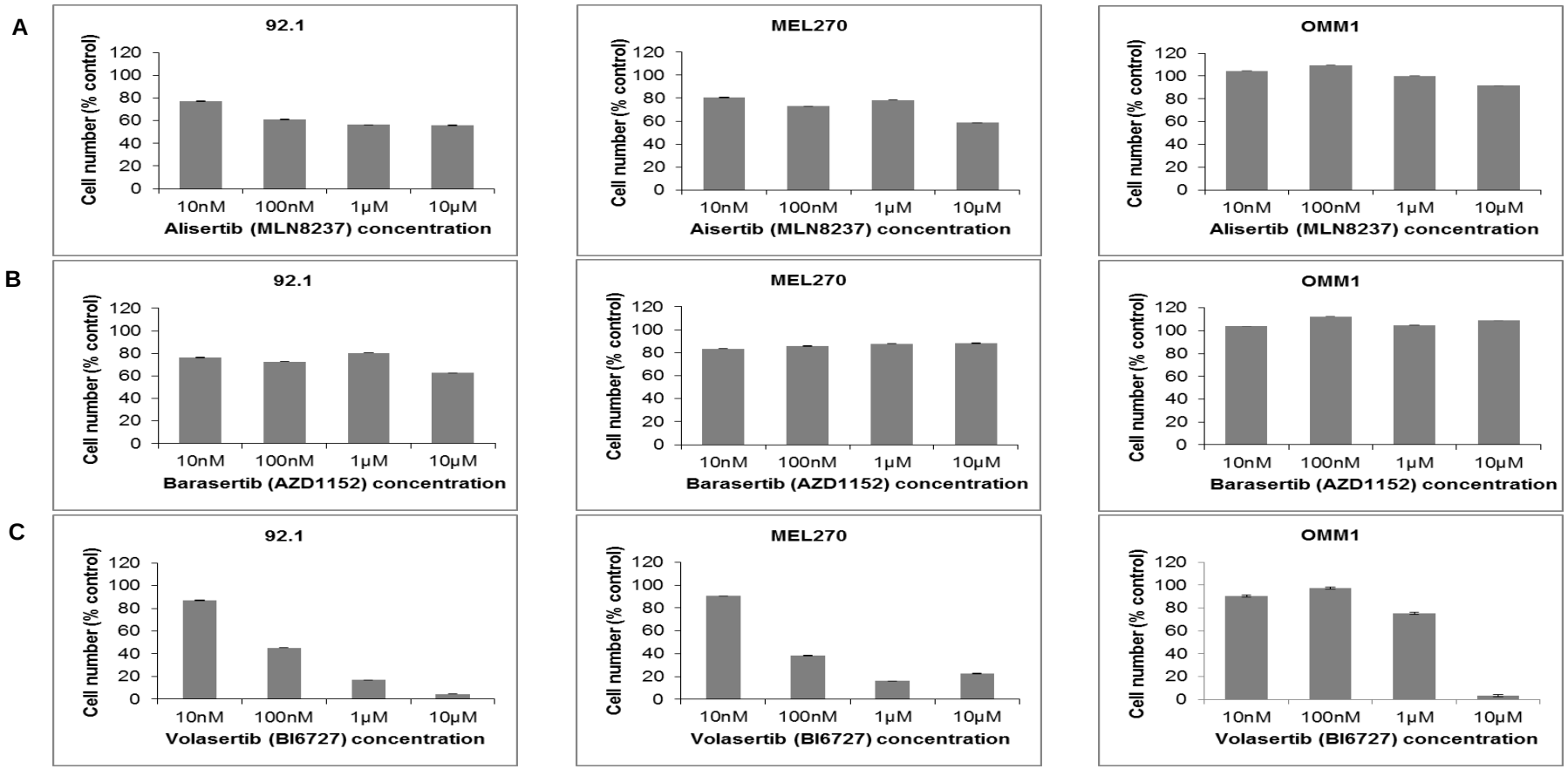

Figure 4.2. Effect of small molecule inhibitors on the growth of UM cell lines. Three UM cell lines, 92.1, MEL270 and OMM1 were examined for the effects of **A.** Aurora A inhibitor Alisertib (MLN8237), **B.** Aurora B inhibitor Barasertib (AZD1152) and **C.** the polo-like kinase inhibitor Volasertib (BI6727) on cell number. Cell lines were exposed to 10-fold serial dilutions over the indicated range. Cell number was quantified using an SRB assay. Bars represent cell number after 72 hours of continuous exposure as compared with DMSO treated control cells. Data are mean ± SEM of 5 technical replicates in a single experiment.

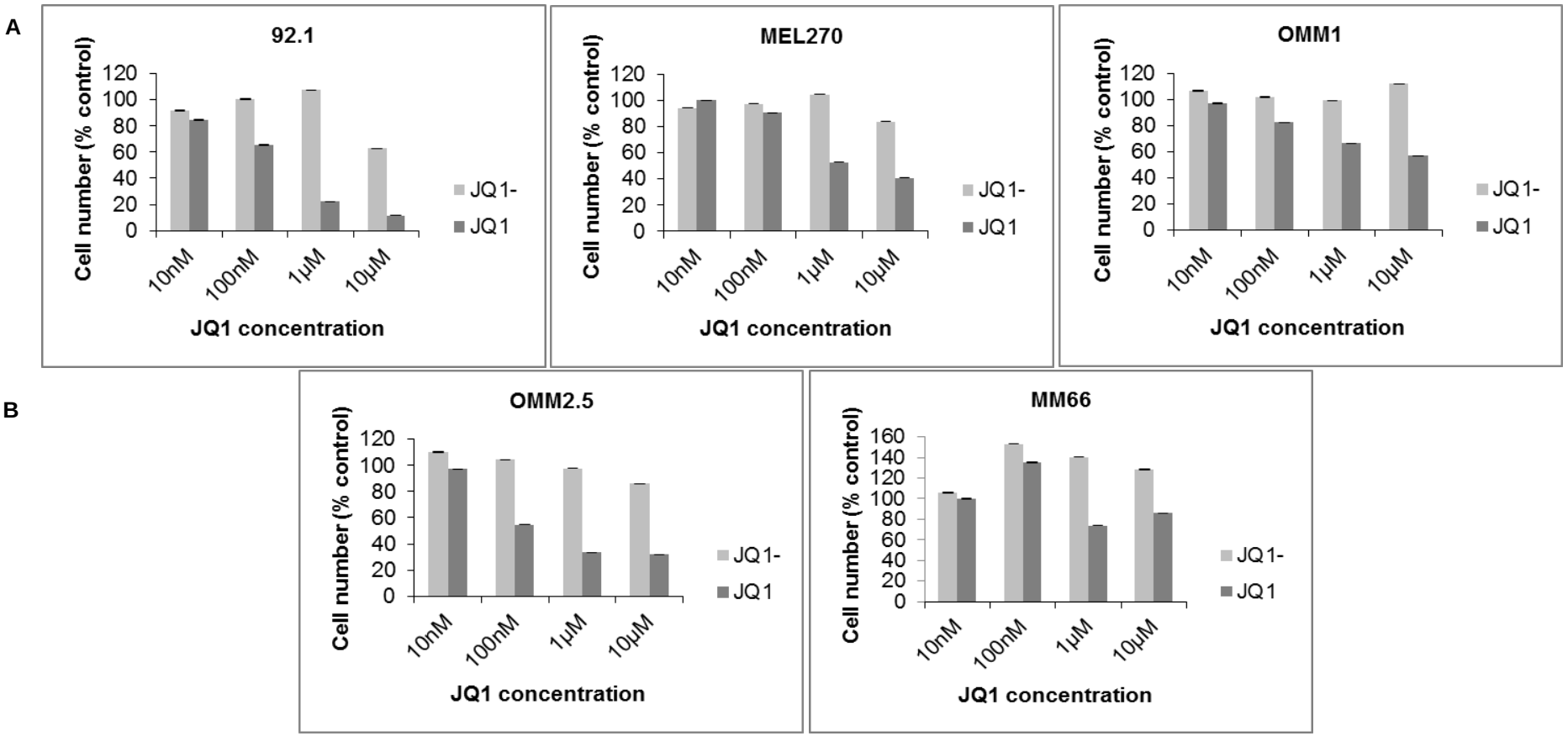

Figure 4.3. Effect of small molecule inhibitor on the growth of UM cell lines. **A** 92.1, MEL270 and OMM1 cell lines and **B**. OMM2.5 and MM66 cell lines. UM cell lines were employed to establish cell numbers after exposure to JQ1 and JQ1-. The cell lines were exposed to 10-fold serial dilutions over the indicated range of the BRD4 PPI inhibitors JQ1 and the inactive stereoisomer JQ1-. Cell number was quantified using an SRB assay. Bars represent cell number after 72 hours of continuous exposure as compared with DMSO treated control cells. Data points are mean ± SEM of 5 technical replicates in a single experiment.

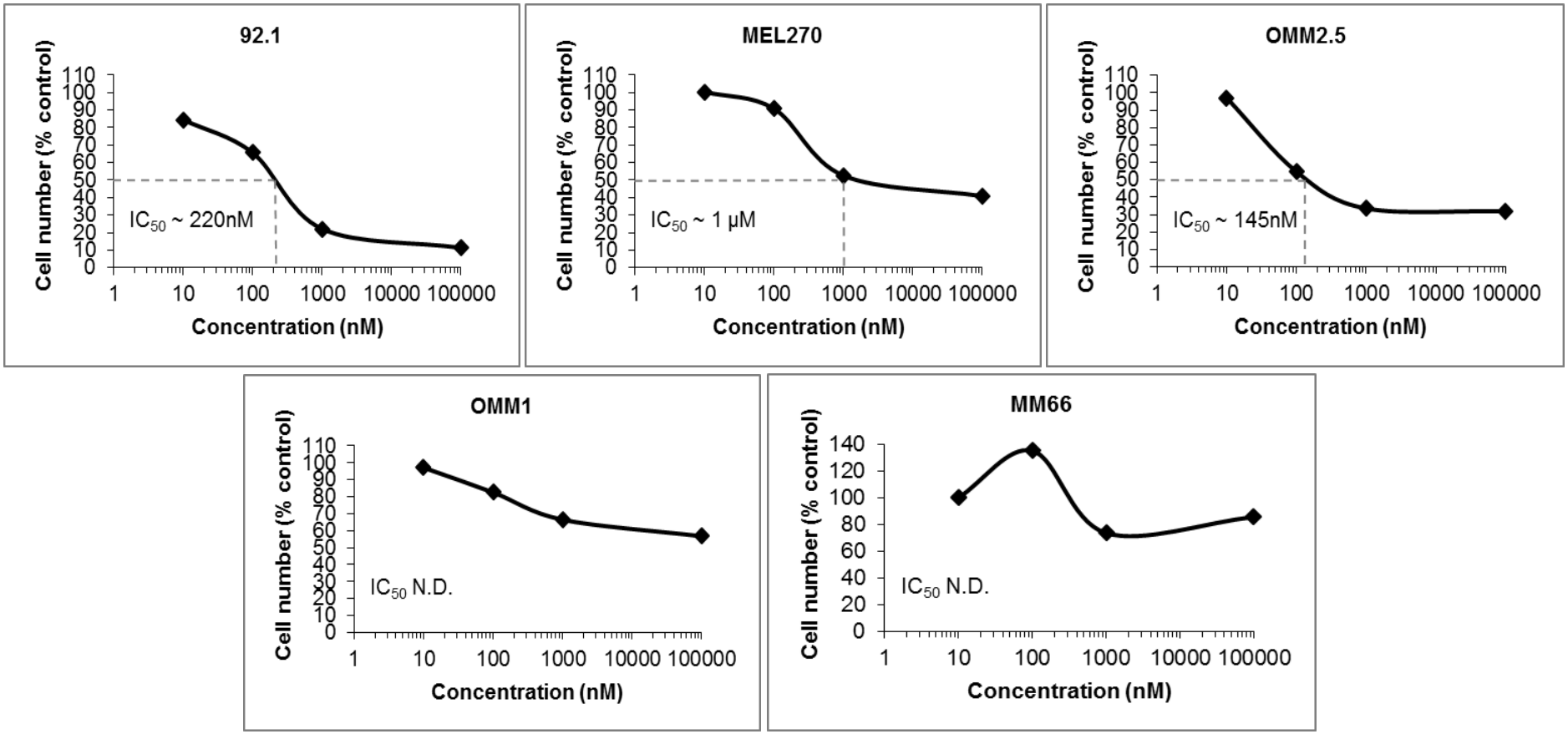

Figure 4.4. Determination of IC_{50} values for JQ1 in UM cell lines. 92.1, MEL270, OMM2.5, OMM1 and MM66 cell lines were exposed to 10-fold serial dilutions of JQ1. IC_{50} values calculated 72 hours after continuous exposure. Cell number was normalised to DMSO-treated cells. Error bars too small to see.

4.3.2 *c-MYC* protein expression levels following treatment of JQ1

Based on the presence of *c-MYC* gene amplification in UM and the previously reported inhibitory effects of JQ1 on c-MYC protein levels, c-MYC protein was examined following treatment of two of the UM cell lines, 92.1 (*GNAQ* mutant) and OMM1 (*GNA11* mutant) with JQ1. To evaluate c-MYC expression, whole cell lysates were prepared at multiple 24-hour intervals following the addition of JQ1. At the IC_{50} concentration of JQ1 (220 nM), c-MYC protein expression was reduced compared with controls in the 92.1 UM cell line. This was seen from 24 hours following compound exposure, and maintained over 72 hours (Figure 4.5 A). The effect was also observed at 1 µM JQ1 in the 92.1 UM cell line at 72 hours following treatment (Figure 4.5 B). However, this effect was not observed with OMM1 cells, where c-MYC barely changed after treatment with 1 µM JQ1 for 24 and 48 hours, and actually increased between 72 and 120 hours after exposure (Figure 4.6).

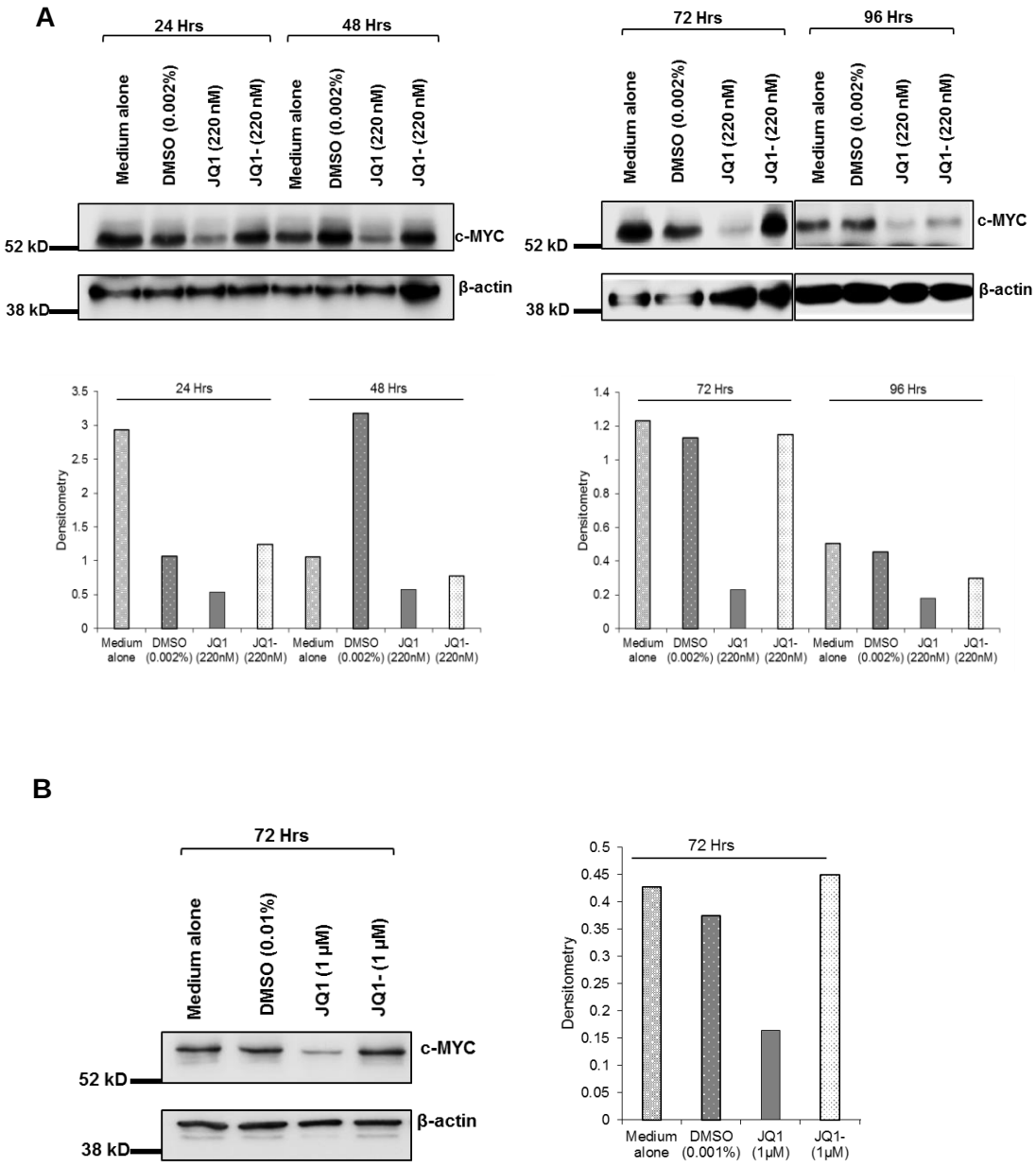

Figure 4.5. JQ1 down-regulates c-MYC expression in 92.1 cells. A. 92.1 cell line was exposed to the IC_{50} concentration of JQ1 (220 nM). Cell lysates were analysed for c-MYC expression and β-actin was used as a loading control, at the indicated time-points after compound addition by western blotting. Respective densitometry also shown. **B.** Cells were exposed to 1 µM JQ1 for 72 hours and processed as in **A.** Respective densitometry also shown.

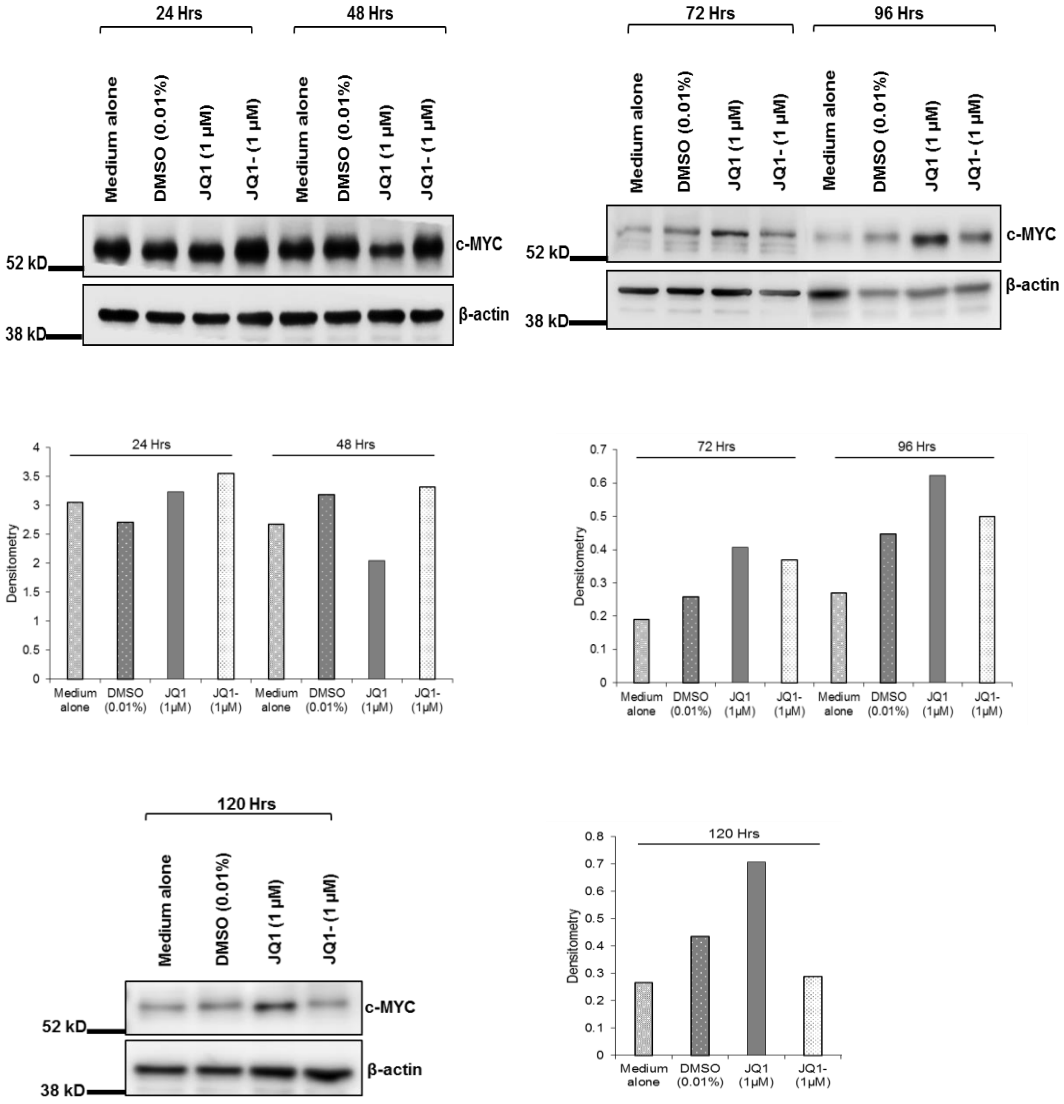

Figure 4.6. Effect of JQ1 on c-MYC expression in OMM1 cells. OMM1 cell line was exposed to 1 µM JQ1. Cell lysates were analysed for c-MYC expression and β-actin was used as a loading control, at the indicated time-points after compound addition by western blotting. Respective densitometry also shown.

4.3.3 Effect of JQ1 on cell cycle profile and apoptosis

Downregulation of *c-MYC* has previously been associated with cell cycle arrest [193]. To investigate the possibility that the JQ1-induced reduction of c-MYC protein levels was also associated with cell cycle arrest, cell cycle profiles (flow cytometry) and western blotting of cyclin D1 levels were examined. 92.1 cells treated with 220 nM JQ1 showed a decrease in the number of cells in S phase with a concomitant increase in cell numbers in G0 / G1 phase as compared with both mock DMSO, JQ1- treated negative control cells. At 24 hours after treatment of 92.1 cells with JQ1, 86% were in G1 phase with only 2% in S phase, compared to 55% and 64% in G1 phase in cells treated with DMSO and JQ1- negative controls respectively, with approximately 20% of cells in S phase in both controls. The G0 / G1 cell cycle arrest was maintained for up to 120 hours following treatment with 220 nM JQ1 (Figure 4.7). A similar G0 / G1 cell cycle arrest was also seen when 92.1 cells were treated at the higher concentration of 1 µM JQ1 over a period of 72 hours (Figure 4.8). Similar results were also obtained with OMM1 cells treated with 1 µM JQ1, with a decrease of cells in S phase and accumulation of cells in the G0 / G1 phase of the cells cycle. At 24 hours after treatment of OMM1 cells with JQ1, 56% were in G1 phase and 6% in S phase compared to DMSO and JQ1- treated negative controls, which showed 48% and 44% in G1 phase and 10% and 15% in S phase respectively. An increase of OMM1 cells in G0 / G1 phase of the cell cycle was maintained up to 120 hours with 86% in G1 and only 2% in S phase compared to 54% and 64% in G1 phase and 20% and 23% in S phase with mock DMSO and JQ1- treated negative control cells (Figure 4.9).

Further assessment of the effects of JQ1 on cell cycle progression was performed by examining cyclin D1 protein levels by western blotting. Cyclin D1 synthesis is required for G1 / S phase transition and accumulates during G1 before being degraded as the cells enter S phase [194]. Upregulation of Cyclin D1 was detected in both 92.1 and

OMM1 cell lines treated with 220 nM and 1 µM JQ1, respectively (Figure 4.10 A and B).

To further understand the mechanism by which JQ1 reduces UM cell number, effects on apoptosis in exposed cells was also evaluated. At the IC_{50} dose, JQ1 failed to induce apoptosis in 92.1 cells, as demonstrated by the Annexin V assay (Figure 4.11). However at the higher concentration of 1 µM JQ1, initiation of apoptosis was detected at 24 hours and this was maintained for up to 72 hours (Figure 4.12). JQ1 at 1 µM failed to induce apoptosis in OMM1 cells (Figure 4.13). These results were further investigated by western blotting with caspase 3, since caspase 3 is one of the executioner caspases activated by proteolytic cleavage during apoptosis. Only uncleaved caspase 3 was observed in the western blots, with no indication of cleaved caspase 3 as a result of apoptosis following treatment with 1 µM JQ1 in either 92.1 or OMM1 cell lines (Figure 4.15 and 4.16). As a control, exposure of both 92.1 and OMM1 cells with 1 µM Staurosporine for 16 hours induced caspase 3 cleavage (Figure 4.14).

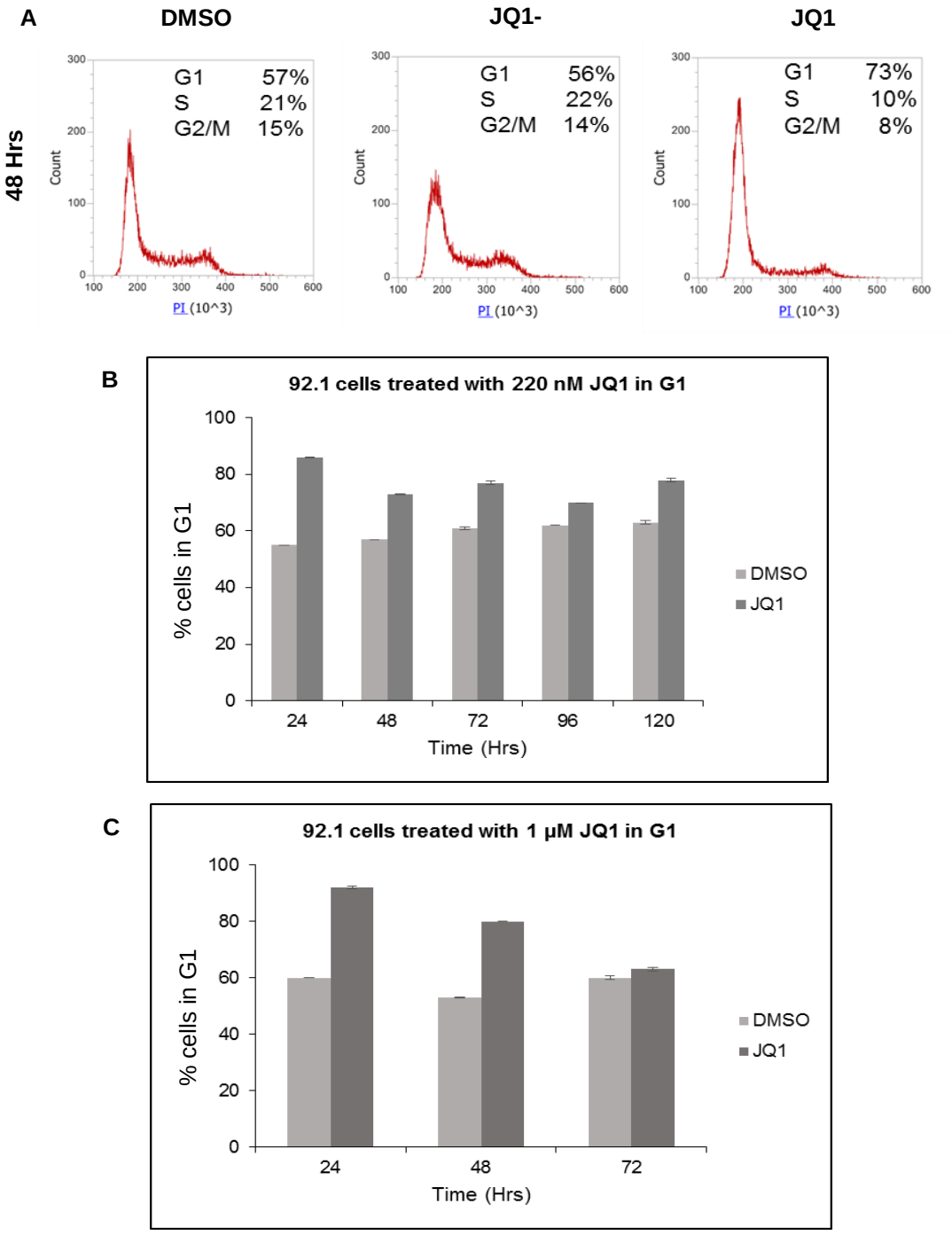

Figure 4.7. Effect of JQ1 on 92.1 cell cycle profile. 92.1 cells were exposed to JQ1 for the indicated times (24 – 120 hours). DNA was stained with PI and the cell cycle distribution was analysed by flow cytometry. **A**. Percentage of cells treated with 220 nM JQ1 in G1, S and G2/M phases are indicated in a representative plot at 48 hours. DNA content was compared to DMSO controls and JQ1-. **B.** Cells treated with 220 nM and **C.** 1 µM JQ1.

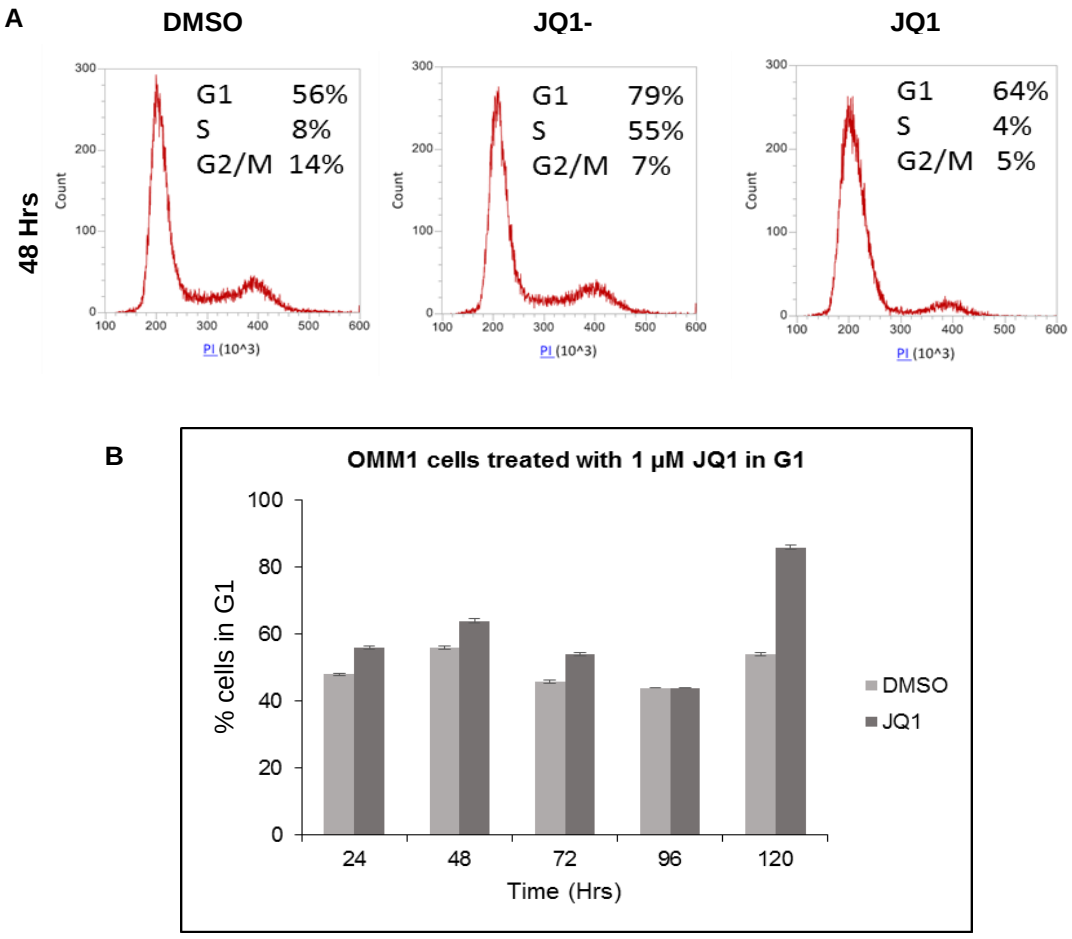

Figure 4.8. Effect of JQ1 on OMM1 cell cycle profile. OMM1 cells were exposed to JQ1 for the indicated times (24 – 120 hours). DNA was stained with PI and the cell cycle distribution was analysed by flow cytometry. **A**. Percentage of cells treated with 220 nM JQ1 in G1, S and G2/M phases are indicated in a representative plot at 48 hours. DNA content was compared to DMSO controls and JQ1-. **B.** Cells treated with 1 µM JQ1.

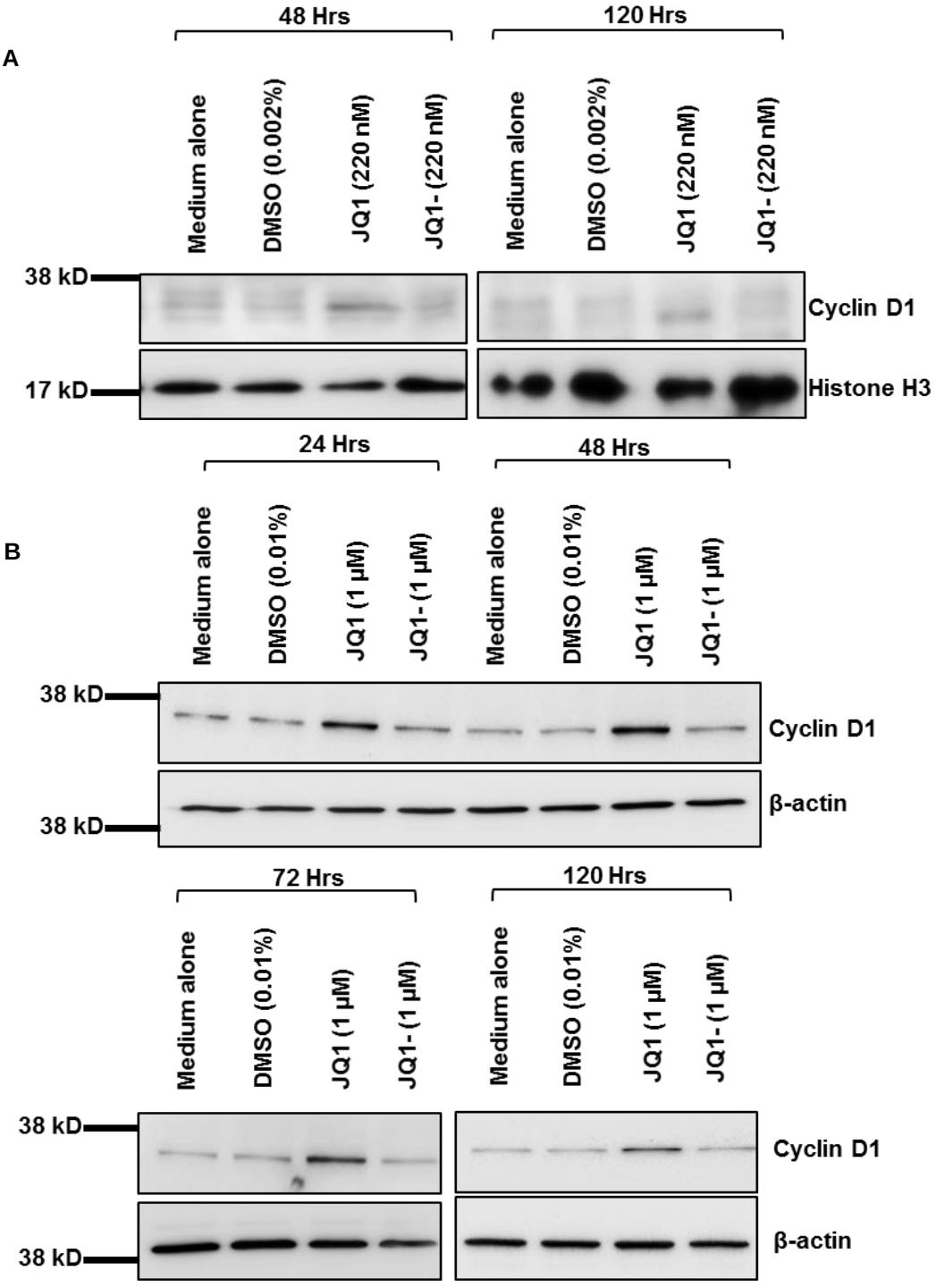

Figure 4.9. JQ1 up-regulates Cyclin D1 expression levels in 92.1 and OMM1 cells. A. 92.1 cells exposed to the EC50 of JQ1 (220 nM) established previously. Cell lysates were analysed for Cyclin D1 levels and Histone H3 was employed as a loading control. **B.** OMM1 cells were exposed to 1 µM JQ1. Cell lysates were analysed for Cyclin D1 levels and β-actin was used as a loading control.

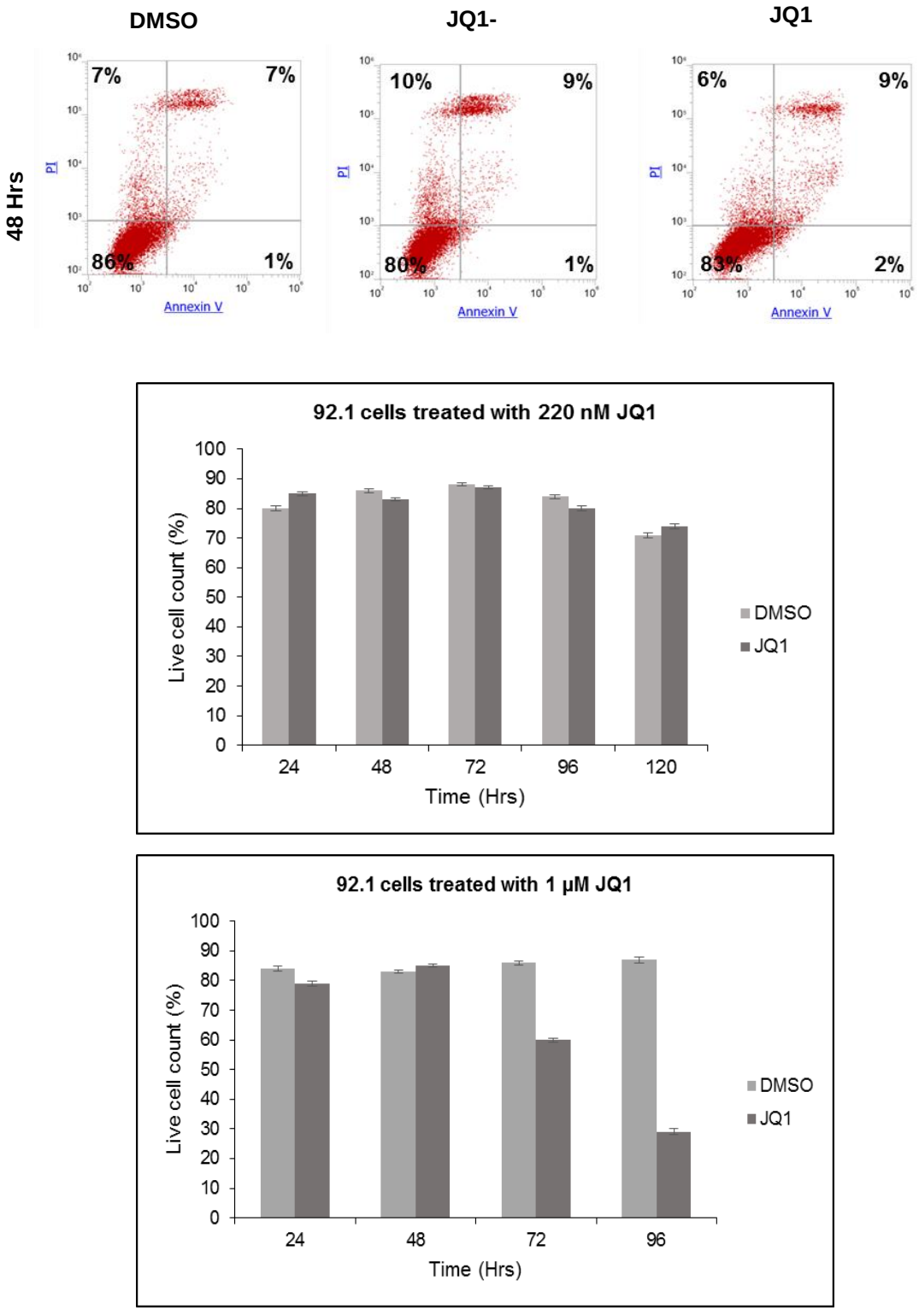

Figure 4.10. Effect of JQ1 on apoptosis in 92.1 cells. A. Analysis of apoptosis by Annexin-V and propidium iodide (PI) double-staining flow cytometry after treatment with 220 nM JQ1, demonstrated in a representative plot at 48 hours. **B.** Percentage of live cells treated with 220 nM JQ1 and **C.** 1 µM JQ1.

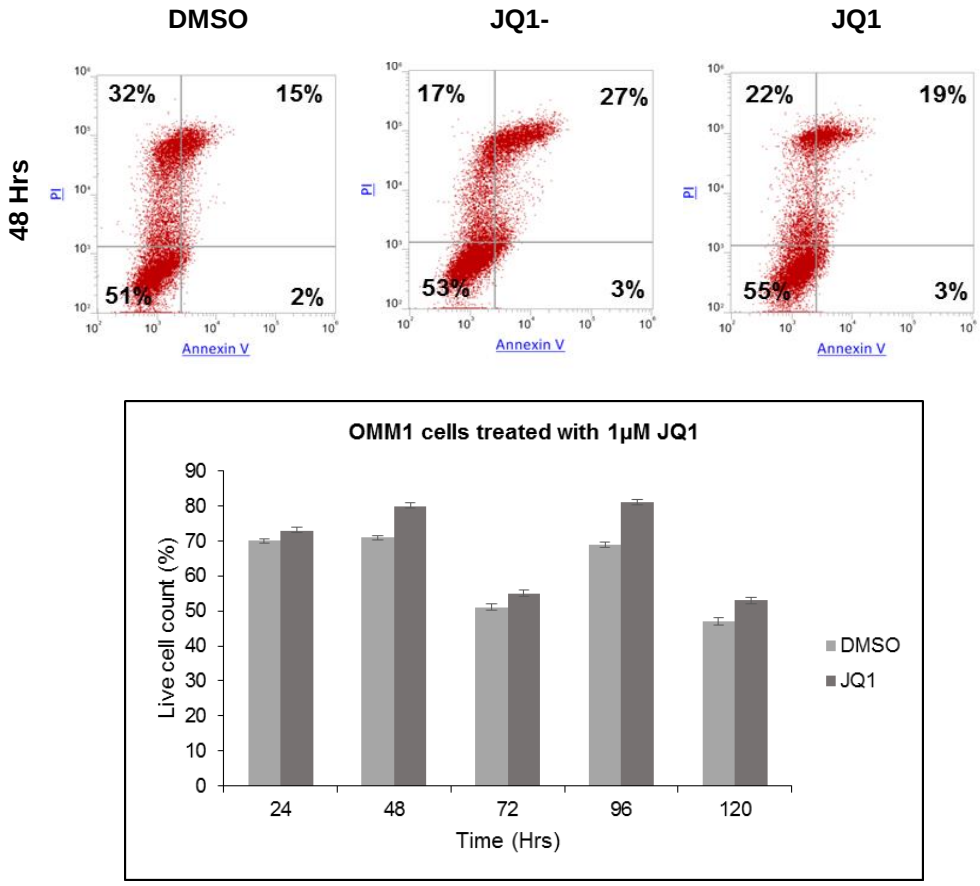

Figure 4.11. Effect of JQ1 on OMM1 cell apoptosis. A. Analysis of apoptosis by Annexin-V and propidium iodide (PI) double-staining flow cytometry after treatment with 1 μM JQ1, demonstrated in a representative plot at 48 hours. **B.** Percentage of live cells treated with 1 μM JQ1.

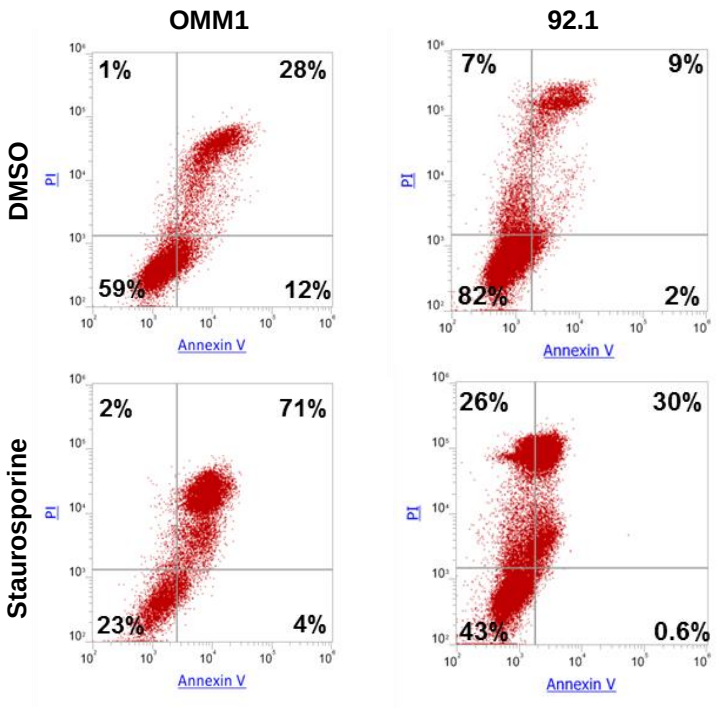

Figure 4.12. Staurosporine causes apoptosis in OMM1 cells and 92.1 cells. Cells were treated with 1μM Staurosporine for 16 hours.

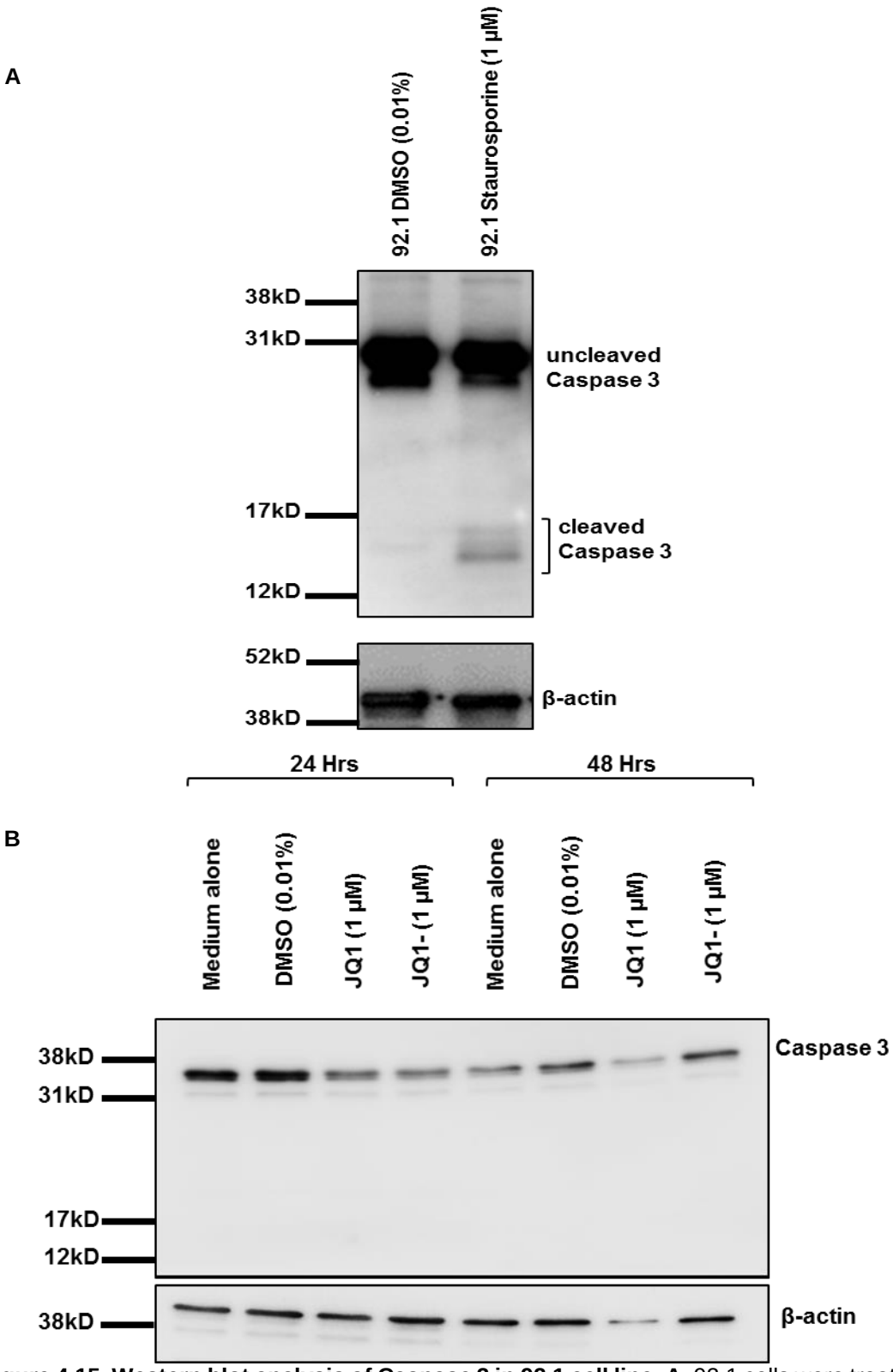

Figure 4.15. Western blot analysis of Caspase 3 in 92.1 cell line. A. 92.1 cells were treated with 1 µM Staurosporine for 16 hours. **B.** 92.1 cells were treated with 1 µM JQ1 at the indicated time points, and lysates subjected to western blot analysis with the indicated antibodies. Note the reduction in total actin and Caspase 3 in 48 hour JQ1 time-point, which may mask effects on cleavage of Caspase 3

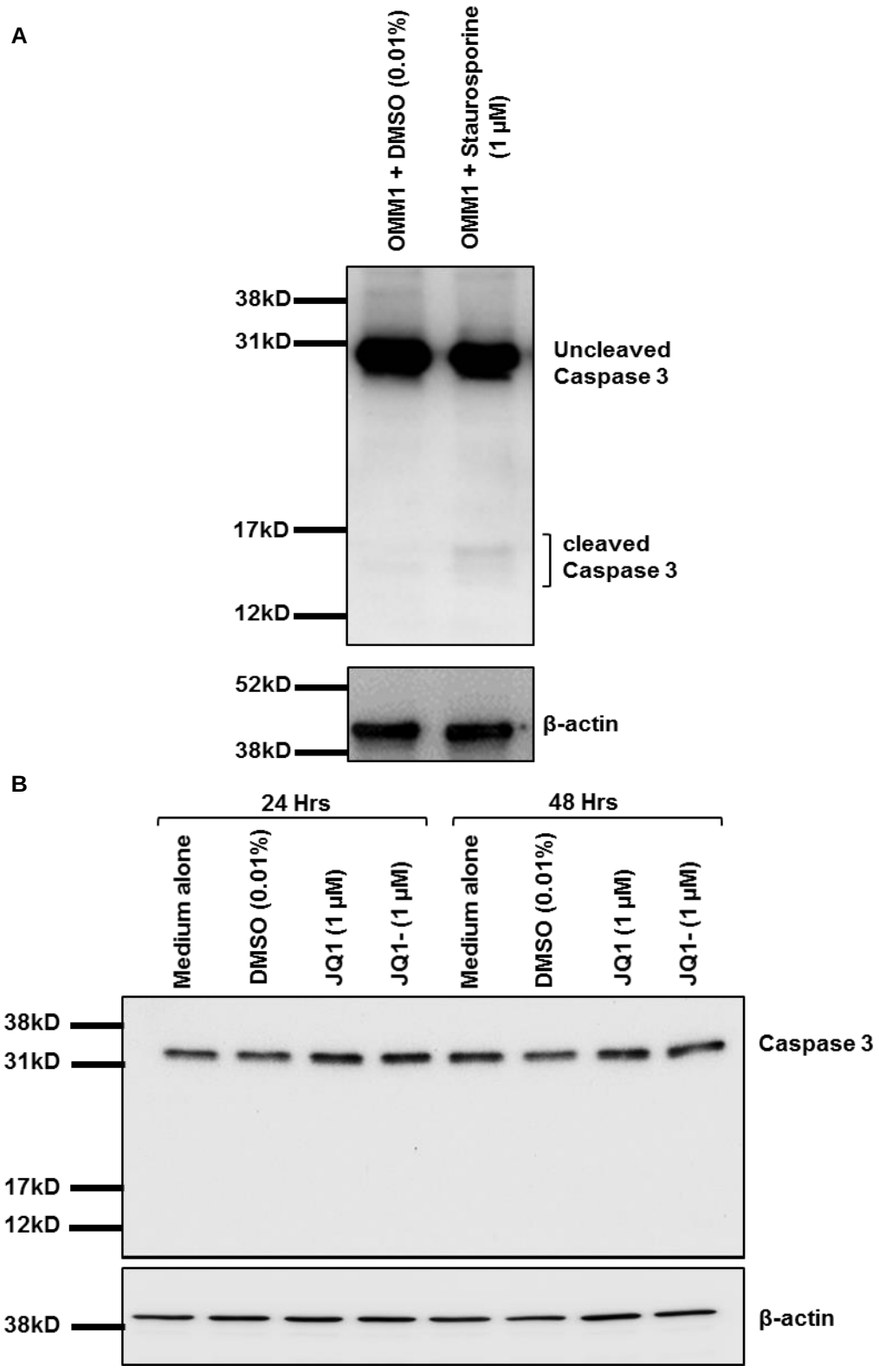

Figure 4.16. Western blot analysis of Caspase 3 in OMM1 cell line. A. OMM1 cells were treated with 1 µM Staurosporine for 16 hours. **B.** OMM1 cells were treated with 1 µM JQ1 at the indicated time points, and lysates subjected to western blot analysis with the indicated antibodies.

4.4 Discussion

Previous studies have demonstrated that extra copies of *MYC* are present in UM [21, 186, 195]. PCR analysis of 600 UM patient samples obtained for prognosis purposes (1998 – 2012) demonstrated amplified *MYC* gene levels in 252 out of the 600 cases (42%). Of these, 155 were also classified as monosomy 3 and survival time of 'high risk' monosomy 3 UM patients is significantly reduced if *MYC* amplification is also present [21]. Unpublished data from MLPA analysis also demonstrated *MYC* amplification in 92.1 cell line, in contrast to the MEL270 cell line. As a result, it has been proposed that *MYC* status represents a novel therapeutic target in a high percentage of 8q-amplified UMs. However, when verifying this with a western blot, there were no obvious differences observed between the c-MYC expression levels of 92.1 and MEL270 cell lines, at least at the protein level. Despite this, interesting results were obtained when the 5 UM cell lines in this study were exposed to a panel of targeted clinical inhibitors that have significant potential for the treatment of human cancer.

Although the Aurora kinase inhibitors did not significantly affect cell number in the UM cell lines here, the Polo-like kinase inhibitor Volasertib and the Bromodomain inhibitor JQ1 reduced 92.1 cell numbers by 84% and 78% respectively (Figure 4.3). Since JQ1 was the most potent drug, and to assess whether a correlation could be confirmed between JQ1 sensitivity and *GNA11* and *GNAQ* mutational status, a further two cell lines OMM2.5 (*GNAQ* mutant) and MM66 (*GNA11* mutant) were evaluated (Figure 4.2). Interestingly, OMM1 and MM66 cell lines, which harbour a *GNA11* mutation, were the least sensitive to JQ1, so that an EC_{50} for each cell line at the range of tested concentrations could not be calculated (Figure 4.4). The other sensitive cell lines tested, including the MEL270 and OMM2.5 cell lines, all harbour *GNAQ* mutations, and are from the same patient as described in Chapter 2. This highlights the importance of different genetic mutations between cell lines and patients, as it shows

how one patient may be less sensitive to a treatment than another based on these mutations. As a result tailoring therapies depending on patients' genetic make-up and molecular profiling are important for targeted therapies and patient stratification. The discovery of key mutations in UM such as *GNAQ / GNA11*, have resulted in significant investigations in the MEK and PKC signalling pathways and consequently in MEK/PKC inhibitors. However, MEK and PKC inhibitors as single target agents have failed to improve overall survival in comparison to chemotherapy; in combination, on the other hand, they have shown promising results, as discussed earlier in this Chapter [175]. Therefore, multiple targeted agents used in combination may be required to effectively treat metastatic UM.

Members of the MYC family of proteins are commonly mutated or amplified in cancers, however it has traditionally been very challenging to target these and to develop drugs that inhibit this transcription factor. Fortunately, experimental BET-domain inhibitors, such as JQ1, have been established as the first of a family of new drugs that inhibit effects of this oncogenic transcription factor and in UM, inhibit tumour progression *in vitro* and also *in vivo* [187]. This is consistent with the findings in this Chapter with JQ1 exposure in 92.1 cell line; however, similar effects were not observed in the OMM1 cell line, in fact an increase in c-MYC levels was seen between 72 and 120 hours following treatment. This could perhaps be due to underlying genetic differences between both cell lines, such as the *GNAQ* / *GNA11* mutations and further cell cycle related proteins. Previous studies have reported alterations in cyclin D1 and related cell-cycle proteins in UM cell lines [196] and UM tissue samples [197]. The latter study, analysed 96 eyes enucleated for UM immunohistochemically for the protein expression of cyclin D1 and related cell-cycle markers. Cyclin D1 positivity (>15% positive tumour cells) was associated with an unfavourable outcome (death from metastasis within the first 5 years). In addition, cyclin D1 positivity was associated with the presence of extraocular melanoma extension, and with the mixed

or epithelioid cell type; therefore, the overexpression of cyclin D1 in UM is associated with a more aggressive course and histologically unfavourable disease [197]. In this investigation, cyclin D1 levels increased in 92.1 and OMM1 cell lines treated with JQ1, consistent with the cell cycle arrest data in this Chapter.

BET inhibitors have been shown to have cytostatic effects in several tumour types, and when used in combination with other drugs, they can induce synergistic effects [198]. Boi and colleagues assessed the preclinical activity of the BET bromodomain inhibitor OTX015 as single agent and in combination in mature B-cell lymphoma models. OTX015 effect was largely cytostatic, with induction of apoptosis in only a genetically defined subset of cell lines, it also inhibits MYC pathway. Furthermore, it shows synergistic or additive effects when combined with several anti-lymphoma agents. Therefore, as mentioned previously, it is likely that multiple targeted agents should be used in combination to effectively treat metastatic disease. It is thought that the *GNAQ/GNA11* mutations are initiating events in UM pathogenesis, as discussed in Chapter 1, and additional mutations, such as inactivating mutations in *BAP1* (located on chromosome 3) are required for metastasis. As a result, HDACi are leading candidates for combination therapy since treatment of UM cells with these inhibitors have shown reduced tumour growth by inducing cell-cycle exit, and a shift to a differentiated, melanocytic gene expression profile [34]. It will be interesting to assess the effects of HDACi on the UM cells employed in this thesis. However, JQ1 independently caused cell cycle arrest in both 92.1 and OMM1 cell lines and as a result, drug combinations may not be necessary for the treatment of some UMs. This was highlighted by Ambrosini and colleagues who showed that combination of JQ1 with other small molecules targeting mutant *GNAQ* signalling did not have a synergistic effect [187].

Further investigations are required to better understand the effects of these compounds on UM cell lines. For example, do the treated UM cells remain in cell cycle

arrest, or do they eventually re-enter the cell cycle and if so, would this pattern be repeated with further application of the compounds. Furthermore, it is unclear why only a slight initiation in apoptosis was seen in 92.1 UM cells treated with JQ1 with no evidence of cleavage of caspase 3, similarly with OMM1 cells. Also of interest for future investigations is Volasertib (BI6727) which, as well as a kinase inhibitor, also targets bromodomains thus acting as a “dual-targeted single agent” [192]. Therefore this compound could potentially offer the same benefits as combination therapies whilst minimising some of the toxic liabilities of combination approaches. Due to time constraints and the necessity to first establish and optimise the baseline assays and drug concentrations, these assays were not conducted in our 3D model. However, these investigations can further be applied to more representative *in vitro* and *in vivo* environments established in this thesis; the compounds can be applied to tumour spheroids where their effect can be observed in a 3D tumour setting outlined in Chapter 2, and further to the chick embryo model system in an *in vivo* environment outlined in Chapter 3. These representative settings will further pave the way for the application of potential clinical trials.

Chapter 5

Conclusions and future perspectives

Advances in the treatment of primary UM have been successful in achieving local tumour control rates of approximately 95%; however metastatic UM remains fatal due to ineffective therapies. Most UM patients who develop liver metastases therefore have a very poor prognosis. The development of *in vitro* and *in vivo* models can provide the necessary tools to better understand disseminated UM, and as pre-clinical models for drug testing.

The scope of this thesis was to develop and characterise *in vitro* and *in vivo* models for the study of UM and its metastases that may be used in preclinical testing. In Chapter 2, the ability to grow and characterise *in vitro* 3D tumour spheroids from patient derived UM samples was described. Attempts with the established UM cell lines to form tumour spheroids proved difficult as they failed to form compact tumour spheroids that were easy to handle. Furthermore, although from the original patient tumour, most established UM cell lines used in studies are limited, since these cell lines have lost many of their original characteristics during repeated passages in culture [199]. In addition, the complexity of cell growth in its *in vivo* environment is far beyond that achieved in 2D culture. 3D spheroid culture using cells isolated from patient tumours is a step towards creating a more representative environment. Chapter 2 demonstrated for the first time that 3D tumour spheroids can be successfully established from UM patient samples in a relatively short timescale and that they retain many morphological and molecular characteristics of the original tumour. For example, the presence of macrophages, a key feature of UM associated with a poorer prognosis, was retained in the tumour spheroids.

Indeed, some of the primary tumour cells failed to form tumour spheroids, however experiments including co-culture experiments to assess the behaviour of the tumour cells with other cells found in their natural environment, such as endothelial cells and / or hepatic cells to mimic the metastatic niche may further enhance the tumour spheroid efficiency and the relevance of these models for pre-clinical testing. In

addition, further studies with a larger panel of tumour cells can provide further insight into determining key mutations and genes that can affect the tumour formation efficiency and what parameters influence spheroid formation. Further investigations of this model as a simple, high throughput method for drug testing and screening warrants investigation and may pave the way to personalised medicine for UM patients. Furthermore, since tumours are enriched with a blood supply in their natural environment, future experiments can recapitulate this by transferring the tumour spheroids to an *in vivo* model.

In Chapter 3, an *in vivo* chick embryo model is described in which not only UM tumour cell morphology, behaviour and migration can be assessed but also with which spontaneous metastasis can be investigated. The majority of animal models are costly, difficult to maintain and time consuming. Currently, there are no representative models of UM; this chapter has presented a cost-effective, efficient and simple chick embryo model with which results can be obtained in a short period of time. A panel of UM cell lines that represent the characteristic genetic and morphological profile in UM were used. Intravenous injections in this model showed homing of the cells to the uveal tract and the liver in a similar manner to UM cells in a patient. Furthermore, the ease of access of this model allowed for a platform, the CAM, for tumour nodule formation. Although these experiments were successfully achieved, certain limitations still remain and future experiments are required to improve this model beyond the initial baseline steps achieved here. For example, spontaneous metastasis was not observed in this model, and there are a substantial number of cells found in organs other than those of interest after intravenous injections of tumour cells. Further studies such as culturing cells in hypoxia and using primary UM cells may lead to spontaneous metastasis demonstrated for other tumours in this model [157]. In addition, longer incubation of the embryos, could determine whether cells found in

other organs would survive. This platform can be further used as an *in vivo* environment to treat these tumour nodules with potential therapeutic drugs.

Although the aims of Chapter 2 and 3 were to optimise the *in vitro* and *in vivo* environments, in order to better understand the processes involved in UM metastasis it is clear that one of the ultimate goals is to establish a preclinical setting in which therapeutic agents can be applied with the aim that they are introduced into clinical trials. Chapter 4 investigated the effects of four targeted clinical inhibitors on UM cell lines. In two UM cell lines, 92.1 and OMM1, JQ1 independently caused cell cycle arrest. Another inhibitor, Volasertib, also showed promising results, however due to time constraints was not examined further. Due to its "dual-targeted single agent" nature discussed in Chapter 4, it would be of great interest to examine its effects further in similar experiments to those performed with JQ1 in this Chapter. The promising results achieved with JQ1 paved the way for many insightful investigations and experiments. Further investigations are required to elaborate on the results achieved in this Chapter; for example, it is unclear why JQ1 causes apoptosis in both 92.1 and OMM1 UM cell lines but does not lead to cleavage of caspase 3, would this effect be observed in additional cell lines and if so, could this be as a result of the different genetic mutations commonly found in UM e.g. *GNA11/GNAQ*. Therefore, these experiments need to be carried out with a larger panel of cell lines that are also representative of common alterations and mutations in UM. For example, the cell lines used in this investigation did not harbour *BAP1* mutations, found in majority of metastasising UM, would these cells behave differently or respond at all, if exposed to the drugs. Furthermore, would the 3D tumour spheroids respond in a similar manner to the cell lines exposed to the drugs in 2D or would they be less / more sensitive or perhaps show no response at all. There is now also accumulating evidence indicating that cell death can occur in a programmed fashion but in complete

absence and independent of caspase activation, therefore, the absence of cleavage of caspase 3 seen here, could also be due to caspase-independent cell death [200].

The 3D tumour spheroids established in Chapter 2 are an ideal next step in assessing the drugs as the 3D environment provides a representative setting that closely represents a solid tumour. A further established environment in Chapter 3, the chick embryo, is an ideal *in vivo* environment with which to assess the effects of these compounds. For example, tumour spheroids can be directly placed onto the CAM and after a period of time when they have recruited blood vessels and adapted to the *in vivo* environment, the compounds can be administered. This can establish a representative *in vivo* setting for pre-clinical drug testing.

Steps such as those uncovered in this thesis can facilitate preclinical analysis of new anticancer compounds against metastatic UM for each UM patient in a time- and cost-effective manner.

Bibliography

1. Kashyap, S., et al., *Uveal melanoma.* Semin Diagn Pathol, 2016.
2. Egan, K.M., et al., *Epidemiologic aspects of uveal melanoma.* Surv Ophthalmol, 1988. **32**(4): p. 239-51.
3. Seddon, J.M., et al., *Host factors, UV radiation, and risk of uveal melanoma. A case-control study.* Arch Ophthalmol, 1990. **108**(9): p. 1274-80.
4. van Hees, C.L., et al., *Are atypical nevi a risk factor for uveal melanoma? A case-control study.* J Invest Dermatol, 1994. **103**(2): p. 202-5.
5. Ewens, K.G., et al., *Genomic profile of 320 uveal melanoma cases: chromosome 8p-loss and metastatic outcome.* Invest Ophthalmol Vis Sci, 2013. **54**(8): p. 5721-9.
6. Singh, A.D., et al., *Uveal melanoma in young patients.* Arch Ophthalmol, 2000. **118**(7): p. 918-23.
7. Damato, B.E. and S.E. Coupland, *Differences in uveal melanomas between men and women from the British Isles.* Eye (Lond), 2012. **26**(2): p. 292-9.
8. Singh, A.D., et al., *Familial uveal melanoma. Clinical observations on 56 patients.* Arch Ophthalmol, 1996. **114**(4): p. 392-9.
9. van Beek, J.G.M., et al., *Diagnosis, Histopathologic and Genetic Classification of Uveal Melanoma*. 2013: INTECH Open Access Publisher.
10. Damato, B. and H. Heimann, *Personalized treatment of uveal melanoma.* Eye (Lond), 2013. **27**(2): p. 172-9.
11. Damato, B., et al., *Proton beam radiotherapy of iris melanoma.* Int J Radiat Oncol Biol Phys, 2005. **63**(1): p. 109-15.
12. Shields, C.L., et al., *Radiation therapy for uveal malignant melanoma.* Ophthalmic Surg Lasers, 1998. **29**(5): p. 397-409.
13. Mashayekhi, A., et al., *Primary transpupillary thermotherapy for choroidal melanoma in 391 cases: importance of risk factors in tumor control.* Ophthalmology, 2015. **122**(3): p. 600-9.
14. Damato, B., et al., *Artificial neural networks estimating survival probability after treatment of choroidal melanoma.* Ophthalmology, 2008. **115**(9): p. 1598-607.
15. Damato, B., et al., *Estimating prognosis for survival after treatment of choroidal melanoma.* Prog Retin Eye Res, 2011. **30**(5): p. 285-95.
16. Damato, B., et al., *Cytogenetics of uveal melanoma: a 7-year clinical experience.* Ophthalmology, 2007. **114**(10): p. 1925-31.
17. Toivonen, P., et al., *Microcirculation and tumor-infiltrating macrophages in choroidal and ciliary body melanoma and corresponding metastases.* Invest Ophthalmol Vis Sci, 2004. **45**(1): p. 1-6.
18. Ksander, B.R., et al., *Uveal melanomas contain antigenically specific and non-specific infiltrating lymphocytes.* Curr Eye Res, 1998. **17**(2): p. 165-73.
19. Prescher, G., et al., *Prognostic implications of monosomy 3 in uveal melanoma.* Lancet, 1996. **347**(9010): p. 1222-5.
20. Coupland, S.E., et al., *Molecular pathology of uveal melanoma.* Eye (Lond), 2013. **27**(2): p. 230-42.
21. Caines, R., et al., *Cluster analysis of multiplex ligation-dependent probe amplification data in choroidal melanoma.* Mol Vis, 2015. **21**: p. 1-11.
22. McCarthy, C., et al., *Insights into genetic alterations of liver metastases from uveal melanoma.* Pigment Cell Melanoma Res, 2016. **29**(1): p. 60-7.

23. White, V.A., et al., *Correlation of cytogenetic abnormalities with the outcome of patients with uveal melanoma.* Cancer, 1998. **83**(2): p. 354-9.
24. Damato, B., J.A. Dopierala, and S.E. Coupland, *Genotypic profiling of 452 choroidal melanomas with multiplex ligation-dependent probe amplification.* Clin Cancer Res, 2010. **16**(24): p. 6083-92.
25. Van Raamsdonk, C.D., et al., *Frequent somatic mutations of GNAQ in uveal melanoma and blue naevi.* Nature, 2009. **457**(7229): p. 599-602.
26. Luke, J.J., et al., *Biology of advanced uveal melanoma and next steps for clinical therapeutics.* Pigment Cell Melanoma Res, 2015. **28**(2): p. 135-47.
27. Griewank, K.G. and R. Murali, *Pathology and genetics of uveal melanoma.* Pathology, 2013. **45**(1): p. 18-27.
28. Harbour, J.W., et al., *Frequent mutation of BAP1 in metastasizing uveal melanomas.* Science, 2010. **330**(6009): p. 1410-3.
29. Farmer, H., et al., *Targeting the DNA repair defect in BRCA mutant cells as a therapeutic strategy.* Nature, 2005. **434**(7035): p. 917-21.
30. Koopmans, A.E., et al., *Clinical significance of immunohistochemistry for detection of BAP1 mutations in uveal melanoma.* Mod Pathol, 2014. **27**(10): p. 1321-30.
31. Kalirai, H., et al., *Lack of BAP1 protein expression in uveal melanoma is associated with increased metastatic risk and has utility in routine prognostic testing.* Br J Cancer, 2014. **111**(7): p. 1373-80.
32. Matatall, K.A., et al., *BAP1 deficiency causes loss of melanocytic cell identity in uveal melanoma.* BMC Cancer, 2013. **13**: p. 371.
33. Abdel-Rahman, M.H., et al., *Germline BAP1 mutation predisposes to uveal melanoma, lung adenocarcinoma, meningioma, and other cancers.* J Med Genet, 2011. **48**(12): p. 856-9.
34. Landreville, S., et al., *Histone deacetylase inhibitors induce growth arrest and differentiation in uveal melanoma.* Clin Cancer Res, 2012. **18**(2): p. 408-16.
35. Harbour, J.W., et al., *Recurrent mutations at codon 625 of the splicing factor SF3B1 in uveal melanoma.* Nat Genet, 2013. **45**(2): p. 133-5.
36. Griewank, K.G., et al., *Genetic and clinico-pathologic analysis of metastatic uveal melanoma.* Mod Pathol, 2014. **27**(2): p. 175-83.
37. Furney, S.J., et al., *SF3B1 mutations are associated with alternative splicing in uveal melanoma.* Cancer Discov, 2013. **3**(10): p. 1122-9.
38. Johansson, P., et al., *Deep sequencing of uveal melanoma identifies a recurrent mutation in PLCB4.* Oncotarget, 2016. **7**(4): p. 4624-31.
39. Martin, M., et al., *Exome sequencing identifies recurrent somatic mutations in EIF1AX and SF3B1 in uveal melanoma with disomy 3.* Nat Genet, 2013. **45**(8): p. 933-6.
40. Eskelin, S., et al., *A prognostic model and staging for metastatic uveal melanoma.* Cancer, 2003. **97**(2): p. 465-75.
41. Augsburger, J.J., Z.M. Correa, and A.H. Shaikh, *Effectiveness of treatments for metastatic uveal melanoma.* Am J Ophthalmol, 2009. **148**(1): p. 119-27.
42. Patel, M., et al., *Therapeutic implications of the emerging molecular biology of uveal melanoma.* Clin Cancer Res, 2011. **17**(8): p. 2087-100.
43. Coupland, S.E., et al., *Metastatic choroidal melanoma to the contralateral orbit 40 years after enucleation.* Arch Ophthalmol, 1996. **114**(6): p. 751-6.
44. Blanco, P.L., et al., *Uveal melanoma dormancy: an acceptable clinical endpoint?* Melanoma Res, 2012. **22**(5): p. 334-40.
45. Grossniklaus, H.E., *Progression of ocular melanoma metastasis to the liver: the 2012 Zimmerman lecture*, in *JAMA Ophthalmol*. 2013: United States. p. 462-9.
46. Dithmar, S., D.M. Albert, and H.E. Grossniklaus, *Animal models of uveal melanoma.* Melanoma Res, 2000. **10**(3): p. 195-211.

47. Tolleson, W.H., et al., *Spontaneous uveal amelanotic melanoma in transgenic Tyr-RAS+ Ink4a/Arf-/- mice.* Arch Ophthalmol, 2005. **123**(8): p. 1088-94.
48. Ma, D. and J.Y. Niederkorn, *Efficacy of tumor-infiltrating lymphocytes in the treatment of hepatic metastases arising from transgenic intraocular tumors in mice*. Invest Ophthalmol Vis Sci, 1995. **36**(6): p. 1067-75.
49. Schiffner, S., et al., *Tg(Grm1) transgenic mice: a murine model that mimics spontaneous uveal melanoma in humans?* Exp Eye Res, 2014. **127**: p. 59-68.
50. Cao, J. and M.J. Jager, *Animal Eye Models for Uveal Melanoma.* Ocul Oncol Pathol, 2015. **1**(3): p. 141-50.
51. Greene, H.S., *A spontaneous melanoma in the hamster with a propensity for amelanotic alteration and sarcomatous transformation during transplantation.* Cancer Res, 1958. **18**(4): p. 422-5.
52. Journee-de Korver, J.G., et al., *Transpupillary thermotherapy (TTT) by infrared irradiation of choroidal melanoma.* Doc Ophthalmol, 1992. **82**(3): p. 185-91.
53. Journee-de Korver, J.G., J.A. Oosterhuis, and G.F. Vrensen, *Light and electron microscopic findings on experimental melanomas after hyperthermia at 50 degrees C.* Melanoma Res, 1995. **5**(6): p. 393-402.
54. Rem, A.I., et al., *Transscleral laser thermotherapy of hamster Greene melanoma: inducing tumour necrosis without scleral damage.* Melanoma Res, 2001. **11**(5): p. 503-9.
55. Bomirski, A., A. Slominski, and J. Bigda, *The natural history of a family of transplantable melanomas in hamsters.* Cancer Metastasis Rev, 1988. **7**(2): p. 95-118.
56. Urbanska, K., et al., *Experimental ruthenium plaque therapy of amelanotic and melanotic melanomas in the hamster eye.* Melanoma Res, 2000. **10**(1): p. 26-35.
57. Romanowska-Dixon, B., et al., *Angiomorphology of the pigmented Bomirski melanoma growing in hamster eye.* Ann Anat, 2001. **183**(6): p. 559-65.
58. Greene, H.S. and E.K. Harvey, *The growth and metastasis of amelanotic melanomas in heterologous hosts.* Cancer Res, 1966. **26**(4): p. 706-14.
59. Rem, A.I., et al., *Transscleral thermotherapy with laser-induced and conductive heating in hamster Greene melanoma.* Melanoma Res, 2004. **14**(5): p. 409-14.
60. Braun, R.D., et al., *Hemodynamic parameters in blood vessels in choroidal melanoma xenografts and rat choroid.* Invest Ophthalmol Vis Sci, 2002. **43**(9): p. 3045-52.
61. Braun, R.D. and K.S. Vistisen, *Modeling human choroidal melanoma xenograft growth in immunocompromised rodents to assess treatment efficacy.* Invest Ophthalmol Vis Sci, 2012. **53**(6): p. 2693-701.
62. Braun, R.D. and A. Abbas, *Orthotopic human choroidal melanoma xenografts in nude rats with aggressive and nonaggressive PAS staining patterns.* Invest Ophthalmol Vis Sci, 2006. **47**(1): p. 7-16.
63. Braun, R.D. and K.S. Vistisen, *Measurement of human choroidal melanoma xenograft volume in rats using high-frequency ultrasound.* Invest Ophthalmol Vis Sci, 2008. **49**(1): p. 16-22.
64. Hill, R.A., et al., *Photodynamic therapy of ocular melanoma with bis silicon 2,3-naphthalocyanine in a rabbit model.* Invest Ophthalmol Vis Sci, 1995. **36**(12): p. 2476-81.
65. Blanco, P.L., et al., *Characterization of ocular and metastatic uveal melanoma in an animal model.* Invest Ophthalmol Vis Sci, 2005. **46**(12): p. 4376-82.
66. Krause, M.H., et al., *MRI of blood volume with MS 325 in experimental choroidal melanoma.* Magn Reson Imaging, 2003. **21**(7): p. 725-32.
67. Krause, M., et al., *MRI of blood volume and cellular uptake of superparamagnetic iron in an animal model of choroidal melanoma.* Ophthalmic Res, 2002. **34**(4): p. 241-50.

68. Krause, M.H., et al., *Treatment of experimental choroidal melanoma with an Nd:yttrium-lanthanum-fluoride laser at 1047 nm.* Arch Ophthalmol, 2003. **121**(3): p. 357-63.
69. Hu, L.K., et al., *Establishment of pigmented choroidal melanomas in a rabbit model.* Retina, 1994. **14**(3): p. 264-9.
70. Mueller, A.J., et al., *Evaluation of the human choroidal melanoma rabbit model for studying microcirculation patterns with confocal ICG and histology.* Exp Eye Res, 1999. **68**(6): p. 671-8.
71. Blanco, G., et al., *Uveal melanoma model with metastasis in rabbits: effects of different doses of cyclosporine A.* Curr Eye Res, 2000. **21**(3): p. 740-7.
72. Bonicel, P., et al., *Establishment of IPC 227 cells as human xenografts in rabbits: a model of uveal melanoma.* Melanoma Res, 2000. **10**(5): p. 445-50.
73. Lopez-Velasco, R., et al., *Efficacy of five human melanocytic cell lines in experimental rabbit choroidal melanoma.* Melanoma Res, 2005. **15**(1): p. 29-37.
74. Marshall, J.C., et al., *The use of a cyclooxygenase-2 inhibitor (Nepafenac) in an ocular and metastatic animal model of uveal melanoma.* Carcinogenesis, 2007. **28**(9): p. 2053-8.
75. Marshall, J.C., et al., *Transcriptional profiling of human uveal melanoma from cell lines to intraocular tumors to metastasis.* Clin Exp Metastasis, 2007. **24**(5): p. 353-62.
76. Di Cesare, S., et al., *The effect of blue light exposure in an ocular melanoma animal model.* J Exp Clin Cancer Res, 2009. **28**: p. 48.
77. Kang, S.J., et al., *In vivo high-frequency contrast-enhanced ultrasonography of choroidal melanoma in rabbits: imaging features and histopathologic correlations.* Br J Ophthalmol, 2013. **97**(7): p. 929-33.
78. Lambrou, F.H., et al., *A new technique for subchoroidal implantation of experimental malignant melanoma.* Invest Ophthalmol Vis Sci, 1988. **29**(6): p. 995-8.
79. Romer, T.J., et al., *Hamster Greene melanoma implanted in the anterior chamber of a rabbit eye: a reliable tumor model?* Ophthalmic Res, 1992. **24**(2): p. 119-24.
80. De Waard-Siebinga, I., et al., *Establishment and characterization of an uveal-melanoma cell line.* Int J Cancer, 1995. **62**(2): p. 155-61.
81. Grossniklaus, H.E., et al., *Anterior vs posterior intraocular melanoma. Metastatic differences in a murine model.* Arch Ophthalmol, 1996. **114**(9): p. 1116-20.
82. Niederkorn, J.Y., *Enucleation in consort with immunologic impairment promotes metastasis of intraocular melanomas in mice.* Invest Ophthalmol Vis Sci, 1984. **25**(9): p. 1080-6.
83. Knisely, T.L. and J.Y. Niederkorn, *Immunologic evaluation of spontaneous regression of an intraocular murine melanoma.* Invest Ophthalmol Vis Sci, 1990. **31**(2): p. 247-57.
84. Grossniklaus, H.E., B.C. Barron, and M.W. Wilson, *Murine model of anterior and posterior ocular melanoma.* Curr Eye Res, 1995. **14**(5): p. 399-404.
85. Ly, L.V., et al., *In aged mice, outgrowth of intraocular melanoma depends on proangiogenic M2-type macrophages.* J Immunol, 2010. **185**(6): p. 3481-8.
86. de Lange, J., et al., *Synergistic growth inhibition based on small-molecule p53 activation as treatment for intraocular melanoma.* Oncogene, 2012. **31**(9): p. 1105-16.
87. Diaz, C.E., et al., *B16LS9 melanoma cells spread to the liver from the murine ocular posterior compartment (PC).* Curr Eye Res, 1999. **18**(2): p. 125-9.
88. Yang, H. and H.E. Grossniklaus, *Constitutive overexpression of pigment epithelium-derived factor inhibition of ocular melanoma growth and metastasis.* Invest Ophthalmol Vis Sci, 2010. **51**(1): p. 28-34.

89. Zhang, Q., et al., *In vivo high-frequency, contrast-enhanced ultrasonography of uveal melanoma in mice: imaging features and histopathologic correlations.* Invest Ophthalmol Vis Sci, 2011. **52**(5): p. 2662-8.
90. Yang, W., et al., *NKT cell exacerbation of liver metastases arising from melanomas transplanted into either the eyes or spleens of mice.* Invest Ophthalmol Vis Sci, 2011. **52**(6): p. 3094-102.
91. Niederkorn, J.Y., et al., *Effect of anti-ganglioside antibodies on the metastatic spread of intraocular melanomas in a nude mouse model of human uveal melanoma.* Curr Eye Res, 1993. **12**(4): p. 347-58.
92. Ma, D., et al., *Association between NM23-H1 gene expression and metastasis of human uveal melanoma in an animal model.* Invest Ophthalmol Vis Sci, 1996. **37**(11): p. 2293-301.
93. Ma, D., et al., *Inhibition of metastasis of intraocular melanomas by adenovirus-mediated gene transfer of plasminogen activator inhibitor type 1 (PAI-1) in an athymic mouse model.* Blood, 1997. **90**(7): p. 2738-46.
94. Ma, D. and J.Y. Niederkorn, *Role of epidermal growth factor receptor in the metastasis of intraocular melanomas.* Invest Ophthalmol Vis Sci, 1998. **39**(7): p. 1067-75.
95. van Ginkel, P.R., et al., *Resveratrol inhibits uveal melanoma tumor growth via early mitochondrial dysfunction.* Invest Ophthalmol Vis Sci, 2008. **49**(4): p. 1299-306.
96. Triozzi, P.L., W. Aldrich, and A. Singh, *Effects of interleukin-1 receptor antagonist on tumor stroma in experimental uveal melanoma.* Invest Ophthalmol Vis Sci, 2011. **52**(8): p. 5529-35.
97. Surriga, O., et al., *Crizotinib, a c-Met inhibitor, prevents metastasis in a metastatic uveal melanoma model.* Mol Cancer Ther, 2013. **12**(12): p. 2817-26.
98. Heegaard, S., M. Spang-Thomsen, and J.U. Prause, *Establishment and characterization of human uveal malignant melanoma xenografts in nude mice.* Melanoma Res, 2003. **13**(3): p. 247-51.
99. Garber, K., *From human to mouse and back: 'tumorgraft' models surge in popularity*, in *J Natl Cancer Inst*. 2009: United States. p. 6-8.
100. Decaudin, D., *Primary human tumor xenografted models ('tumorgrafts') for good management of patients with cancer.* Anticancer Drugs, 2011. **22**(9): p. 827-41.
101. Nemati, F., et al., *Establishment and characterization of a panel of human uveal melanoma xenografts derived from primary and/or metastatic tumors.* Clin Cancer Res, 2010. **16**(8): p. 2352-62.
102. Amirouchene-Angelozzi, N., et al., *Establishment of novel cell lines recapitulating the genetic landscape of uveal melanoma and preclinical validation of mTOR as a therapeutic target.* Mol Oncol, 2014. **8**(8): p. 1508-20.
103. Griewank, K.G., et al., *Genetic and molecular characterization of uveal melanoma cell lines.* Pigment Cell Melanoma Res, 2012. **25**(2): p. 182-7.
104. van der Ent, W., et al., *Embryonic Zebrafish: Different Phenotypes after Injection of Human Uveal Melanoma Cells.* Ocul Oncol Pathol, 2015. **1**(3): p. 170-81.
105. Kim, T.H., et al., *The delivery of doxorubicin to 3-D multicellular spheroids and tumors in a murine xenograft model using tumor-penetrating triblock polymeric micelles.* Biomaterials, 2010. **31**(28): p. 7386-97.
106. Vinci, M., et al., *Advances in establishment and analysis of three-dimensional tumor spheroid-based functional assays for target validation and drug evaluation.* BMC Biol, 2012. **10**: p. 29.
107. Sutherland, R.M., J.A. McCredie, and W.R. Inch, *Growth of multicell spheroids in tissue culture as a model of nodular carcinomas.* J Natl Cancer Inst, 1971. **46**(1): p. 113-20.

108. Achilli, T.M., J. Meyer, and J.R. Morgan, *Advances in the formation, use and understanding of multi-cellular spheroids.* Expert Opin Biol Ther, 2012. **12**(10): p. 1347-60.
109. Frith, J.E., B. Thomson, and P.G. Genever, *Dynamic three-dimensional culture methods enhance mesenchymal stem cell properties and increase therapeutic potential.* Tissue Eng Part C Methods, 2010. **16**(4): p. 735-49.
110. Desroches, B.R., et al., *Functional scaffold-free 3-D cardiac microtissues: a novel model for the investigation of heart cells.* Am J Physiol Heart Circ Physiol, 2012. **302**(10): p. H2031-42.
111. Ivascu, A. and M. Kubbies, *Diversity of cell-mediated adhesions in breast cancer spheroids.* Int J Oncol, 2007. **31**(6): p. 1403-13.
112. Landry, J., et al., *Spheroidal aggregate culture of rat liver cells: histotypic reorganization, biomatrix deposition, and maintenance of functional activities.* J Cell Biol, 1985. **101**(3): p. 914-23.
113. Kelm, J.M., et al., *Method for generation of homogeneous multicellular tumor spheroids applicable to a wide variety of cell types.* Biotechnol Bioeng, 2003. **83**(2): p. 173-80.
114. Tung, Y.C., et al., *High-throughput 3D spheroid culture and drug testing using a 384 hanging drop array.* Analyst, 2011. **136**(3): p. 473-8.
115. Angi, M., M. Versluis, and H. Kalirai, *Culturing Uveal Melanoma Cells.* Ocul Oncol Pathol, 2015. **1**(3): p. 126-32.
116. Verbik, D.J., et al., *Melanomas that develop within the eye inhibit lymphocyte proliferation.* Int J Cancer, 1997. **73**(4): p. 470-8.
117. Lake, S.L., et al., *Comparison of formalin-fixed and snap-frozen samples analyzed by multiplex ligation-dependent probe amplification for prognostic testing in uveal melanoma.* Invest Ophthalmol Vis Sci, 2012. **53**(6): p. 2647-52.
118. Kaliki, S., C.L. Shields, and J.A. Shields, *Uveal melanoma: estimating prognosis.* Indian J Ophthalmol, 2015. **63**(2): p. 93-102.
119. LaBarbera, D.V., B.G. Reid, and B.H. Yoo, *The multicellular tumor spheroid model for high-throughput cancer drug discovery.* Expert Opin Drug Discov, 2012. **7**(9): p. 819-30.
120. Nyga, A., U. Cheema, and M. Loizidou, *3D tumour models: novel in vitro approaches to cancer studies.* J Cell Commun Signal, 2011. **5**(3): p. 239-48.
121. Holliday, D.L., et al., *Novel multicellular organotypic models of normal and malignant breast: tools for dissecting the role of the microenvironment in breast cancer progression.* Breast Cancer Res, 2009. **11**(1): p. R3.
122. Kaur, P., et al., *Human breast cancer histoid: an in vitro 3-dimensional co-culture model that mimics breast cancer tissue.* J Histochem Cytochem, 2011. **59**(12): p. 1087-100.
123. Abu-Absi, S.F., et al., *Structural polarity and functional bile canaliculi in rat hepatocyte spheroids.* Exp Cell Res, 2002. **274**(1): p. 56-67.
124. Riccalton-Banks, L., et al., *Long-term culture of functional liver tissue: three-dimensional coculture of primary hepatocytes and stellate cells.* Tissue Eng, 2003. **9**(3): p. 401-10.
125. Ohmori, T., et al., *Blockade of tumor cell transforming growth factor-betas enhances cell cycle progression and sensitizes human breast carcinoma cells to cytotoxic chemotherapy.* Exp Cell Res, 1998. **245**(2): p. 350-9.
126. Duval, M.M., *Atlas D'Embryologie* 1889: Kessinger Publishing.
127. Hamburger, V. and H.L. Hamilton, *A series of normal stages in the development of the chick embryo. 1951.* Dev Dyn, 1992. **195**(4): p. 231-72.
128. *PA, R., A SARCOMA OF THE FOWL TRANSMISSIBLE BY AN AGENT SEPARABLE FROM THE TUMOR CELLS. Journal of Experimental Medicine*, 1911. **13**: p. 397-411.

129. P, R., M. JB, and T. WH, *The role of injury in the production of a chicken sarcoma by a filterable agent.* JAMA, 1912. **59**: p. 1793–1794.
130. Murphy, J.B., *FACTORS OF RESISTANCE TO HETEROPLASTIC TISSUE-GRAFTING : STUDIES IN TISSUE SPECIFICITY. III.* J Exp Med, 1914. **19**(5): p. 513-22.
131. Murphy, J.B., *STUDIES IN TISSUE SPECIFICITY : II. THE ULTIMATE FATE OF MAMMALIAN TISSUE IMPLANTED IN THE CHICK EMBRYO.* J Exp Med, 1914. **19**(2): p. 181-6.
132. Ribatti, D., *The chick embryo chorioallantoic membrane as a model for tumor biology.* Exp Cell Res, 2014.
133. Tong, Q., et al., *Embryonic development and the physiological factors that coordinate hatching in domestic chickens.* Poult Sci, 2013. **92**(3): p. 620-8.
134. Wong, G.K. and M.J. Cavey, *Development of the liver in the chicken embryo. I. Hepatic cords and sinusoids.* Anat Rec, 1992. **234**(4): p. 555-67.
135. Bellairs and Osmond, *Atlas of Chick Development, 3rd Edition*. 2014: Academic Press.
136. AL, R., *The Avian Embryo*. 1960.
137. Weber, W.T. and R. Mausner, *Migration patterns of avian embryonic bone marrow cells and their differentiation to functional T and B cells.* Adv Exp Med Biol, 1977. **88**: p. 47-59.
138. Lokman, N.A., et al., *Chick Chorioallantoic Membrane (CAM) Assay as an In Vivo Model to Study the Effect of Newly Identified Molecules on Ovarian Cancer Invasion and Metastasis.* Int J Mol Sci, 2012. **13**(8): p. 9959-70.
139. Hagedorn, M., et al., *Accessing key steps of human tumor progression in vivo by using an avian embryo model.* Proc Natl Acad Sci U S A, 2005. **102**(5): p. 1643-8.
140. Subauste, M.C., et al., *Evaluation of metastatic and angiogenic potentials of human colon carcinoma cells in chick embryo model systems.* Clin Exp Metastasis, 2009. **26**(8): p. 1033-47.
141. Conn, E.M., et al., *Comparative analysis of metastasis variants derived from human prostate carcinoma cells: roles in intravasation of VEGF-mediated angiogenesis and uPA-mediated invasion.* Am J Pathol, 2009. **175**(4): p. 1638-52.
142. Deryugina, E.I., et al., *Unexpected effect of matrix metalloproteinase down-regulation on vascular intravasation and metastasis of human fibrosarcoma cells selected in vivo for high rates of dissemination.* Cancer Res, 2005. **65**(23): p. 10959-69.
143. Xiao, X., et al., *Chick Chorioallantoic Membrane Assay: A 3D Animal Model for Study of Human Nasopharyngeal Carcinoma.* PLoS One, 2015. **10**(6): p. e0130935.
144. Chambers, A.F., R. Shafir, and V. Ling, *A model system for studying metastasis using the embryonic chick.* Cancer Res, 1982. **42**(10): p. 4018-25.
145. Busch, C., J. Krochmann, and U. Drews, *The chick embryo as an experimental system for melanoma cell invasion.* PLoS One, 2013. **8**(1): p. e53970.
146. Koop, S., et al., *Fate of melanoma cells entering the microcirculation: over 80% survive and extravasate.* Cancer Res, 1995. **55**(12): p. 2520-3.
147. Taizi, M., et al., *A novel and rapid in vivo system for testing therapeutics on human leukemias.* Exp Hematol, 2006. **34**(12): p. 1698-708.
148. Shioda, T., et al., *Early events of metastasis in the microcirculation involve changes in gene expression of cancer cells. Tracking mRNA levels of metastasizing cancer cells in the chick embryo chorioallantoic membrane.* Am J Pathol, 1997. **150**(6): p. 2099-112.
149. Bobek, V., et al., *Development of a green fluorescent protein metastatic-cancer chick-embryo drug-screen model.* Clin Exp Metastasis, 2004. **21**(4): p. 347-52.
150. Luyten, G.P., et al., *A chicken embryo model to study the growth of human uveal melanoma.* Biochem Biophys Res Commun, 1993. **192**(1): p. 22-9.
151. Berube, M., et al., *MMP-2 expression in uveal melanoma: differential activation status dictated by the cellular environment.* Mol Vis, 2005. **11**: p. 1101-11.

152. Laurent, C., et al., *High PTP4A3 phosphatase expression correlates with metastatic risk in uveal melanoma patients.* Cancer Res, 2011. **71**(3): p. 666-74.
153. Falini, B., et al., *Evolutionary conservation in various mammalian species of the human proliferation-associated epitope recognized by the Ki-67 monoclonal antibody.* J Histochem Cytochem, 1989. **37**(10): p. 1471-8.
154. Balke, M., et al., *Morphologic characterization of osteosarcoma growth on the chick chorioallantoic membrane.* BMC Res Notes, 2010. **3**: p. 58.
155. Stetler-Stevenson, W.G., S. Aznavoorian, and L.A. Liotta, *Tumor cell interactions with the extracellular matrix during invasion and metastasis.* Annu Rev Cell Biol, 1993. **9**: p. 541-73.
156. Semenza, G.L., *Targeting HIF-1 for cancer therapy.* Nat Rev Cancer, 2003. **3**(10): p. 721-32.
157. Herrmann, A., et al., *Cellular memory of hypoxia elicits neuroblastoma metastasis and enables invasion by non-aggressive neighbouring cells.* Oncogenesis, 2015. **4**: p. e138.
158. Bilzer, M., F. Roggel, and A.L. Gerbes, *Role of Kupffer cells in host defense and liver disease.* Liver Int, 2006. **26**(10): p. 1175-86.
159. Borthwick, N.J., et al., *The biology of micrometastases from uveal melanoma.* J Clin Pathol, 2011. **64**(8): p. 666-71.
160. MacDonald, I.C., et al., *Intravital videomicroscopy of the chorioallantoic microcirculation: a model system for studying metastasis.* Microvasc Res, 1992. **44**(2): p. 185-99.
161. Morris, V.L., et al., *Mammary carcinoma cell lines of high and low metastatic potential differ not in extravasation but in subsequent migration and growth.* Clin Exp Metastasis, 1994. **12**(6): p. 357-67.
162. Gomez, D., et al., *The Liverpool uveal melanoma liver metastases pathway: outcome following liver resection.* J Surg Oncol, 2014. **109**(6): p. 542-7.
163. L, D., et al., *andomised study on adjuvant therapy by DTIC in choroidal melanoma.* Ophtalmologie, 1998. **12**: p. 168–173.
164. Voelter, V., et al., *Adjuvant intra-arterial hepatic fotemustine for high-risk uveal melanoma patients.* Melanoma Res, 2008. **18**(3): p. 220-4.
165. Lane, A.M., et al., *Adjuvant interferon therapy for patients with uveal melanoma at high risk of metastasis.* Ophthalmology, 2009. **116**(11): p. 2206-12.
166. Davies, H., et al., *Mutations of the BRAF gene in human cancer.* Nature, 2002. **417**(6892): p. 949-54.
167. Korn, E.L., et al., *Meta-analysis of phase II cooperative group trials in metastatic stage IV melanoma to determine progression-free and overall survival benchmarks for future phase II trials.* J Clin Oncol, 2008. **26**(4): p. 527-34.
168. Krishna, Y., et al., *Genetic findings in treatment-naive and proton-beam-radiated iris melanomas.* Br J Ophthalmol, 2016.
169. Van Raamsdonk, C.D., et al., *Mutations in GNA11 in uveal melanoma.* N Engl J Med, 2010. **363**(23): p. 2191-9.
170. Griner, E.M. and M.G. Kazanietz, *Protein kinase C and other diacylglycerol effectors in cancer.* Nat Rev Cancer, 2007. **7**(4): p. 281-94.
171. Shoushtari, A.N. and R.D. Carvajal, *GNAQ and GNA11 mutations in uveal melanoma.* Melanoma Res, 2014. **24**(6): p. 525-34.
172. Carvajal, R.D., et al., *Study design and rationale for a randomised, placebo-controlled, double-blind study to assess the efficacy of selumetinib (AZD6244; ARRY-142886) in combination with dacarbazine in patients with metastatic uveal melanoma (SUMIT).* BMC Cancer, 2015. **15**: p. 467.
173. JJ, S., et al., *Sunitinib versus dacarbazine as first-line treatment in patients with metastatic uveal melanoma.* J Clin Oncol, 2013.

174. PD, N., et al., *A Cancer Research UK two-stage multicenter phase II study of imatinib in the treatment of patients with c-kit positive metastatic uveal melanoma (ITEM).* J Clin Oncol, 2013.
175. Chen, X., et al., *Combined PKC and MEK inhibition in uveal melanoma with GNAQ and GNA11 mutations.* Oncogene, 2014. **33**(39): p. 4724-34.
176. Musi, E., et al., *The phosphoinositide 3-kinase alpha selective inhibitor BYL719 enhances the effect of the protein kinase C inhibitor AEB071 in GNAQ/GNA11-mutant uveal melanoma cells.* Mol Cancer Ther, 2014. **13**(5): p. 1044-53.
177. Garcia, P.L., et al., *The BET bromodomain inhibitor JQ1 suppresses growth of pancreatic ductal adenocarcinoma in patient-derived xenograft models.* Oncogene, 2016. **35**(7): p. 833-45.
178. Delmore, J.E., et al., *BET bromodomain inhibition as a therapeutic strategy to target c-Myc.* Cell, 2011. **146**(6): p. 904-17.
179. Bandopadhayay, P., et al., *BET bromodomain inhibition of MYC-amplified medulloblastoma.* Clin Cancer Res, 2014. **20**(4): p. 912-25.
180. Lee, S., et al., *Bromodomain and extraterminal inhibition blocks tumor progression and promotes differentiation in neuroblastoma.* Surgery, 2015. **158**(3): p. 819-26.
181. Cheng, Z., et al., *Inhibition of BET bromodomain targets genetically diverse glioblastoma.* Clin Cancer Res, 2013. **19**(7): p. 1748-59.
182. Segura, M.F., et al., *BRD4 sustains melanoma proliferation and represents a new target for epigenetic therapy.* Cancer Res, 2013. **73**(20): p. 6264-76.
183. Filippakopoulos, P., et al., *Selective inhibition of BET bromodomains.* Nature, 2010. **468**(7327): p. 1067-73.
184. Shao, Q., et al., *BET protein inhibitor JQ1 attenuates Myc-amplified MCC tumor growth in vivo.* Cancer Res, 2014. **74**(23): p. 7090-102.
185. Lake, S.L., et al., *Single nucleotide polymorphism array analysis of uveal melanomas reveals that amplification of CNKSR3 is correlated with improved patient survival.* Am J Pathol, 2013. **182**(3): p. 678-87.
186. Parrella, P., et al., *Detection of c-myc amplification in uveal melanoma by fluorescent in situ hybridization.* Invest Ophthalmol Vis Sci, 2001. **42**(8): p. 1679-84.
187. Ambrosini, G., et al., *BRD4-targeted therapy induces Myc-independent cytotoxicity in Gnaq/11-mutatant uveal melanoma cells.* Oncotarget, 2015. **6**(32): p. 33397-409.
188. Sos, M.L., et al., *A framework for identification of actionable cancer genome dependencies in small cell lung cancer.* Proc Natl Acad Sci U S A, 2012. **109**(42): p. 17034-9.
189. Durlacher, C.T., et al., *An update on the pharmacokinetics and pharmacodynamics of alisertib, a selective Aurora kinase A inhibitor.* Clin Exp Pharmacol Physiol, 2016. **43**(6): p. 585-601.
190. Gonzalez-Loyola, A., et al., *Aurora B Overexpression Causes Aneuploidy and p21Cip1 Repression during Tumor Development.* Mol Cell Biol, 2015. **35**(20): p. 3566-78.
191. Pujade-Lauraine, E., et al., *Volasertib Versus Chemotherapy in Platinum-Resistant or -Refractory Ovarian Cancer: A Randomized Phase II Groupe des Investigateurs Nationaux pour l'Etude des Cancers de l'Ovaire Study.* J Clin Oncol, 2016. **34**(7): p. 706-13.
192. Ciceri, P., et al., *Dual kinase-bromodomain inhibitors for rationally designed polypharmacology.* Nat Chem Biol, 2014. **10**(4): p. 305-12.
193. Hoffman, B. and D.A. Liebermann, *Apoptotic signaling by c-MYC.* Oncogene, 2008. **27**(50): p. 6462-72.
194. Baldin, V., et al., *Cyclin D1 is a nuclear protein required for cell cycle progression in G1.* Genes Dev, 1993. **7**(5): p. 812-21.
195. Blom, D.J., et al., *Inverse correlation between expression of HLA-B and c-myc in uveal melanoma.* J Pathol, 1997. **181**(1): p. 75-9.

196. Mouriaux, F., et al., *Differential expression of G1 cyclins and cyclin-dependent kinase inhibitors in normal and transformed melanocytes.* Invest Ophthalmol Vis Sci, 1998. **39**(6): p. 876-84.
197. Coupland, S.E., et al., *The prognostic value of cyclin D1, p53, and MDM2 protein expression in uveal melanoma.* J Pathol, 2000. **191**(2): p. 120-6.
198. Boi, M., et al., *The BET Bromodomain Inhibitor OTX015 Affects Pathogenetic Pathways in Preclinical B-cell Tumor Models and Synergizes with Targeted Drugs.* Clin Cancer Res, 2015. **21**(7): p. 1628-38.
199. Kasai, F., et al., *Changes of heterogeneous cell populations in the Ishikawa cell line during long-term culture: Proposal for an in vitro clonal evolution model of tumor cells.* Genomics, 2016. **107**(6): p. 259-66.
200. Broker, L.E., F.A. Kruyt, and G. Giaccone, *Cell death independent of caspases: a review.* Clin Cancer Res, 2005. **11**(9): p. 3155-62.

Appendices

Appendix 1. Representative Immunohistochemistry staining of S093-15 case plated at 8000 cells per well. **A.** H&E Cross section of enucleated patient eye followed by higher power of tumour cells within patient eye and tumour cells cultured in 2D. **B.** H&E and Ki67 staining of tumour cells cultured in 3D at day 3, 6 and 9. **C.** MelanA, BAP1 and CD68 staining of tumour cells cultured in 3D at day 3.

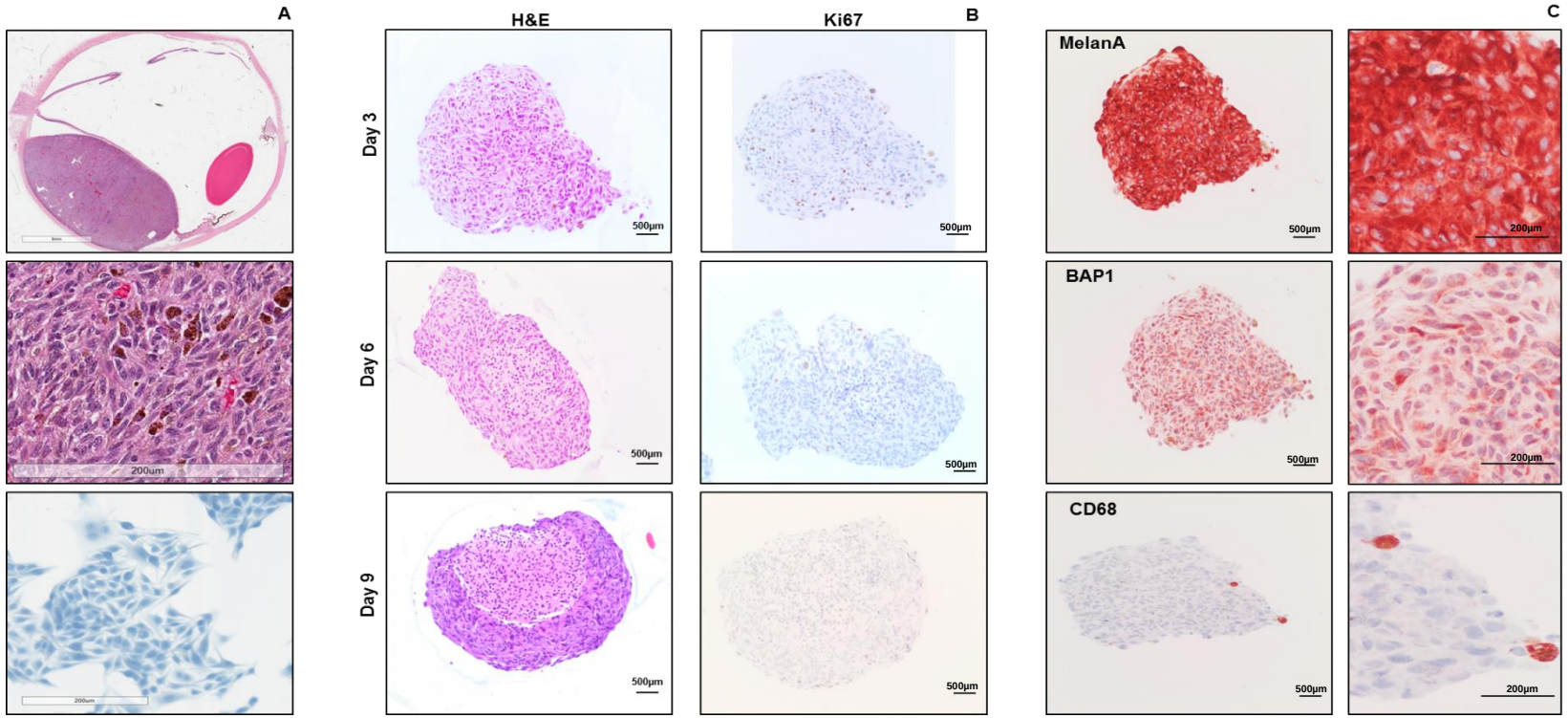

Appendix 2. Representative Immunohistochemistry staining of S119-15 case plated at 8000 cells per well. **A.** H&E Cross section of enucleated patient eye followed by higher power of tumour cells within patient eye and tumour cells cultured in 2D. **B.** H&E and Ki67 staining of tumour cells cultured in 3D at day 9 . **C.** MelanA, BAP1 and CD68 staining of tumour cells cultured in 3D at day 9.

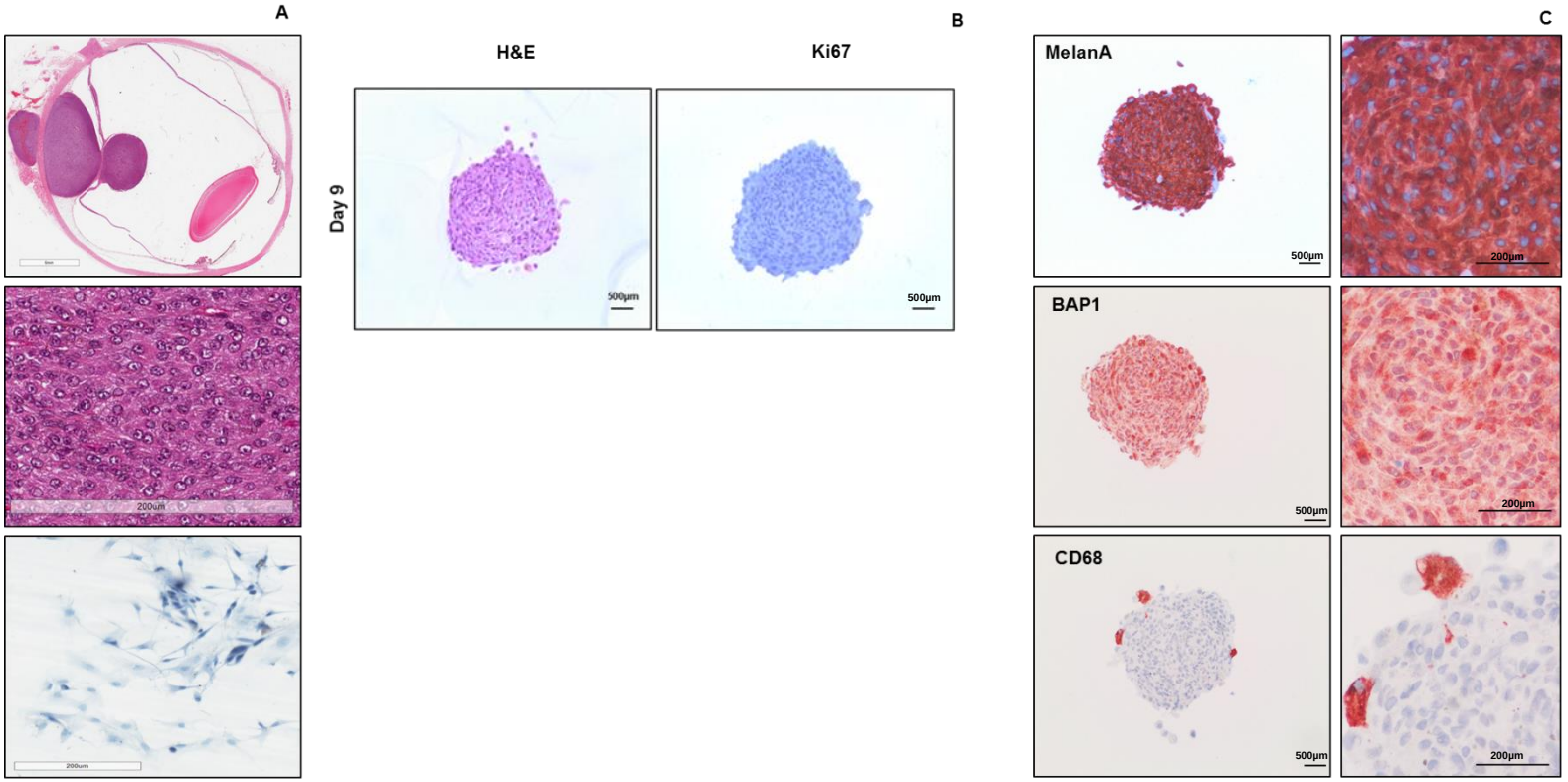

Appendix 3. Representative Immunohistochemistry staining of S084-15 case plated at 8000 cells per well. **A.** H&E Cross section of enucleated patient eye followed by higher power of tumour cells within patient eye. **B.** H&E and Ki67 staining of tumour cells cultured in 3D at day 6 and 9. **C.** MelanA, BAP1 and CD68 staining of tumour cells cultured in 3D at day 9.

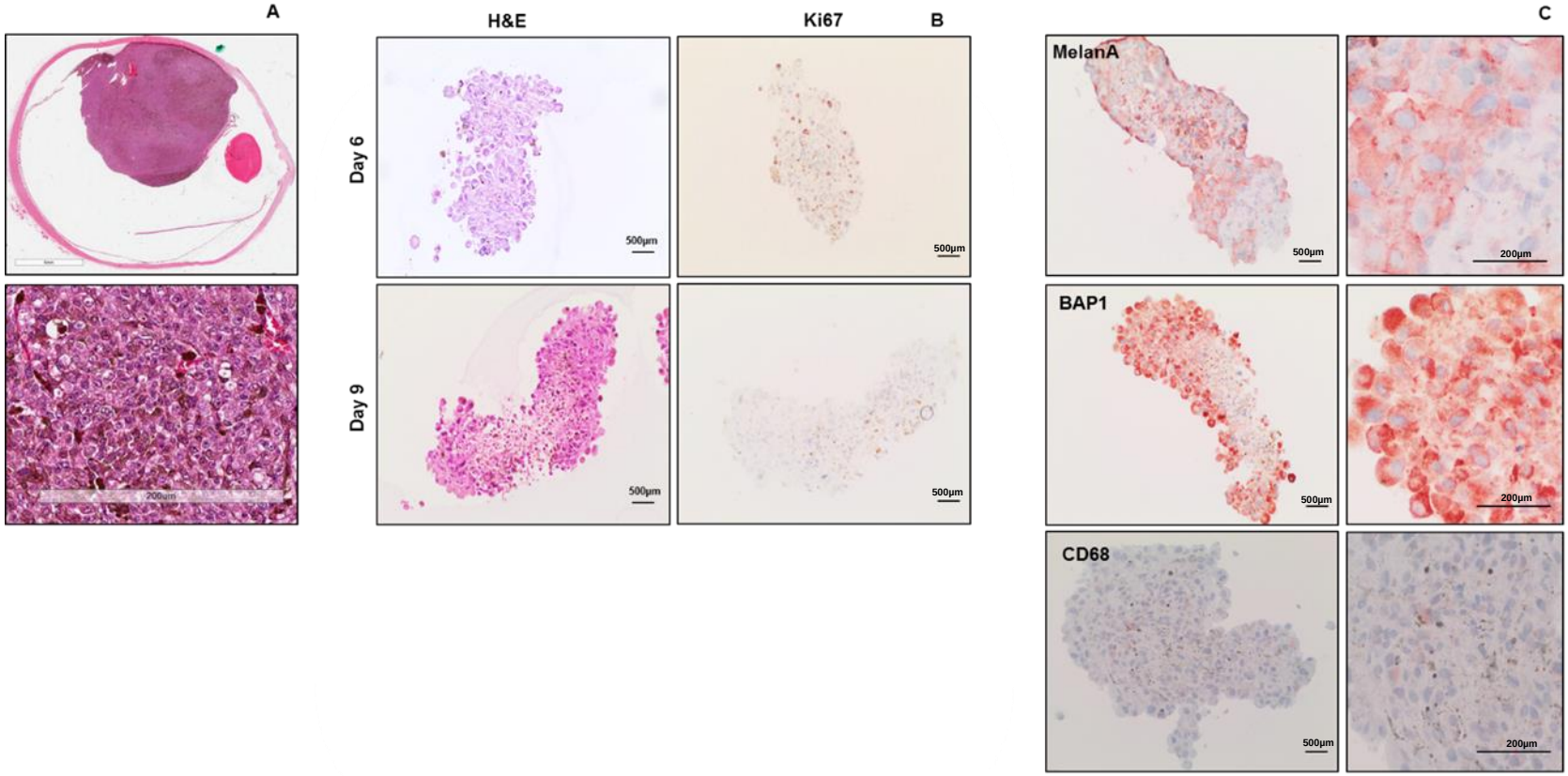

Appendix 4. Representative Immunohistochemistry staining of S121-15 case plated at 8000 and 16000 cells per well. **A.** H&E Cross section of enucleated patient eye followed by higher power of tumour cells within patient eye. **B.** H&E and Ki67 staining of tumour cells cultured in 3D at day 9. **C.** MelanA, BAP1 and CD68 staining of tumour cells cultured in 3D at day 9.

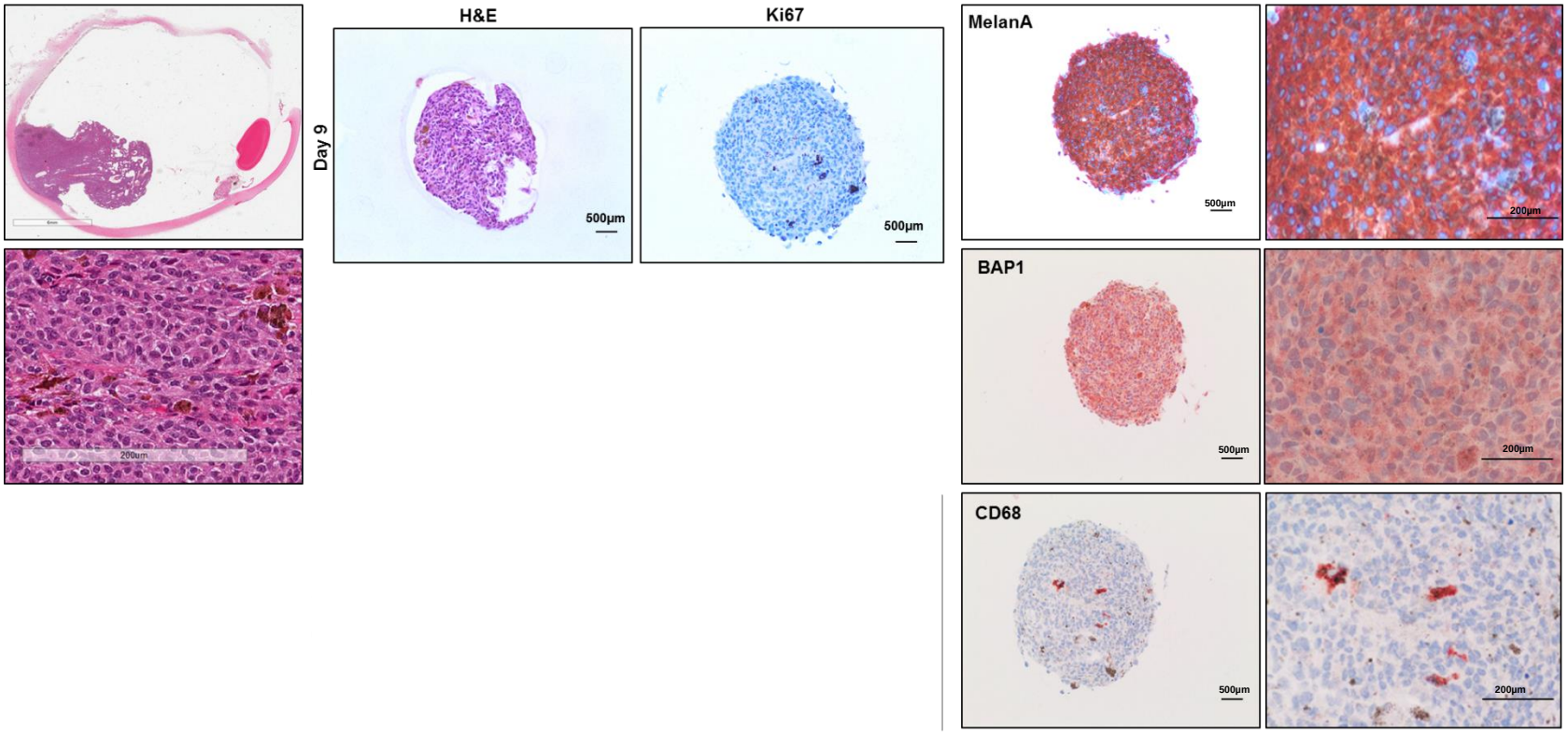

Appendix 5. Representative Immunohistochemistry staining of S125-15 case plated at 4000 and 8000 cells per well. **A.** H&E Cross section of enucleated patient eye followed by higher power of tumour cells within patient eye. **B.** H&E and Ki67 staining of tumour cells cultured in 3D at day 9. **C.** MelanA, BAP1 and CD68 staining of tumour cells cultured in 3D at day 9.

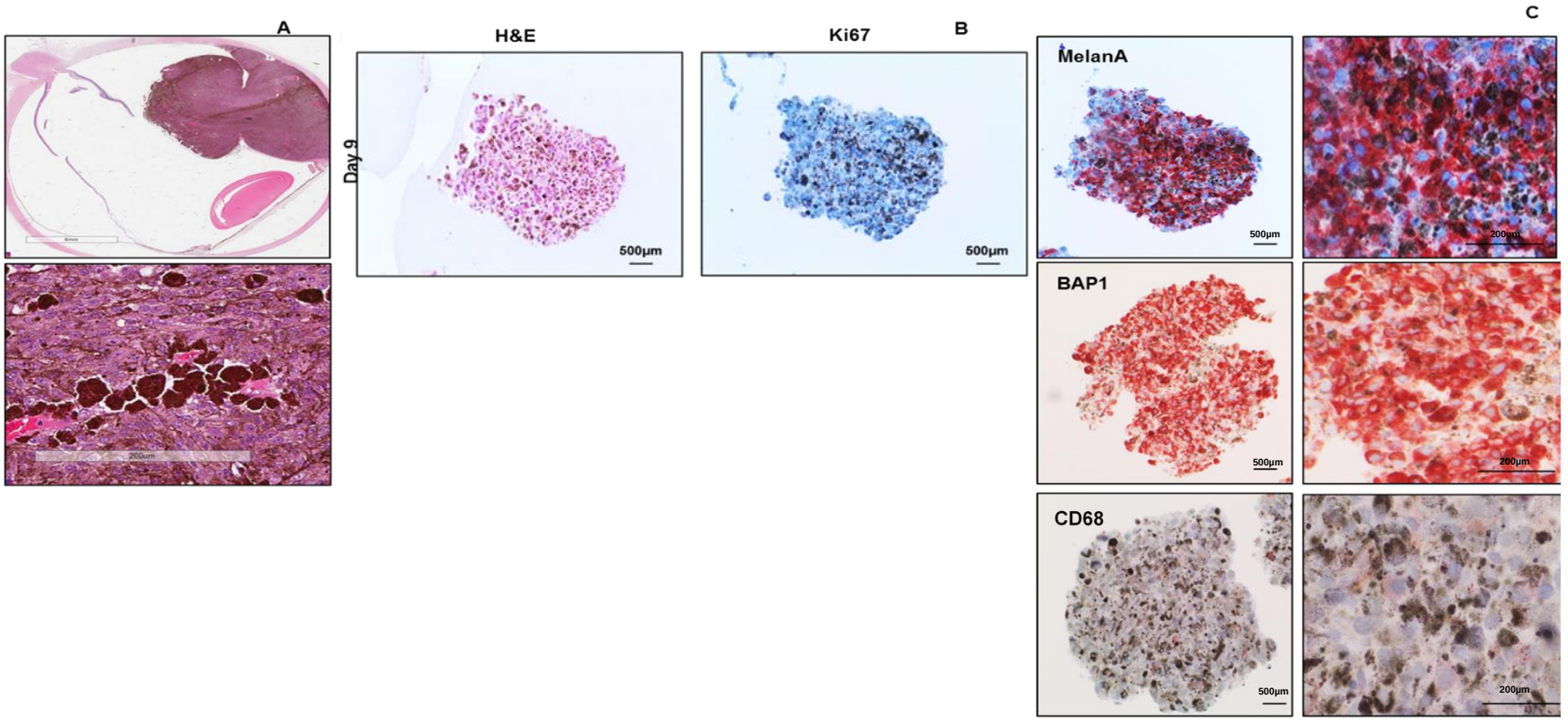

Appendix 6. Representative Immunohistochemistry staining of S104-15 case plated at 8000 cells per well. Since this case was an endoresection cross section of enucleated patient eye was not possible **A.** H&E and Ki67 staining of tumour cells cultured in 3D at day 3, 6 and 9. **B.** MelanA, BAP1 and CD68 staining of tumour cells cultured in 3D at day 9

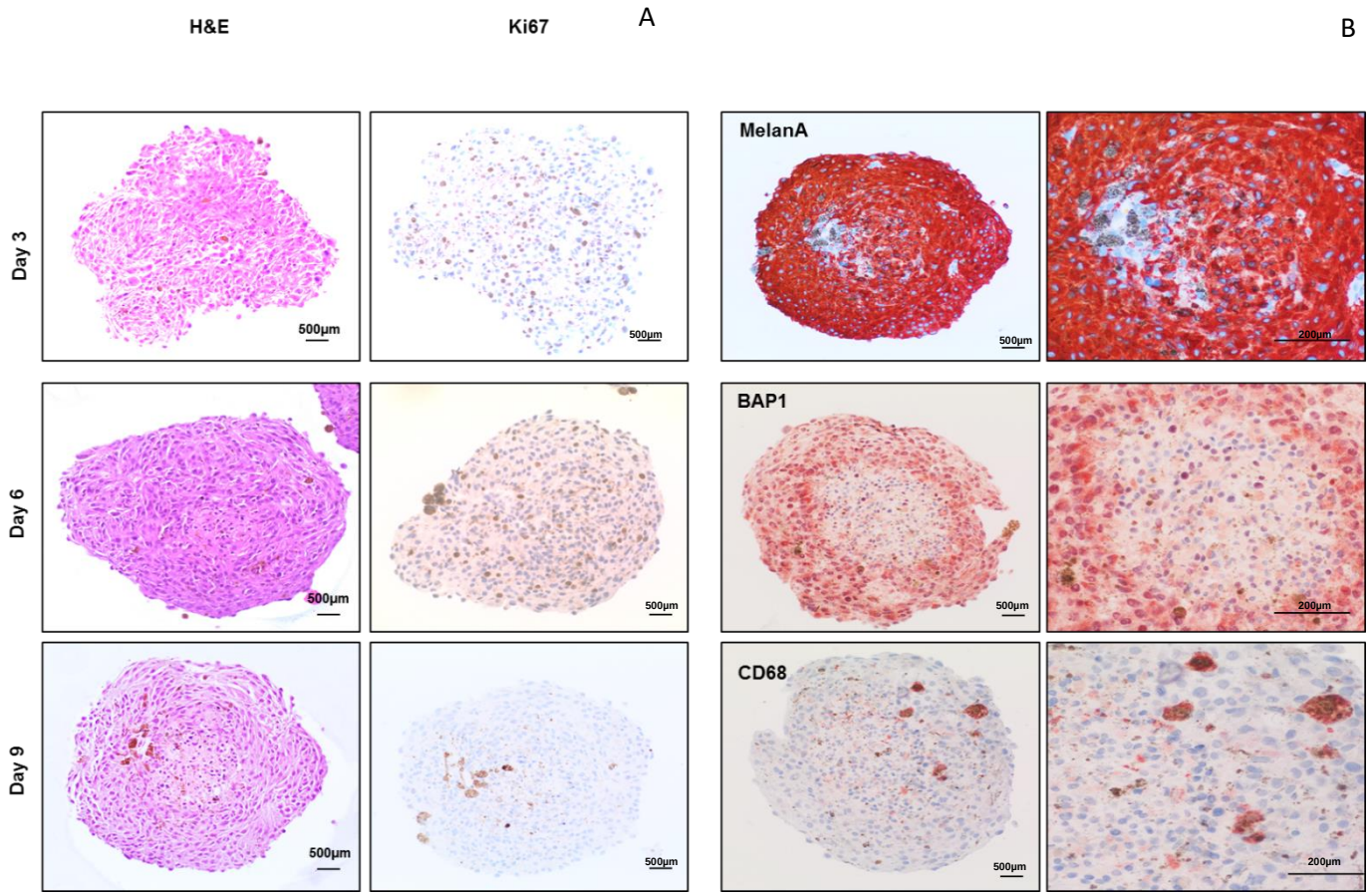

Appendix 7. Success rate of UM tumour nodule formation of GFP-labelled cell lines at E14, 7 days following CAM laceration.

92.1		
Experiment	**Number of surviving embryos**	**Nodule formation**
1	3	1
2	4	4
3	2	1
4	5	3
5	3	2
Total	17	11

OMM1		
Experiment	**Number of surviving embryos**	**Nodule formation**
1	2	1
2	2	2
3	2	2
Total	6	5

OMM2.3		
Experiment	**Number of surviving embryos**	**Nodule formation**
1	4	0
2	4	0
3	5	0
Total	13	0

MEL270		
Experiment	**Number of surviving embryos**	**Nodule formation**
1	5	0
2	4	0
3	5	0
Total	14	0

Appendix 8. PolyAcrylamide Gel, membrane probing and development

Acrylamide gels (10% Running/Resolving and 5% Stacking gels) were prepared for a Bio-Rad minigel apparatus (Bio-Rad laboratories Ltd). 4 ml resolving gel buffer (Geneflow, Lichfield, UK) was mixed with 5.3 ml acrylamide solution (19:1 Acrylamide/Bisacrylamide, Geneflow) and 6.7 ml H_2O. 75 µl of 10% ammonium persulphate (APS) (Sigma-Aldrich, UK) and 15 µl of tetramethylethylenediamine (TEMED) (Sigma-Aldrich, UK) were added to initiate polymerisation and left for 30 minutes at room temperature. This solution was sufficient to prepare 2 X 1.5 mm PAGE gels. A 5% polyacrylamide stacking gel was prepared by mixing 1.5 ml stacking gel buffer (Geneflow) with 1 ml acrylamide solution and 3.5 ml H_2O, 10% APS and TEMED were then added followed immediately by inserting a 10 or 15 well comb to create wells in the gels. The combs were gently removed once the stacking gel had set; generally after 15 minutes at room temperature. The electrophoresis tank was filled with 1X running buffer (25 mM Tris, 192 mM glycine, 0.1% SDS pH=8.3). 10 µg of total protein was loaded per lane of gel. The Full-Range Rainbow Molecular Weight Marker (GE Healthcare Life Sciences, UK) was also loaded for sizing. Gels were run at 35 V per gel constant voltage for 1 hour.

The separated proteins were subsequently transferred to polyvinylidene difluoride (PVDF) membranes (0.45 µm pore size, Roche Diagnostic Limited, UK). The membranes were briefly dipped in methanol followed by cold transfer buffer (25 mM Tris, 190 mM glycine, 0.1% SDS pH=8.3). A transfer sandwich was prepared and placed in the apparatus with cold transfer buffer. An electrical current of 400 mA (constant current) was applied for 1 hour at 4°C.

Membranes were blocked with the blocking buffer (5% milk in TBS-T (150 mM NaCl, 25 mM Tris pH 7.5, 0.1% Tween 20)) for an hour to reduce non-specific binding between the membranes and antibodies. The membranes were then probed with the primary antibodies, as detailed in Table 4.2, diluted with blocking buffer overnight at

4 ºC with gentle agitation. Membranes were then washed with TBS-T four times and incubated with the appropriate secondary antibody (Table 4.3). After a final wash with TBST, membranes were developed with Immobilon™ Western Chemiluminescent HRP substrate (MerckMillipore, Watford, UK), and imaged using an LAS-1000 imager (Fujifilm, Japan). Equal protein loading was confirmed by probing the blots with anti β-Actin or Histone H3 antibodies (Table 4.3).